Issue 4 2016 | Volume 12

The Journal on Advanced Studies in Theoretical and Experimental Physics, including Related Themes from Mathematics

PROGRESS IN PHYSICS

"All scientists shall have the right to present their scientific research results, in whole or in part, at relevant scientific conferences, and to publish the same in printed scientific journals, electronic archives, and any other media." — Declaration of Academic Freedom, Article 8

ISSN 1555-5534

The Journal on Advanced Studies in Theoretical and Experimental Physics, including Related Themes from Mathematics

PROGRESS IN PHYSICS

A quarterly issue scientific journal, registered with the Library of Congress (DC, USA). This journal is peer reviewed and included in the abstracting and indexing coverage of: Mathematical Reviews and MathSciNet (AMS, USA), DOAJ of Lund University (Sweden), Scientific Commons of the University of St. Gallen (Switzerland), Open-J-Gate (India), Referativnyi Zhurnal VINITI (Russia), etc.

Electronic version of this journal:
http://www.ptep-online.com

Postal Address

Department of Mathematics and Science,
University of New Mexico,
705 Gurley Ave., Gallup, NM 87301, USA

ISSN: 1555-5534 (print)
ISSN: 1555-5615 (online)

Standard Address Number: 297-5092
Printed in the United States of America

October 2016 **Vol. 12, Issue 4**

CONTENTS

Consiglio J. Take Fifteen Minutes to Compute the Fine Structure Constant (*Letters to Progress in Physics*) 305

Bilbao L. Does the Velocity of Light Depend on the Source Movement? 307

Marquet P. Vacuum Background Field in General Relativity 313

Marquet P. On the Physical Nature of the de Broglie Wave 318

Daywitt W. C. Antigravity and Vacuum Propulsion in the Planck Vacuum Theory 323

Ogiba F. On the Quantum-Relativistic Behavior of Moving Particles 325

Faizuddin A. Type III Spacetime with Closed Timelike Curves 329

Seaver J. R. Experimental and Theoretical Test of Cahill's Detection of Absolute Velocity in Gas-mode Interferometer Experiments 332

Heymann Y. Dark Matter, the Correction to Newton's Law in a Disk 347

Zhang T. X. Principle of Spacetime Black Hole Equivalence 353

Seaver J. R. Attempt to Replicate Cahill's Quantum Gravity Experiment to Measure Absolute Velocity 362

Marquet P. Some Insights on the Nature of the Vacuum Background Field in General Relativity (*Letters to Progress in Physics*) 366

Heymann Y. Conservation Laws and Energy Budget in a Static Universe 368

Information for Authors

Progress in Physics has been created for rapid publications on advanced studies in theoretical and experimental physics, including related themes from mathematics and astronomy. All submitted papers should be professional, in good English, containing a brief review of a problem and obtained results.

All submissions should be designed in LaTeX format using *Progress in Physics* template. This template can be downloaded from *Progress in Physics* home page http://www.ptep-online.com

Preliminary, authors may submit papers in PDF format. If the paper is accepted, authors can manage LaTeXtyping. Do not send MS Word documents, please: we do not use this software, so unable to read this file format. Incorrectly formatted papers (i.e. not LaTeXwith the template) will not be accepted for publication. Those authors who are unable to prepare their submissions in LaTeXformat can apply to a third-party payable service for LaTeX typing. Our personnel work voluntarily. Authors must assist by conforming to this policy, to make the publication process as easy and fast as possible.

Abstract and the necessary information about author(s) should be included into the papers. To submit a paper, mail the file(s) to the Editor-in-Chief.

All submitted papers should be as brief as possible. Short articles are preferable. Large papers can also be considered. Letters related to the publications in the journal or to the events among the science community can be applied to the section *Letters to Progress in Physics*.

All that has been accepted for the online issue of *Progress in Physics* is printed in the paper version of the journal. To order printed issues, contact the Editors.

Authors retain their rights to use their papers published in *Progress in Physics* as a whole or any part of it in any other publications and in any way they see fit. This copyright agreement shall remain valid even if the authors transfer copyright of their published papers to another party.

Electronic copies of all papers published in *Progress in Physics* are available for free download, copying, and re-distribution, according to the copyright agreement printed on the titlepage of each issue of the journal. This copyright agreement follows the *Budapest Open Initiative* and the *Creative Commons Attribution-Noncommercial-No Derivative Works 2.5 License* declaring that electronic copies of such books and journals should always be accessed for reading, download, and copying for any person, and free of charge.

Consideration and review process does not require any payment from the side of the submitters. Nevertheless the authors of accepted papers are requested to pay the page charges. *Progress in Physics* is a non-profit/academic journal: money collected from the authors cover the cost of printing and distribution of the annual volumes of the journal along the major academic/university libraries of the world. (Look for the current author fee in the online version of *Progress in Physics*.)

LETTERS TO PROGRESS IN PHYSICS

Take Fifteen Minutes to Compute the Fine Structure Constant

Jacques Consiglio

52 Chemin de Labarthe, 31600 Labastidette, France
E-mail: Jacques.Consiglio@gmail.com

This note complements the calculus of the fine structure constant provided in [2] in agreement with the theory of mass/resonances developed therein. It shows that the value of α can be predicted from geometry using a) the assumption of integral resonances, b) de Broglie's thesis, and c) the Wheeler-Feynman absorber theory and its time-symmetry; hence independently of precision measurement.

1 Introduction

Using Quantum Electro-Dynamics (QED), precise measurement of the electron magnetic moment anomaly enables to compute the value of the fine structure constant.

In this note, we show that the resulting value of α pulls us back almost to square one, namely Bohr's model and de Broglie's thesis, since the assumption of integral resonances used in [2] and its use of the Wheeler-Feynman absorber theory [5], [6] give the same result, straight from geometry.

2 The calculus

In order to complete the calculus, we shall need two assumptions used sequentially:

- All elementary particles are integral-number based resonances of physical currents. We uses the verb "to be" in its full sense: there is nothing else to deal with.
- The Wheeler-Feynman absorber theory [5], [6], is close to the right picture. The universe expands in a 4^{th} spatial dimension and we live at some sort of boundary or membrane that expands spherically. Up and Down-time currents exist making particles.

Now according to de Broglie [1] the phase coherence of the wave gives the Bohr orbits. Second, consider the first orbit and imagine the figure, a helicoid, in x, y, t. Considering a system of unit where the Bohr radius is 1 in x, y, and its Compton frequency is 1 on the time axis, the helix length is:

$$L_h^2 = 137^2 + (2\pi)^2.$$

According to the assumptions, this expression is the effect of a resonance, but α is the coupling of the electron with the field; therefore it is the amplitude *and the geometry* from which L_h develops. Since $\alpha < 1$, we necessarily have:

$$\alpha \leftarrow L_h^{-1}.$$

But the electron makes one turn when the helix makes two turns. With respect to the electron "being" a resonance, its rotational path length must be reduced by half and we get a resonance length:

$$L_r^2 \approx 137^2 + \pi^2.$$

Now we need to take into account the wavelength h/p as part of the electron resonance. According to de Broglie, its phase velocity is $V = c^2/v$, with v the electron velocity; here distances are inverted and velocity dependent. Its length around the proton is then $1/274$ (the electron phase repeats every 274 Compton periods). But when the wave makes one turn the electron progresses; therefore the resonance makes 275 turns when the electron resonance makes a full turn. The wave misses 1 turn over 275, which gives a negative term:

$$L_r^2 \approx 137^2 + \pi^2 - \frac{1}{275}.$$

Here the negative term is not squared. The explanation is a little less trivial than the rest of the calculus. Denoting a_n the radius of the n^{th} Bohr orbit and λ_{dn} the associated de Broglie wavelength, we have:

$$a_n = n^2\, a_0; \lambda_{dn} = n\, \lambda_{d0}\,.$$

Those quantities are physical. The round trip of the wave is $n\,\lambda_{dn} = n^2\,\lambda_{d0}$ and corresponds to quantized angular momentum; at the opposite, the same trip includes $137\,n^2$ Compton periods. Therefore a different treatment is needed for 137 and $1/275$. The former is squared in (1) and associated to n^2; then since the latter is associated to n, it cannot be squared; otherwise this expression would be orbit dependent in n. This is the physical aspect, it means that on any Bohr orbit we can use a system of units in the space dimensions where $n^2\,a_0 = 1$, and the de Broglie wavelength and its angle (its phase velocity) defines the unit for $V > c$. We end-up with a system of units which is entirely defined by de Broglie's geometry, where all quantities are defined by h or $\hbar$, and the electron mass.

Let us now use the second assumption. The field is time-symmetrical for an observer which is fixed in time (this is also the perspective of QED). Time symmetry implies that the electron is composite of up and down-time currents: Up-time $= -e/2$, down-time $= +e/2$. Those currents are cen-

tered like the electron resonance (on the helix) and manifest an electric charge which contribution (sign) depends on their own sign and time-orientation. Their interaction gives $(-e/2)(+e/2) = -e^2/4$, which compares to $-e^2$, the interaction electron-proton.

We must apply the same reasoning to the wave; by symmetry it is also composed of two currents of opposite directions, but of identical charges, centered on the electron. Then we just add $1/4$ as follows:

$$L_r^2 = 137^2 + \pi^2 - \frac{1}{275}\left(1 + \frac{1}{4}\right). \quad (1)$$

Last we compute the inverse of this length to get α:

$$(1) \rightarrow L_r^{-1} = 7.29\,735\,256\,656\,433\,e^{-3}. \quad (2)$$

Compare with CODATA 2014:

$$\alpha = 7.29\,735\,256\,64\,(12)\,e^{-3}. \quad (3)$$

The difference is on the last digit and $1/7^{th}$ the uncertainty.

You can stop your chronometer.

3 Conclusions

The fine structure constant was computed from de Broglie's geometry under the following assumptions:

- The electron "is" an integral resonance,
- The existence of symmetrical currents, where we see the signature of a resonant system,
- Asymmetry in currents between space and time, which is implicit in the reasoning.

This result completes the calculus provided in [2] where a logical origin of 137 is uncovered.

Interestingly, it was possible to predict this value of α about 70 years ago pushing Wheeler-Feynman's absorber theory to its natural consequences in terms of time-symmetry, since $\alpha \approx 1/137$ was known.

By the way, it also requires to use de Broglie's geometry in its full extent; not only the wavelength $\lambda_d = h/p$, but also the phase velocity $V = c^2/v > c$ for which no experimental verification exists. We showed that this velocity is consistent with the current best estimate of α.

Last but not least, the coefficient $1/4$ in (1) addresses the wave compositeness; an aspect of importance, or rather a possibility meaning the incompleteness of wave mechanics, quantum mechanics and field theory.

Submitted on July 5, 2016 / Accepted on July 7, 2016

References

1. De Broglie L. Recherches sur la théorie des quanta. *Annales de Physique* — 10e sérié — Tome III — Janvier-Février 1925.
2. Consiglio J. On quantization and the resonance paths. *Progress in Physics*, 2016, v. 12(3), 259–275.
3. Consiglio J. On the absorber in gravitation. *Progress in Physics*, 2016, v. 12(1), 20–25.
4. Cramer J. The transactional interpretation of quantum mechanics. *Rev. Mod. Phys.*, 1986, v. 58(3).
5. Wheeler J.A., Feynman R.P. Interaction with the absorber as the mechanism of radiation. *Reviews of Modern Physics*, 1945, v. 17(2–3), 157–161.
6. Wheeler J.A., Feynman R.P. Classical electrodynamics in terms of direct interparticle action. *Reviews of Modern Physics*, 1949, v. 21(3), 425–433.

Does the Velocity of Light Depend on the Source Movement?

Luis Bilbao
Universidad de Buenos Aires. Consejo Nacional de lnvestigaciones Científicas y Técnicas.
Instituto de Física del Plasma (INFIP). Facultad de Ciencias Exactas y Naturales. Buenos Aires, Argentina.
E-mail: bilbao@df.uba.ar

Data from spacecrafts tracking exhibit many anomalies that suggest the dependence of the speed of electromagnetic radiation with the motion of its source. This dependence is different from that predicted from emission theories that long ago have been demonstrated to be wrong. By relating the velocity of light and the corresponding Doppler effect with the velocity of the source at the time of detection, instead of the time of emission, it is possible to explain quantitatively and qualitatively the spacecraft anomalies. Also, a formulation of electromagnetism compatible with this conception is possible (and also compatible with the known electromagnetic phenomena). Under this theory the influence of the velocity of the source in the speed of light is somewhat subtle in many practical situations and probably went unnoticed (i.e. below the detection limit) in other measurements.

1 Introduction

In these lines I intend to show that there exists consistent evidence pointing to the need of revision and further study of what seem at present a settled issue, namely the independence of the speed of electromagnetic radiation on the motion of its source.

The main point in the evidence is the range disagreement during the Earth flyby of the spacecraft NEAR in 1998. Its range was measured near the point of closest approach using two radar stations, Millstone and Altair, of the Space Surveillance Network, and compared with the trajectory obtained from the Deep Space Network [1]. As for the range, the two measurements should match within a meter-level accuracy (the resolution is 5 m for Millstone and 25 m for Altair), but actual data showed a difference that varies linearly with time (with different slopes for the two radar stations) up to a maximum difference of about 1 km, i.e. more than 100 times larger than the accuracy of the equipment used (see figure 10 of [1]). Further, when NEAR crossed the orbits of Global Positioning System (GPS) satellites, orbital radius 26,600 km, the measured range difference was 650 m, that is, a time difference of 2 μs. Is it reasonable that any standard GPS receiver performs better than the Deep Space Network or the Space Surveillance Network?

There has not been a complete explanation for the range discrepancy. It is very difficult to find any physical reason that may produce this anomaly, for any physical disturbance of the path of the spacecraft should manifest equally in the Deep Space Network and the Space Surveillance Network data. Guruprasad [2] proposed an explanation that points to a time lag in the Deep Space Network signals proportional to the range, but the model is, at best, within 10% of the measured data (i.e. larger than the instrumental error) and, more important, it fails to explain an important feature, that is, the different slope for the two radars. If we assume that systems are working properly, then the measured range difference (time lag) could be due to different propagation time of the employed signals.

Additional points in the evidence come from anomalies related to the tracking of spacecrafts, present in both Doppler and ranging data. The Pioneer anomaly [3] and the flyby anomaly [4] refer to small residuals of the differences between measured and modeled Doppler frequencies of the radio signals emitted by the spacecrafts. Although these residuals are very small (less than 1 Hz on GHz signals) the problem is that they follow a non-random pattern, indicating failures of the model. According to the temporal variation of those residuals the Pioneer anomaly exhibits a main term, an annual term, a diurnal term and a term that appears during planetary encounters. It should be clarified that a few years ago an explanation of the Pioneer anomaly was published [5]. However, it is a very specific solution that applies only to the main term of the Pioneer spacecraft anomaly, but left unresolved many other anomalies, including those of the spaceships Cassini, Ulysses and Galileo; the annual term; the diurnal term; the increases of the anomaly during planetary encounters; the flyby anomaly; and the possible link between all them (it is hard to think that there are so many different causes for the mentioned anomalies). For all this, I believe that the issue can not be closed as it stands.

2 Range disagreement

As a matter of fact, the range difference between the Space Surveillance Network and the Deep Space Network, δR, is perfectly fitted with

$$\delta R(t) = -\frac{\mathbf{R}(t)\cdot\mathbf{v}(t)}{c}\,, \tag{1}$$

where $\mathbf{R}(t)$ is a vector range pointing from the spacecraft to the radar, $\mathbf{v}(t)$ the spacecraft velocity relative to the radar,

and c the speed of light. Figure 1 shows this fit and its comparison with measured data. The orbital and measured data were taken from [1]. Although the exact location of the radar stations are unknown to the author (approximate values are: Millstone 42.6° N 71.43° W, and Altair 9.18° N 167.42° E), the fit is statistically significant for both radar stations ($p < 10^{-3}$) including the first outliers points. It reproduces the (almost) linear dependence with time during the measured interval, and the two different slopes for Millstone and Altair stations due to their different locations.

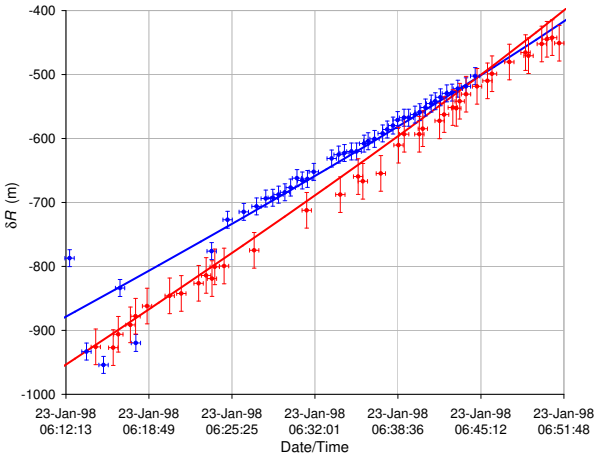

Fig. 1: Range disagreement between the Space Surveillance Network and the Deep Space Network, for 1998 NEAR flyby (Millstone blue points, upper trace, and Altair red points, lower trace). Also the fit (1) is plotted (full lines, Millstone in blue and Altair in red). For Millstone, the error bars refer to the uncertainties in the extraction of the data from figure 10 of [1], rather than to its tracking error (5 m), while for Altair, the accuracy is 25 m.

Since range measurements are based on time-of-flight techniques, the validity of (1) means that the electromagnetic waves (microwave) of the Deep Space Network and the Space Surveillance Network travel at different speeds. Specifically, in the radar frame of reference, if the Space Surveillance Network waves travel at c, then the Deep Space Network waves travel at c plus the projection of the spacecraft velocity in the direction of the beam, in sharp contrast with the Second Postulate of the Special Relativity Theory.

In view of the above result one may ask what is established, at present, about the relation of the speed of electromagnetic radiation (light for short) to the motion of the source. In order to elaborate this point the following questions are of relevance:

1. Are there *simultaneous* measurements of the speed of light from different moving macroscopic sources (not moving images) with different velocities?;
2. Since ballistic (emission) theories are ruled out (see, for example, DeSitter [6,7], Brecher [8] and Alväger et al [9]), how else could the speed of light depend on the source movement?;
3. How is it possible that there is a first order difference in v/c in spacecraft range measurements, while at the same time there are many experiments on time dilation that are consistent with Special Relativity Theory to second order in v/c (see, for example, [10])?;
4. If the velocity of light depend on the velocity of the source, why has this not been observed in other phenomena in the past?

In answer to the previous questions, so far as the author is aware, there is no known experimental work that simultaneously measures the speed of light from two different sources (not images), or that simultaneously measures the speed of light and that of its source. For example, in the work by Alväger et al, [9] the speed of light is measured at a later time (≈ 200 ns) than the emission time, and there is no measurement of the speed of the source at the time of the *detection* of the light.

Note that measurements involving moving images produce different results from those produced by mobile sources. For example, under Special Relativity Theory, a moving source is affected by time dilation while a moving image is not. Therefore, to ensure the independence of the speed of light from its source movement, it is essential to have two sources with different movements.

Although controversial and beyond the scope of the this note, time dilatation phenomena may be of different physical origin from first order terms, as it may be inferred from the work of Schrödinger [11]. Thus, measurements of time dilatation phenomena in accordance with Special Relativity Theory, does not necessarily imply the independence of the speed of light with the movement of the source.

The experiments mentioned above [6–9] only rule out ballistic theories in which radiation maintains the speed of the source at the time of *emission*, but do not rule out other ideas, like Faraday's 1846 [12].

3 Faraday's ray vibrations

In order to remove the ether, Faraday introduced the concept of vibrating rays [12], in which an electric charge is conceived as a center of force with attached "rays" that extend to infinity. The rays move with their center, but without rotating. According to this view, the phenomenon of electromagnetic radiation corresponds to the vibration of these "rays", that propagates at speed c relative to the rays (and the center). That is, the radiation remains linked to the source even after emitted. Today we could describe the interaction as a kind of entanglement between the charge and the photon. A framework for the electromagnetic phenomena according to Faraday's ideas was developed. It was called "Vibrating Rays Theory" [13] in reference to Faraday's "vibrating rays".

Under Faraday's idea, the velocity of radiation at a given epoch will be equal to c plus the velocity of the source at the *same* epoch, in contrast with ballistic theories in which

the emitted light retains the speed of the source at the *emission* epoch. In this sense the radiation is always linked to the charge at every time after the emission. Consequently, the measured Doppler Effect corresponds to the speed of the source at the time of *reception*, as well.

Further, a difference between active and passive reflection is expected, since the latter is still related to the original source according to Vibrating Rays Theory. The Deep Space Network works with the so called active reflection (the spacecraft re-emits in real time a signal in phase with the received signal from Earth), while the Space Surveillance Network works with passive radar reflection. In consequence, the down-link signal from the approaching spacecraft will propagate faster that the reflected one. Using the available orbital data [1] we found that, under Vibrating Rays Theory, the theoretical time-of-flight difference between active and passive reflection gives exactly the same range disagreement as (1), see Part 6 of [13].

4 Pioneer anomaly

The Pioneer anomaly refers to the fact that the received Doppler frequency differs from the modeled one by a blue shift that varies almost linearly with time, and whose derivative is

$$\frac{d(\Delta f)}{dt} \approx -6 \times 10^{-9}\ \text{Hz/s}, \tag{2}$$

where Δf is the frequency difference between the measured and the modeled values.

In the case of a source with variable speed, the main difference in Doppler (to first order) between Vibrating Rays Theory and Special Relativity Theory, is that Special Relativity Theory relates to the speed of the source at the time of *emission*, while Vibrating Rays Theory relates to the speed of the source at the time of *reception*. Precisely, this difference seems to be present in the spacecraft anomalies.

If Vibrating Rays Theory is valid, it automatically invalidates all calculations and data analysis of spacecraft tracking which are based on Special Relativity Theory. So, it is not easy to make a direct comparison between the expected results from Special Relativity Theory and Vibrating Rays Theory. However, to see whether or not the main features predicted by Vibrating Rays Theory are present in the measurements, we can evaluate the residual by simulating a measured Doppler signal assuming that light propagates in accordance to Vibrating Rays Theory but analyzed according to Special Relativity Theory.

Calling t_2 the emission time of the downlink signal from the spacecraft toward Earth and t_3 the reception time at Earth, the first order difference of the Doppler shift between Vibrating Rays Theory and Special Relativity Theory is (see [13] Part 4)

$$\Delta f = f_{VRT} - f_{SRT} \approx f_0 \hat{\mathbf{r}} \cdot \frac{\mathbf{v}_2 - \mathbf{v}_3}{c}, \tag{3}$$

where $\mathbf{v}_2$ and $\mathbf{v}_3$ represent the velocities of the spacecraft at the corresponding epoch, $\hat{\mathbf{r}}$ is the unit vector from the spaceship to the antenna, and f_0 the proper frequency of the signal. That is, the velocity used in the Special Relativity Theory formula is that at the time of *emission* while according to Vibrating Rays Theory is that corresponding at the time of *reception*.

Since the spacecraft slows down as it moves away, then $\hat{\mathbf{r}} \cdot (\mathbf{v}_2 - \mathbf{v}_3) > 0$, therefore the difference corresponds to a small blue shift mounted over the large red shift, as it has been observed in the Pioneer anomaly. It should be noted that this difference appears because of the active reflection produced by the on-board transmitter. In case of a passive reflection (for example, by means of a mirror) the above difference vanishes.

4.1 Main term

An estimate of the order of magnitude of 3 is obtained by using that the variation of the velocity of the spacecraft between the time of emission and reception is approximately

$$\mathbf{v}_2 - \mathbf{v}_3 \approx \mathbf{a}\,(t_2 - t_3), \tag{4}$$

where $\mathbf{a}$ is a mean acceleration during the down-link interval. An estimate for the duration of the down-link is simply

$$t_3 - t_2 \approx \frac{r}{c}, \tag{5}$$

where r is a mean position of the spaceship between t_2 and t_3, therefore

$$\Delta f \approx -f_0 \frac{\mathbf{r} \cdot \mathbf{a}}{c^2}.$$

Since

$$\mathbf{a} = -\frac{GM}{r^2}\hat{\mathbf{r}},$$

where G is the gravitational constant, and M the mass of the Sun, then, the time derivative becomes

$$\frac{d\,(\Delta f)}{dt} \approx f_0 \frac{\mathbf{v} \cdot \mathbf{a}}{c^2}. \tag{6}$$

If the difference (6) is interpreted as an anomalous acceleration we get

$$a_a \approx \frac{v}{c}\, a, \tag{7}$$

that is, the so-called anomalous acceleration is v/c times the actual acceleration of the spacecraft.

Using data from HORIZONS Web-Interface [14] for the spacecraft ephemeris, some characteristic value for a_a can be obtained. Consider the anomalous acceleration detected at the shortest distance of the Cassini spacecraft during solar conjunction in June, 2002. The spacecraft was at a distance of 7.42 AU moving at a speed of 5.76 km/s. The anomalous acceleration given by (7) is $a_a \approx 2 \times 10^{-9}$ m/s^2 of the same order of the measured one ($\approx 2.7 \times 10^{-9}$ m/s^2). Also, the closest distance at which the Pioneer anomaly has been detected was

about 20 AU. the anomalous acceleration predicted by (7) at that distance is $a_a \approx 7.3 \times 10^{-10}$ m/s^2 of the same order as the measured one.

The "anomaly" given by (7) decreases in time in a way that has not been observed. Note, however, that according to Markwardt [15] the expected frequency at the receiver includes an additional Doppler effect caused by small effective path length changes, given by

$$\Delta f_{path} = -\frac{2f_0}{c}\frac{dl}{dt}, \tag{8}$$

where dl/dt is the rate of change of effective photon trajectory path length along the line of sight. This is a first order effect that can partially hide the difference between Special Relativity Theory and Vibrating Rays Theory. Therefore, a more careful analysis should take into account the additional contribution of (8) in (7).

Further, other first order effects may appear, for example, by a slight rotation of the orbital plane. Due to spacecraft maneuvers or random perturbations the orbital parameters are obtained by periodically fitting the measurements with theoretical orbits. Therefore there is no straightforward way to weight the importance of these fittings in (7). In other words, data acquisition and analysis may hide part of the Vibrating Rays Theory signature.

4.2 Annual term

Apart from the residual referred to in the preceding paragraph there is also an annual term. According to Anderson et al [16] the problem is due to modeling errors of the parameters that determine the spacecraft orientation with respect to the reference system. Anyway, Levy et al [17] claim that errors such as errors in the Earth ephemeris, the orientation of the Earth spin axis or the stations coordinates are strongly constrained by other observational methods and it seems difficult to modify them sufficiently to explain the periodic anomaly.

The advantage of studying the annual term over the main term, is that the former is less sensitive to the first order correction mentioned above, and, for the case of Pioneer, also to the thermal propulsion correction [5]. Clearly, the Earth orbital position does not modify those terms.

As before, the annual term is explained by the difference between the velocity of the spacecraft at the time of emission and that at the moment of detection, which depends on whether the spaceship is in opposition or in conjunction relative to the Sun. When the spacecraft is in conjunction, light takes longer to get back to Earth than in opposition. The time difference between emission and reception will be increased by the time the light takes in crossing the Earth orbit. Specifically, taking into account the delay due to the position of Earth in its orbit, in opposition equation (5) should be written as

$$t_3 - t_2 \approx \frac{r + R_{orb}}{c}, \tag{9}$$

while in conjunction it would be

$$t_3 - t_2 \approx \frac{r - R_{orb}}{c}, \tag{10}$$

where R_{orb} is the mean orbital radius of Earth.

Therefore, an estimate of the magnitude of the amplitude of the annual term is

$$\Delta f \approx f_0 \frac{aR_{orb}}{c^2}. \tag{11}$$

For the case of Pioneer 10 at 40 AU we get

$$\Delta f \approx 14 \text{ mHz}, \tag{12}$$

and at 69 AU

$$\Delta f \approx 4.8 \text{ mHz}, \tag{13}$$

in good agreement with the observed values.

Using data from HORIZONS Web-Interface [14] a more complete analysis of the time variation of Δf has be performed. The residual (that is, simulated Doppler using Vibrating Rays Theory but interpreted under Special Relativity Theory) during 12 years time span is plotted in figure 2. Also the dumped sine best fit of the 50 days average measured by Turyshev et al [18] is plotted showing an excellent agreement between measurements and Vibrating Rays Theory prediction. The negative peaks (i.e., maximum anomalous acceleration) occur during conjunction when the Earth is further apart from the spacecraft, and positive peaks during opposition. Also, the amplitude is larger at the beginning of the plotted interval and decreases with time, as it was observed [4, 18].

5 Flyby anomaly

Like the Pioneer anomaly, the Earth flyby anomaly can be associated to a modeling problem, in the sense that relativistic Doppler includes terms that are absent in the measured signals. The empirical equation of the flyby anomaly is given by Anderson et al [4], which, notably, can be derived using Vibrating Rays Theory, as is done in Part 6 of [13].

Consider the case of NEAR tracked by 3 antennas located in USA, Spain, and Australia (a full description of the tracking system is found in a series of monographs of the Jet Propulsion Laboratory [19]). The receiving antenna was chosen as that having a minimum angle between the spacecraft and the local zenith.

Using available orbital data, a simulated Doppler signal has been calculated using Vibrating Rays Theory. Thus, the simulated residual is obtained by subtracting the theoretical Special Relativity Theory Doppler, from the Vibrating Rays Theory calculation. We observed, however, that the term that contains the velocity of the antennas, that is

$$d = \frac{\gamma_{u_3}}{\gamma_{u_1}} \frac{1 - \hat{\mathbf{r}}_{23} \cdot \mathbf{u}_3/c}{1 - \hat{\mathbf{r}}_{12} \cdot \mathbf{u}_1/c}, \tag{14}$$

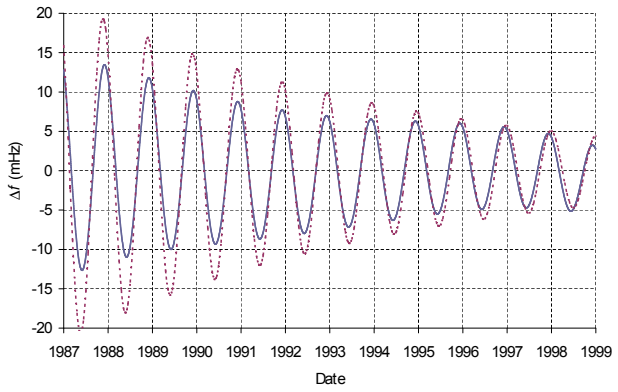

Fig. 2: Annual variation of the frequency difference between Vibrating Rays Theory and Special Relativity Theory (full line) and anomalous dumped sine best fit of the 50 days average measured by Turyshev et al [18] (dashed line), for Pioneer 10 from January 1987 to January 1999.

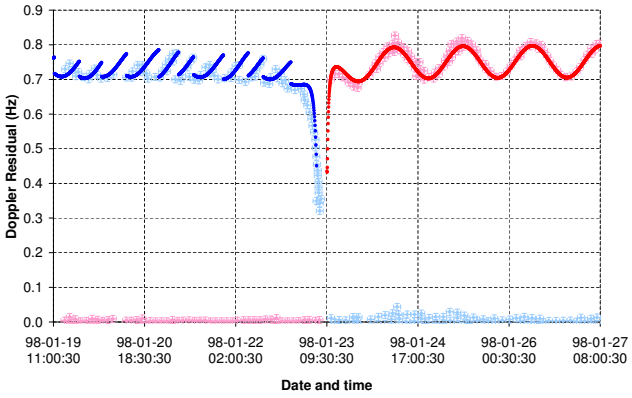

Fig. 3: Fitting the pre- (right half, in red) and post-encounter (left half, in blue) X-band Doppler data residual, for the NEAR flyby under an ideal hyperbolic orbit. Solid lines simulated according to Vibrating Rays Theory. Crosses, actual data extracted from reference [4].

is not enough to completely remove the first order (in u/c) Earth signature (**u** is the velocity of the antenna, 1 refers to the emission epoch and 3 to the reception epoch, as in [13] Part 4).

This is so because the velocity of the antennas is not uniform and the evaluation of the emission time is different for Vibrating Rays Theory and Special Relativity Theory. Then, a small first order term remains. Anyway, since orbital parameters are obtained by periodically fitting the measurements to theoretical orbits, thus a similar procedure is needed for Vibrating Rays Theory. Curiously, by doing so, the first order term is removed. The only difference between orbits adjusted by Special Relativity Theory and Vibrating Rays Theory is a slight rotation of the orbit plane, as mentioned above. Note that in the case of range disagreement (discussed above) two different orbital adjustment would be needed by the Deep Space Network and the Space Surveillance Network due to the different propagation speed. In consequence, it will be impossible to fit a simultaneous measurement, as it seems to happen with the range disagreement.

The final result shows that each antenna produces a sinusoidal residual with a phase shift at the moment of maximum approach. Therefore, if we fit the data with the pre-encounter sinusoid a post-encounter residual remains and vice versa.

In figure 3 are simultaneously plotted the result of fitting the residual by pre-encounter data (right half in red, corresponding to figure 2a of [4]) and by post-encounter data (left half in blue, corresponding to figure 2b of [4]).

Note that the simulated plots are remarkably similar to the reported ones, including the amplitude and phase (i.e., minima and maxima) of the corresponding antenna. The fitting of post-encounter data (blue) can be improved by appropriately setting the exact switching times of the antennas (which are unknown to the author). The flyby Doppler residual exhibits a clean signature of the Vibrating Rays Theory.

6 Conclusions

In this work I have presented observational evidence favoring a dependence of the speed of light on that of the source, in the manner implied in Faraday's ideas of "vibrating rays".

It is remarkable and very suggestive that, as derived from Faraday's thoughts, simply by relating the velocity of light and the corresponding Doppler effect with the velocity of the source at the time of detection, is enough to quantitatively and qualitatively explain a variety of spacecraft anomalies.

Also, it is worth mentioning that a formulation of electromagnetism compatible with Faraday's conception is possible, as shown in [13] Part 8, which is also compatible with the known electromagnetic phenomena. The most remarkable fact of this new formalism is the simultaneous presence of instantaneous (static terms) and delayed (radiative terms) interactions (i.e., local and nonlocal phenomena in the same interaction).

Finally, under Vibrating Rays Theory the manifestation of the movement of the source in the speed of light is more subtle than the naive $c + kv$ hypothesis (k is a constant, $0 \leq k \leq 1$) usually used to test their dependence [8]. Thus, it is also of fundamental importance the fact that, from the experimental point of view, it is very difficult to detect differences between Vibrating Rays Theory and Special Relativity Theory, as discussed in [13], which is also manifest in the smallness of the measured anomalies, and in the non clear manifestation of the effect in usual experiments and observations. For example, it produces a negligible effect on satellite positioning systems, see Part 7 of [13].

I am aware of how counterintuitive these conceptions are to the modern scientist, but also believe that, given the above evidence, a conscientious experimental research is needed to settle the question of the dependence of the speed of light on that of its source as predicted by Vibrating Rays Theory, and

that has been observed during the 1998 NEAR flyby. As a closure, I recall Fox's words regarding the possibility of conducting an experiment on the propagation of light relative to the motion of the source: "*Nevertheless if one balances the overwhelming odds against such an experiment yielding anything new against the overwhelming importance of the point to be tested, he may conclude that the experiment should be performed*" [20].

Acknowledgements

I am thankful to Fernando Minotti who read this paper and improved the manuscript significantly, although he may not agree with all of the interpretations provided in this paper.

Submitted on July 4, 2016 / Accepted on July 8, 2016

References

1. Antreasian P.G., Guinn J. R. Investigations into the unexpected Delta-V increases during the Earth gravity assists of Galileo and NEAR. AIAA Paper No. 98-4287 presented at the AIAA/AAS Astrodynamics Specialist Conference and Exhibit (Boston, August 10-12, 1998).
2. Guruprasad V. Observational evidence for travelling wave modes bearing distance proportional shifts. *E*PL, 2015, v. 110, 54001.
3. Anderson J.D., Laing P.A., Lau E.L., Liu A.S., Nieto M.M., Turyshev S.G. Indication, from Pioneer 10/11, Galileo, and Ulysses Data, of an Apparent Anomalous, Weak, Long-Range Acceleration. *Phys. Rev. Lett.*, 1998, v. 81, 2858–2861.
4. Anderson J.D., Campbell J.K., Ekelund J.E., Ellis J., Jordan J.F. Anomalous Orbital-Energy Changes Observed during Spacecraft Flybys of Earth. *Phys. Rev. Lett.*, 2008, v. 100, 091102.
5. Turyshev S.G., Toth V.T., Kinsella G., Lee S.-C., Lok S.M., Ellis J. Support for the Thermal Origin of the Pioneer Anomaly. *Phys. Rev. Lett*, 2012, v. 108, 241101.
6. de Sitter W. Ein astronomischer Beweis für die Konstanz der Lichgeshwindigkeit. *Z. Phys.*, 1913, v. 14, 429.
7. de Sitter W. Über die Genauigkeit, innerhalb welcher die Unabhängigkeit der Lichtgeschwindigkeit von der Bewegung der Quelle behauptet werden kann. *Z. Phys.*, 1913, v. 14, 1267.
8. Brecher K. Is the Speed of Light Independent of the Velocity of the Source? *Phys. Rev. Lett.*, 1977, v. 39, 1051.
9. Alväger T., Farley F.J.M., Kjellman J., Wallin I. Test of the second postulate of special relativity in the GeV region. *Phys. Lett.*, 1964, v. 12, 260–262.
10. Botermann B., Bing D., Geppert C., et al. Test of Time Dilation Using Stored Li+ Ions as Clocks at Relativistic Speed. *Phys. Rev. Lett.*, 2014, v. 113, 120405.
11. Schrödinger E. Die erfüllbarkeit der relativitätsforderung in der klassischen mechanik. *Ann. der Physik*, 1925, v. 77, 325–336.
12. Faraday M. Thoughts on ray-vibrations. *Phil. Mag. Series 3*, 1846, v. 28, 345.
13. Bilbao L., Bernal L., Minotti F. Vibrating Rays Theory. arXiv: 1407.5001.
14. http://ssd.jpl.nasa.gov
15. Markwardt C.B. Independent Confirmation of the Pioneer 10 Anomalous Acceleration. arXiv: gr-qc/0208046.
16. Anderson J.D., Laing P.A., Lau E.L., Liu A.S., Nieto M.M., Turyshev S.G. Study of the anomalous acceleration of Pioneer 10 and 11. *Phys. Rev. D*, 2002, v. 65, 082004.
17. Levy A., Christophe B., Reynaud S., Courty J-M., Brio P., Mtris G. Pioneer 10 data analysis: investigation on periodic anomalies. Journées scientifiques de la SF2A, Paris, France, 2008, 133–136 (hal-00417743).
18. Turyshev S.G., Anderson J.D., Laing P.A., Lau E.L., Liu A.S., Nieto M.M. The Apparent Anomalous, Weak, Long-Range Acceleration of Pioneer 10 and 11. arXiv: gr-qc/9903024.
19. DESCANSOTeam, Jet Propulsion Laboratory, California Institute of Technology. http://descanso.jpl.nasa.gov/Monograph/mono.cfm (accessed July 2014).
20. Fox J.G. Experimental Evidence for the Second Postulate of Special Relativity. *Am. J. Phys.*, 1962, v. 30, 297.

Editorial Comment

This paper plays an importance in the understanding of the physical observable velocity of light that differs from the world-invariant in the General Theory of Relativity.

Defining physical observable quantities in the General Theory of Relativity is not a trivial problem. This is because we are looking at objects in a four-dimensional space-time, and we have to determine which components of these four-dimensional tensor quantities are physically observable. A complete mathematical theory for calculating physically observable quantities in the four-dimensional space (space-time) of General Relativity was introduced in 1944 by Abraham Zelmanov, and is known as the *theory of chronometric invariants*[*]. Landau and Lifshitz in §84 of their *The Classical Theory of Fields* also introduced physically observable time and observable three-dimensional intervals similar to Zelmanov. But they limited themselves only to this particular case, while only Zelmanov arrived at the versatile mathematical theory. A compendium of Zelmanov's theory of physical observable quantities can also be found in the books[†].

In short, physically observable are the projections of four-dimensional quantities onto the time line and the three-dimensional spatial section of the observer, which can be non-uniform, deformed, curved and rotating. These projections are calculated through the special projecting operators which take all the aforementioned factors into account. In particular, the physical observable velocity of light differs from the world-invariant, and is depended on the gravitational potential and the rotation velocity of the observer's space. In ultimate physical conditions, as is shown in Chapter 5 of *Particles Here and Beyond the Mirror*[†], the observable velocity of light can even become zero, that is verified by the frozen light experiment (Lene Hau, 2001).

Even more. In a physical space (space-time metric) wherein is a shift at one of the spatial directions (that means a spatial anisotropy), the observable velocity of light is depended on the signal source's velocity at this preferred direction. We drafted such a space-time metric in the last decade.

Einstein's postulates have now only a historical meaning. Once Einstein moved his theory on the mathematical basis of Riemannian geometry, he found that all the postulates are the manifestations of geometry of Riemannian spaces. It is as well true about the world-invariant of the velocity of light. In a space, which is free of gravitation, is uniform, non-deformed, and non-rotating, the physical observable velocity of light coincides with the world-invariant. However in a real physical space it does not.

For this reason the experimental compendium and the analysis presented in Bilbao's paper will maybe give a new fresh stream in search for the further theoretical predictions of the General Theory of Relativity.

Dmitri Rabounski, Editor-in-Chief
Larissa Borissova, Assoc. Editor

[*]Zelmanov A. Chronometric invariants. American Research Press, Rehoboth (NM), 2006. Zelmanov A. Chronometric invariants and accompanying frames of reference in the General Theory of Relativity. *Soviet Physics Doklady*, 1956, v. 1, 227–230.

[†]Borissova L. and Rabounski D. Fields, Vacuum, and the Mirror Universe. 2nd ed., Svenska fysikarkivet, Stockholm, 2009. Rabounski D. and Borissova L. Particles Here and Beyond the Mirror. 3rd ed., American Research Press, Rehoboth (NM), 2012.

Vacuum Background Field in General Relativity

Patrick Marquet

18 avenue du Président Wilson, 62100 Calais, France
E-mail: patrick.marquet6@wanadoo.fr

We assume here a slightly varying cosmological term which readily induces a permanent background field filling the physical vacuum. A precise form of the variable cosmological term is introduced containing an infinitesimal Killing vector which accounts for the space-time variation of this term. As a result the term can be added to the Einstein Lagrangian without affecting the varied action δS. As a result, we showed in an earlier publications that the permanent background field filling the vaccum is excited in the vicinity of matter which precisely corresponds to its gravitational field classically described by a pseudo-tensor. With this preparation, the global energy-momentum tensor of matter and gravity field is no longer a pseudo-tensor and is formally conserved like the Einstein tensor. In the excited state, this antisymmetric tensor can be conveniently symmetrized by applying the Belinfante procedure which automatically self excludes far from matter since the background field tensor is naturally symmetric.

Introduction

The substance of this study is inspired by the following considerations. In the framework of the Theory of General Relativity (GR), the Einstein tensor exhibits a *conceptually* conserved property, while any corresponding stress-energy tensor does not, which leaves the theory with a major inconsistency. When pure matter is the source, a so-called "pseudo-tensor" describing its gravitational field is introduced so that the four-momentum of both matter and its gravity field is conserved [1]. Unfortunately in this approach, the gravitational field maybe transformed away at any point and by essence, its pseudo-tensor cannot appear in the Einstein's field equations, as it should be.

We will tackle the problem in another way : Restricting our study to neutral massive flow, we proceed as follows. We introduce a space-time variable term that supersedes the so-called cosmological term Λg_{ab} in the Einstein's field equations [2]. Under this latter assumption, we formally show that the gravity field of a massive source is no longer described by a vanishing *pseudo-tensor*, but it is represented by a *true* tensor which can explicitly appear with the bare matter tensor together with another specific field, on the right hand side of the Einstein's field equations. Inspection also shows that this *global* stress-energy tensor now complies with the intrinsic conservation property of the Einstein tensor as it should be. As a result, the physical vacuum is here filled with a *homogeneous vacuum background field* which is always present in the so-called Einstein's "source free" equations and whose tensor exhibits a conserved property. Our theory leads to admit that matter causes the surrounding background field to produce its gravitational field which decreases asymptotically to the level of this vacuum field. Naturally, since we will deal with energy-momentum canonical field tensors which are not symmetric, the total angular momentum of the isolated system is not conserved. In this case, it is always possible to apply the symmetrizing procedure to these tensors according to J. Belinfante [3]. In the absence of matter, the inferred Belinfante tensor reduces to the symmetric background field tensor as it should be.

Notations

Space-time Latin indices run from $a = b$: 0, 1, 2, 3, while spatial Greek indices run from $\alpha = \beta$: 1, 2, 3. The space-time signature is -2. In the present text, $\varkappa$ is Einstein's constant $4\pi G/c^4$, where G is Newton's gravitational constant.

1 The field equations in General Relativity

1.1 The problem of the conserved gravity tensor

The General Theory of Relativity requires a 4-dimensional pseudo-Riemannian manifold. A Riemannian manifold is characterized by the line element $ds^2 = g_{ab}\, dx^a dx^b$. It is well known that by varying the action $\mathcal{S} = \mathfrak{L}_E d^4x$ with respect to the metric tensor g_{ab} with the Lagrangian density given by

$$\mathfrak{L}_E = \sqrt{-g}\, g_{ab}\left[\left\{{e \atop ab}\right\}\left\{{d \atop de}\right\} - \left\{{d \atop ae}\right\}\left\{{e \atop bd}\right\}\right], \tag{1.1}$$

$$g = \det \| g_{ab} \|. \tag{1.2}$$

Also one infers the symmetric Einstein tensor

$$G_{ab} = R_{ab} - \frac{1}{2}\, g_{ab}\, R\,, \tag{1.3}$$

where

$$R_{bc} = \partial_a \left\{{a \atop bc}\right\} - \partial_c \left\{{a \atop ba}\right\} - \left\{{d \atop bc}\right\}\left\{{a \atop da}\right\} - \left\{{d \atop ba}\right\}\left\{{a \atop dc}\right\} \tag{1.4}$$

is the Ricci tensor with its contraction R, the curvature scalar (the $\left\{{e \atop ab}\right\}$ denote the Christoffel symbols of the second kind). The 10 source free field equations are

$$G_{ab} = 0\,. \tag{1.5}$$

The second rank Einstein tensor G_{ab} is symmetric and is only function of the metric tensor components g_{ab} and their first and second order derivatives. The relations

$$\nabla_a G^a_b = 0 \tag{1.6}$$

are the conservation identities provided that the tensor G_{ab} has the form [4]

$$G_{ab} = k\left[R_{ab} - \frac{1}{2}\, g_{ab}\,(R + 2\Lambda)\right], \tag{1.7}$$

where k is a constant, which is here assumed to be 1, while Λ is usually named the *cosmological constant*.

Einstein's field equations for a source free field are

$$G_{ab} = R_{ab} - \frac{1}{2}\, g_{ab}\, R - \Lambda g_{ab} = 0\,. \tag{1.8}$$

In the case where the field source is present, the field equations become

$$G_{ab} = R_{ab} - \frac{1}{2}\, g_{ab}\, R - \Lambda g_{ab} = \varkappa\, T_{ab}\,, \tag{1.8 bis}$$

where T_{ab} is the energy-momentum tensor of the source.

However, unlike the Einstein tensor G_{ab} which is *conceptually conserved*, the conditions

$$\nabla_a T^a_b = 0 \tag{1.9}$$

are never satisfied in a general coordinates system [5]. Therefore, the Einstein tensor G_{ab} which *intrinsically* obeys a conservation condition inferred from the Bianchi's identities, is generally related with a tensor T_{ab} which obviously *fails to satisfy the same requirement*.

Hence, we are faced here with a major inconsistency in GR which can be removed in the case of a neutral massive source upon a small constraint.

1.2 The tensor density representation

We first set

$$\mathfrak{g}^{ab} = \sqrt{-g}\, g^{ab} \tag{1.10}$$

thus the Einstein tensor density is

$$\mathfrak{G}^{ab} = \sqrt{-g}\, G^{ab}\,, \tag{1.10 bis}$$

$$\mathfrak{G}^c_a = \sqrt{-g}\, G^c_a\,, \tag{1.10 ter}$$

$$\mathfrak{R}^{ab} = \sqrt{-g}\, R^{ab}\,. \tag{1.11}$$

In the density notations, the field equations with a source (1.8) will read

$$\mathfrak{G}^{ab} = \mathfrak{R}^{ab} - \frac{1}{2}\, g^{ab}\, \mathfrak{R} - \sqrt{-g}\, g^{ab}\, \Lambda = \varkappa\, \mathfrak{T}^{ab}\,, \tag{1.12}$$

where $\mathfrak{T}^{ab} = \sqrt{-g}\, T^{ab}$.

2 The new approach on gravity

2.1 The canonical gravity pseudo-tensor

Let us consider the energy momentum tensor for neutral matter density ρ

$$T_{ab} = \rho\, c^2 u_a u_b \tag{2.1}$$

as the right hand side of the standard field equations

$$G_{ab} = R_{ab} - \frac{1}{2}\, g_{ab}\, R = \varkappa\, T_{ab}\,. \tag{2.2}$$

The conservation condition for this tensor are written

$$\nabla_a T^a_b = \sqrt{-g}\, \partial_a T^a_b - \frac{1}{2}\, T_{ac} \partial_b\, g_{ac} = 0 \tag{2.3}$$

with the tensor density

$$\mathfrak{T}^a_b = \sqrt{-g}\, T^a_b\,. \tag{2.4}$$

However, across a given hypersurface dS_b, the integral

$$P^a = \frac{1}{c} \int T^{ab} \sqrt{-g}\, dS_b \tag{2.5}$$

is conserved only if [6]

$$\partial_a\, \mathfrak{T}^a_b = 0\,. \tag{2.6}$$

This problem can be cured only if the metric admits a Killing vector field [7]. If this is not so, we write (2.3) for the *bare* matter tensor density

$$\partial_a (\mathfrak{T}^a_b)_{\text{matter}} = \frac{1}{2}\, (\mathfrak{T}^{cd})_{\text{matter}}\, \partial_b\, g_{cd}\,. \tag{2.7}$$

Inspection then shows that

$$R_{il}\, d\mathfrak{g}^{il} = \sqrt{-g}\left[-R^{ie} + \frac{1}{2}\, g^{ie} R\right] dg_{ie} = \\ = -\varkappa\, (\mathfrak{T}^{ie})_{\text{matter}}\, dg_{ie}\,. \tag{2.8}$$

Taking now into account the Lagrangian formulation for R_{il} which is

$$R_{il} = \frac{d\mathfrak{Q}_E}{\mathfrak{g}^{il}} = \partial_k \left[\frac{\partial \mathfrak{Q}_E}{\partial(\partial_k\, \mathfrak{g}^{il})}\right] - \frac{d\mathfrak{Q}_E}{\partial\, \mathfrak{g}^{il}}\,, \tag{2.9}$$

we obtain

$$-\varkappa\, (\mathfrak{T}^{il})_{\text{matter}}\, dg_{il} = \left\{\partial_k \left[\frac{\partial \mathfrak{Q}_E}{\partial\, (\partial_k\, \mathfrak{g}^{il})}\right] - \frac{\partial \mathfrak{Q}_E}{\partial \mathfrak{g}^{il}}\right\} d\mathfrak{g}^{il} = \\ = \partial_k \left[\frac{\partial \mathfrak{Q}_E\, d\mathfrak{g}^{il}}{\partial\, (\partial_k\, \mathfrak{g}^{il})}\right] - d\mathfrak{Q}_E$$

or

$$-\varkappa\, (\mathfrak{T}^{il})_{\text{matter}}\, \partial_m\, g_{il} = \partial_k \left[\frac{\partial \mathfrak{Q}_E\, \partial_m(\partial \mathfrak{g}^{il})}{\partial(\partial_k\, \mathfrak{g}^{il})} - \delta^k_m\, \mathfrak{Q}_E\right] = \\ = 2\varkappa\, \partial_k (\mathfrak{t}^k_m)_{\text{field}}\,, \tag{2.10}$$

where $(\mathfrak{t}^k_m)_{\text{field}}$ denotes the field tensor density extracted from

$$2\varkappa\,(\mathfrak{t}^k_m)_{\text{field}} = \frac{\partial \mathfrak{Q}_E\,\partial_m(\partial \mathfrak{g}^{il})}{\partial(\partial_k\,\mathfrak{g}^{il})} - \delta^k_m\,\mathfrak{Q}_E \tag{2.11}$$

so that we have the explicit canonical form

$$(\mathfrak{t}^k_m)_{\text{field}} = \frac{1}{2\varkappa}\left\{\frac{\partial \mathfrak{Q}_E\,\partial_m(\partial \mathfrak{g}^{il})}{\partial(\partial_k\,\mathfrak{g}^{il})} - \delta^k_m\,\mathfrak{Q}_E\right\} \tag{2.12}$$

where

$$\partial_k(\mathfrak{T}^k_i)_{\text{matter}} = \frac{1}{2}\,(\mathfrak{T}^{ek})_{\text{matter}}\,\partial_k\,g_{ei} = -\partial_k(\mathfrak{t}^k_i)_{\text{field}}$$

that is, the required conservation relation is

$$\partial_k\left[(\mathfrak{T}^k_i)_{\text{matter}} + (\mathfrak{t}^k_i)_{\text{field}}\right] = 0\,. \tag{2.13}$$

Looking back of the deduction, (2.12) defines the *canonical gravity pseudo-tensor density of matter*

$$(\mathfrak{t}^k_m)_{\text{pseudogravity}} = \frac{1}{2\varkappa}\left\{\frac{\partial \mathfrak{Q}_E\,\partial_m(\partial \mathfrak{g}^{il})}{\partial(\partial_k\,\mathfrak{g}^{il})} - \delta^k_m\,\mathfrak{Q}_E\right\}. \tag{2.14}$$

Expressed with the explicit form of the Lagrangian density $\mathfrak{Q}_E$ (1.1), (2.14) can be written in the form

$$(\mathfrak{t}^k_m)_{\text{pseudogravity}} = \\ = \frac{1}{2\varkappa}\left(\left\{{k \atop il}\right\}\partial_m\,\mathfrak{g}^{il} - \left\{{i \atop il}\right\}\partial_m\,\mathfrak{g}^{lk} - \delta^k_m\,\mathfrak{Q}_E\right). \tag{2.15}$$

This is the *mixed Einstein-Dirac pseudo-tensor density* [8] which is not symmetric on k and m, and therefore is not suitable for basing a definition of angular momentum on.

Thus, our aim is to look for:

- A *true* tensor;
- A *symmetric* tensor.

2.2 The new canonical tensor

In the density notations, the field equations with a massive source (1.8 bis) can be re-written as

$$\mathfrak{G}^{ab} = \mathfrak{R}^{ab} - \frac{1}{2}\,\mathfrak{g}^{ab}\,\mathfrak{R} - \mathfrak{g}^{ab}\,\zeta = \varkappa\,(\mathfrak{T}^{ab})_{\text{matter}}\,, \tag{2.16}$$

where in place of the constant cosmological term $\Lambda\sqrt{-g}$, we have introduced a *scalar density* denoted as

$$\zeta = \Xi\sqrt{-g}\,. \tag{2.17}$$

Unlike Λ, the scalar Ξ is slightly space-time variable and can be regarded as a Lagrangian characterizing a *specific vacuum background field*.

We will choose the variation of Ξ as follows

$$\Xi = \nabla_a\,\kappa^a, \tag{2.17 bis}$$

where κ^a is a Killing vector. Hence

$$\zeta = \sqrt{-g}\,\nabla_a\,\kappa^a. \tag{2.17 ter}$$

We will first write the field equations with a massive source together with its gravity tensor density

$$\mathfrak{G}^{ab} = \mathfrak{R}^{ab} - \frac{1}{2}\,g^{ab}\,\mathfrak{R} = \varkappa\left[(\mathfrak{T}^{ab})_{\text{matter}} + (\mathfrak{t}^{ab})_{\text{gravity}}\right] \tag{2.18}$$

where $(\mathfrak{t}^{ab})_{\text{gravity}}$ is related to ζ as

$$\mathfrak{G}^{ab} = \mathfrak{R}^{ab} - \frac{1}{2}\,g^{ab}\,\mathfrak{R} = \varkappa\left[(\mathfrak{T}^{ab})_{\text{matter}} + \frac{g^{ab}\zeta}{2\varkappa}\right]. \tag{2.19}$$

Re-instating the term ζ accordingly, the gravitational field tensor density now reads

$$(\mathfrak{t}^k_m)_{\text{gravity}} = \frac{1}{2\varkappa}\left\{\frac{\partial \mathfrak{Q}_E\,\partial_m(\partial \mathfrak{g}^{il})}{\partial(\partial_k\,\mathfrak{g}^{il})} - \delta^k_m\,(\mathfrak{Q}_E - \zeta)\right\}. \tag{2.20}$$

A first inspection shows that ζ represents the Lagrangian density of the background field, therefore the modified field equations (2.19) should be derived from an Einstein Lagrangian density different from $\mathfrak{Q}_E$ (1.1) and which includes ζ.

By choosing the form (2.17 ter), we check that

$$\zeta = \sqrt{-g}\,\nabla_a\,\kappa^a = \partial_a\left(\sqrt{-g}\,\kappa^a\right).$$

Now, if we write the new action as

$$\mathcal{S}_M = \int \mathfrak{Q}_M\,d^4x = \int \mathfrak{Q}_E\,d^4x + \int \partial_a\left(\sqrt{-g}\,\kappa^a\right)d^4x$$

due to Gauss' theorem we see that the last integral can be transformed in an integral extended to an hyperfurface which does not contribute in the variation of $\mathcal{S}_M$ and

$$\delta\int \mathfrak{Q}_M\,d^4x = \delta\int \mathfrak{Q}_E\,d^4x\,.$$

Therefore, it is legitimate to maintain $(\mathfrak{t}^k_m)_{\text{gravity}}$ as per (2.20).

The presence of the scalar density ζ characterizing the background field is here of central importance, as it means that $(\mathfrak{t}^k_m)_{\text{gravity}}$ can never be zero in contrast to the classical theory where the gravitational field is only described by an awkward *pseudo-tensor*.

The quantity $(\mathfrak{t}^k_m)_{\text{gravity}}$ constitutes thus a *true* tensor density describing the gravity field attached to the neighbouring matter.

It is then easy to show that we have the conserved quantity

$$\partial_a\left[(\mathfrak{T}^b_a)_{\text{matter}} + (\mathfrak{t}^b_a)_{\text{gravity}}\right] = 0\,. \tag{2.21}$$

In this picture and examining (2.20), we clearly see that the gravitational field of matter appears as an *excited state* of the homogeneous background energy field which permanently fills the physical vacuum.

Far from its matter source, the field sharply decreases down to the level of the background field described by the tensor density $(\mathfrak{t}^{ab})_{\text{background field}}$. Therefore the "source free" field equations should always retain a non-zero right hand side according to

$$\mathfrak{G}^{ab} = \mathfrak{R}^{ab} - \frac{1}{2}\, g^{ab}\, \mathfrak{R} = \varkappa\, (\mathfrak{t}^{ab})_{\text{background field}} \qquad (2.22)$$

which are the equivalent of (1.8)

$$\mathfrak{G}^{ab} = \mathfrak{R}^{ab} - \frac{1}{2}\, g^{ab}\, \mathfrak{R} = \varkappa\, \frac{g^{ab}\,\zeta}{2\varkappa}\,. \qquad (2.23)$$

In this case, the conservation law applied to the right hand side of the tensor density field equations is straightforward

$$\partial_a(\mathfrak{t}^b_a)_{\text{background field}} = \partial_a\left(\frac{\zeta}{2\varkappa}\,\delta^b_a\right) = 0\,. \qquad (2.24)$$

2.3 Symmetrization of the gravity tensor

Let us consider the new gravity tensor expressed with the explicit form of the Lagrangian density $\mathfrak{L}_E$ (1.1):

$$(\mathfrak{t}^k_m)_{\text{gravity}} = \\ = \frac{1}{2\varkappa}\left[\left\{{k \atop il}\right\}\partial_m\mathfrak{g}^{il} - \left\{{i \atop il}\right\}\partial_m\mathfrak{g}^{lk} - \delta^k_m\,(\mathfrak{L}_E - \zeta)\right]. \qquad (2.25)$$

Like we mentioned, this tensor includes the Einstein-Dirac pseudo-tensor which is not symmetric. We can however follow the *Belinfante procedure* used to symmetrize the canonical tensor $(\Theta^k_m)_{\text{gravity}}$ that extracted from $(\mathfrak{t}^k_m)_{\text{gravity}} = \sqrt{-g}\,(\Theta^k_m)_{\text{gravity}}$.

The *total angular momentum* is known to be the sum

$$M^{cba} = x^b(\Theta^{ca})_{\text{gravity}} - x^a(\Theta^{cb})_{\text{gravity}} + S^{cab}, \qquad (2.26)$$

where S^{cab} is the contribution of the *intrinsic angular momentum*. By definition,

$$S^{cab} = -S^{cba}.$$

Local conservation of the total angular momentum, i.e. $\nabla_c M^{cab} = 0$, requires that

$$\nabla_c S^{cab} = (\Theta^{ab})_{\text{gravity}} - (\Theta^{ba})_{\text{gravity}}\,. \qquad (2.27)$$

We now add a tensor Υ^{bca} which is antisymmetric with respect to the first two indices b, c:

$$(\mathfrak{t}^{ca})_{\text{gravity}} = (\Theta^{ca})_{\text{gravity}} + \nabla_b\,\Upsilon^{bca}, \qquad (2.28)$$

where

$$\Upsilon^{cba} = \frac{1}{2}\left(S^{cba} + S^{bab} - S^{acb}\right). \qquad (2.29)$$

The $(\mathfrak{t}^{ab})_{\text{gravity}}$ should be identified to the *Belinfante-Rosenfeld tensor* [9] which is found to be symmetric.

In addition, the antisymmetry of Υ^{cba} guarantees that the conservation law remains unchanged

$$\nabla_a(\Theta^a_b)_{\text{gravity}} = \nabla_a(\mathfrak{t}^a_b)_{\text{gravity}} = 0\,. \qquad (2.30)$$

Staying far distant from matter (unexcited state), we have

$$(\Theta^{ab})_{\text{gravity}} \longrightarrow (\mathfrak{t}^{ab})_{\text{background field}}\,, \qquad \Upsilon^{cba} = 0\,.$$

By essence, $(\mathfrak{t}^{ab})_{\text{background field}}$ is thus symmetric.

Conclusions and outlook

Like we mentioned in an earlier publication, from the beginning of General Relativity, the cosmological constant Λ has played an unsavory rôle Einstein included this constant in his theory, because he wanted to have a cosmological model of the Universe which he wrongly thought static. Shortly after the works published by De Sitter and Lemaître, he decided to reject it.

But to-day, despite its smallness, a term like Λ seems to be badly needed to explain some astronomical observations, all related with the basic dynamical expanding model (Robertson-Walker et al.), even though its occurrence was never clearly explained.

In the classical General Relativity, the space-time is either filled with ponderomotive energy or devoid of source, which is accepted as a physical vacuum. However, numerous experiments predict that quantum vacuum is not "empty" but permanently subjected to virtual particles exchanges of energy.

Heisenberg's Uncertainty Principle, which allows for this process to take a place, has not been used in our demonstration, but it certainly plays a role in the variable property of the cosmological background field which our study relied on.

To sum up all that above, we have eventually reached the following important results:

- The gravitational energy can be represented by a true tensor;
- Its nonlocalizability doesnot hold anymore;
- The existence of a vacuum field is inferred from GR, which confirms the quantum predictions.

This last conclusion is noteworthy since our theory shows that General Relativity and Quantum Physics have convergent results.

Submitted on July 8, 2016 / Accepted on July 14, 2016

References

1. Landau L. and Lifshitz E. The Classical Theory of Fields. Addison-Wesley, Reading (Massachusetts), 1962, p. 402 (French translation).
2. Marquet P. The gravitational field: A new approach. *Progress in Physics*, 2013, v. 9, issue 3, 62–66.
3. Belinfante J. *Physica*, 1939, v. 6, 887.
4. Cartan E. La Géométrie des Espaces de Riemann. Re-print de 1925, Gauthier-Villars, Paris, 1946.

5. Straumann N. General Relativity and Relativistic Astrophysics. Springer-Verlag, Berlin, 1984, p. 159.
6. Tonnelat M.A. Les Théories Unitaires de l'Electromagnétisme et de la Gravitation. Gauthier-Villars, Paris, 1959, p. 18.
7. Hawking S.W., Ellis G.F.R. (1987). The Large Scale Structure of Space time. Cambridge University Press, 1987, p. 62.
8. Dirac P.A.M. General Theory of Relativity. Princeton University Press, 2nd edition, 1975, p. 61.
9. Rosenfeld L. Sur le tenseur d'Impulsion-Energie. Palais des Académies Roy. de Belgique, Serie: "Mémoires de Classes de Sciences", tome 18, Bruxelles, 1940.

On the Physical Nature of the de Broglie Wave

Patrick Marquet

18 avenue du Président Wilson, 62100 Calais, France
E-mail: patrick.marquet6@wanadoo.fr

Here is revisited de Broglie's Wave Mechanics Theory of Double Solution wherein a particle endowed with a variable proper mass is required to propagate within a hidden medium in order to describe a physical scalar wave carrying its own associated mass. Since the experiment that detected the wave applied to electrons, we extend the de Broglie's theory to the Dirac spinor, so that we can outline the physical reality of this fermion field.

Introduction

Some hundred years ago, was established the famous relation $E = h\nu$ later verified for the photon. On this basis, in 1924, Louis de Broglie extended the wave dualism to all massive particles. The predicted original wave function associated with a given particle was soon detected in 1927 by Davisson and Germer in their famous experience on electrons diffraction by a nickel crystal lattice [1]. The wave producing physical effects, was an overwhelming evidence of its true existence.

Nevertheless, since the *Brussels Solvay Symposium* was held in 1927, official physics interpretation prevailed which considered quantum mechanics on the pure statistical grounds and then leading to accept the notion of *non-real* wave functions.

Although it is unquestionable that use of a probabilistic wave and its generalization did lead to accurate prediction and fruitful theories, de Broglie could never believe that observable physical phenomena follow from abstract mathematical wave functions. In his opinion, the wave function had to remain an objective physical entity which is intimately related with its mass, rather than the subjective probabilistic representation currently adopted in modern quantum physics. Since the real wave was detected by means of electrons scattering, we will here formally show that there is a strict identity between its phase and the one of its associated wave which therefore physically carries the particle. To make this identity possible, the electron proper mass must be variable according to the Planck-Laue relation [2]. Within this frame, de Broglie's theory inferred a so-called "guidance formulae" which forces the electron to be always in motion. However, because of the stationary property of energy levels inside an atom, a static electron is not compatible with its dynamic guided state. de Broglie then postulated the existence of a *hidden medium* which permanently exchanges energy and momentum with the electron causing it to oscillate and then avoiding a motionless location.

When I first met Louis de Broglie in summer 1966, this issue was debated with a great deal of speculation. Today, another explanation can be pushed forward.

Notations

Space-time Latin indices run from $a = b$: 0, 1, 2, 3, while spatial Greek indices run from $\alpha = \beta$: 1, 2, 3. The space-time signature is -2.

1 Spinor field-electron duality

1.1 The origins of the Double Solution Theory

1.1.1 Basics of the wave mechanics

From standard optics, we first recall the definition of the classical wave with a frequency v

$$\psi = a(n)\exp\left[i(\nu t - \boldsymbol{k}\cdot\boldsymbol{r})\right] \tag{1.1}$$

which propagates along the direction of the unit vector $\boldsymbol{n}$. (Here $\boldsymbol{k}$ is the 3-wave vector, $\boldsymbol{k}\cdot\boldsymbol{r} = \phi$ is the wave spatial phase, n is the refractive index of the medium.)

Formula (1.1) is a solution of the classical propagation equation

$$\Delta\psi = \frac{1}{w^2}\frac{\partial^2\psi}{c^2\partial t^2}\,, \tag{1.2}$$

where w is the wave phase velocity of the wave moving in a dispersive medium whose refractive index is $n(\nu)$ generally depending on the coordinates, and which is defined by

$$\frac{1}{w} = \frac{n(\nu)}{c}\,. \tag{1.3}$$

This medium is assumed to be homogeneous and only depends on the frequency ν. The (constant) phase ϕ of the wave is progressing along the given direction with a separation given by a distance $\lambda = w/\nu$, called wavelength.

Consider now the superposition of a group of stationary (monochromatic) waves having each a very close frequency along the x-axis

$$\psi = \int_{\nu_0-\Delta\nu}^{\nu_0+\Delta\nu} a(n)\exp\left[i(\nu t - \phi(\nu))\right]. \tag{1.4}$$

Such a group of waves moves with a constant velocity called group velocity v_g according to the Rayleigh's formula

$$\frac{1}{v_g} = \frac{d(\nu/v)}{d\nu} = \frac{1}{\nu_0}\frac{\partial n\nu}{\partial\nu}\,. \tag{1.5}$$

The wave mechanics eventually shows that the group velocity v_g of waves associated with a particle of rest mass m_0, coincides with the velocity of this particle whose momentum along the x-axis (in vacuum) is given by the famous de Broglie's relation [3]

$$p_x = m_0 v_x = \frac{h}{\lambda}\,. \tag{1.6}$$

We clearly note that there is an obvious *first* physical link between the particle and its associated wave which will be further substantiated.

1.1.2 Double nature of the wave function

Like we mentioned above, de Broglie was firmly convinced that the wave associated with a massive particle should be a *real observable quantity*, therefore, he introduced a *true plane wave* of the usual form

$$\psi = a(x^\alpha) \exp\left[\frac{i}{h}\,\phi(x^\alpha)\right], \tag{1.7}$$

which is connected to a probabilistic Ω-wave by the relation

$$\Omega = f\,\psi\,, \tag{1.8}$$

where f is a constant normalizing factor.

The original wave mechanics is thus complemented with the Double Solution Theory [4], for Ω and ψ are two solutions of the same propagation equation. The Ω-wave (normed in the usual quantum machanical formalism), has the nature of a *subjective* probability representation formulated by means of the objective ψ-wave.

Defining ψ^* as the complex conjugate of ψ, it is well known that $\psi^2 dV = \psi\,\psi^* dV$ gives the absolute value of finding the particle in the volume element dV so that the normalization condition is adapted with f as

$$\int_V \Omega\,\Omega^* dV = 1\,. \tag{1.8 bis}$$

This guarantees that the particle is present in the arbitrary volume V.

The Ω and ψ have the same phase ϕ, but the constant f ought to be much larger than 1. Indeed, the current theory which only uses the Ω-function assumes this quantity to be spread out over the whole wave, i.e. spread out over a related physical quantity b (e.g. energy of the particle) according to

$$\int_V \Omega\,\Omega^* dV = b\,. \tag{1.8 ter}$$

In the double solution theory however, b should be concentrated in a very small region occupied by the particle and the integral of $a^2 b\,dV$ taken over the ψ-wave in the volume V is much smaller than b, which eventually leads to $|b| \gg 1$.

2 Extension to the spinor

2.1 The real spinor wave

2.1.1 The Dirac operators and Dirac equation (reminder)

In order to write the Schrödinger equation under a relativistic form, P. A. M. Dirac has defined a specific four-components wave function Ψ^A called *spinor* [5] which must necessarily apply to any spin-1/2 particles thus in our case, the electron. (Capital Latin spinorial indices are: $A = B = 1, 2, 3, 4$.)

To this effect, he introduced a system of (4×4) non local trace free matrices $\gamma_a = (\gamma_a{}^A{}_B)$. (In the classical theory, it is customary to omit the spinorial indices.)

The matrices γ a can display the standard following components [6]:

$$\gamma_0 = \begin{pmatrix} 0 & 0 & 0 & -1 \\ 0 & 0 & -1 & 0 \\ 0 & 1 & 0 & 0 \\ 1 & 0 & 0 & 0 \end{pmatrix}, \quad \gamma_1 = \begin{pmatrix} 0 & 0 & 0 & -1 \\ 0 & 0 & 1 & 0 \\ 0 & 1 & 0 & 0 \\ -1 & 0 & 0 & 0 \end{pmatrix},$$
$$\gamma_2 = \begin{pmatrix} 1 & 0 & 0 & 0 \\ 0 & 1 & 0 & 0 \\ 0 & 0 & -1 & 0 \\ 0 & 0 & 0 & -1 \end{pmatrix}, \quad \gamma_3 = \begin{pmatrix} 0 & 0 & -1 & 0 \\ 0 & 0 & 0 & -1 \\ -1 & 0 & 0 & 0 \\ 0 & -1 & 0 & 0 \end{pmatrix} \tag{2.1}$$

in order to satisfy the fundamental relation

$$\gamma_a \gamma_b + \gamma_b \gamma_a = -2\,\eta_{ab}\,\mathbf{I}\,, \tag{2.2}$$

where η_{ab} is the Minkowskian tensor, and $\mathbf{I}$ is the unit matrix.

Formula $W = \gamma^a \partial_a$ is known as the Dirac operator where the Planck constant h is absorbed in the ∂_a.

For a free massive spin 1/2-field, the Dirac equation is eventually written as

$$(W - m_0 c)\,\Psi = 0\,, \tag{2.3}$$

where the proper mass m_0 is attributed to the associated spin 1/2-electron.

2.1.2 The normed spinor density

Since we are here considering a spin 1/2-fermion particle we must look for a wave which is a *real* spinor Ψ that physically carries the electron. From the classical Dirac theory, it is well known that the probability density of the electron's presence. is the time component of the (real) Dirac current vector density [7]

$$(J^a)_{\mathrm{D}} = i\,(^\sharp\Psi \gamma^a \Psi)\,, \tag{2.4}$$

where $^\sharp\Psi$ is the Dirac adjoint spinor $\Psi^+\gamma^0$, and Ψ^+ is the (complex) conjugate transpose of Ψ. So, this density of the electron reads

$$(J^0)_{\mathrm{D}} = i\,(^\sharp\Psi \gamma^0 \Psi) \tag{2.4 bis}$$

which is easily shown to be always definite and positive. Without the loss of generality, we could express Ψ under the form of a plane wave spinor [8] as

$$\Psi = \varpi(x^a) \exp\left[\frac{i}{h}\,\phi(x^a)\right],$$

where the wave spinor amplitude ϖ and the phase ϕ are *real local* functions. The Dirac spinor amplitudes ϖ could then be tuned so as to possess the orthogonality and completeness properties that guarantee that the plane waves Ψ have the adequate *normalization* to delta functions [9]. However, only a single spinor Ψ can be considered as a physical wave function, whereas we are left with 4-components Ψ^A. Then, at first glance, one might be tempted to consider the simple combination

$$\mathbf{\Psi} = \Psi^1 + \Psi^2 + \Psi^3 + \Psi^4.$$

Unfortunately, the Ψ-components are defined with respect to a spinorial frame $S(V_4)$ distinct from the structural Minkowski space, which renders those physically irrelevant. Instead, we will follow another extremely simple way: since ρ is here a real value, we have always the freedom to define a scalar wave function Φ such that

$$\Phi\,\Phi^* = \rho\,. \tag{2.5}$$

Moreover, we assume that this wave function has the same form as ψ (1.7)

$$\Phi = \omega(x^a)\exp\left[\frac{i}{h}\,\phi(x^a)\right]. \tag{2.6}$$

We state that Φ is the true wave function of the electron which was actually detected in the Davisson and Germer experiment upon a given set of gamma matrices γ^a, simply because it is derived from a real quantity which is itself inferred from the 1/2-spinor definition (2.4 bis) as it should.

Thus, we apply the same hypothesis conjectured by de Broglie (1.8 bis), and we are now able to write the normed expression as

$$\int_V \Xi\,\Xi^*\,dV = 1\,, \tag{2.7}$$

where

$$\Xi = g\,\Phi \tag{2.7 bis}$$

is the subjective wave function and g is a normalizing factor which satisfies (2.7).

In all the following text, Φ will be denoted as the "spinor wave".

2.1.3 Internal frequency of the electron

From (2.6), the energy and momentum of the electron located at x^a are

$$E = \partial_t\phi\,, \tag{2.8}$$

$$\boldsymbol{P} = P_a = -\mathrm{grad}\,\phi\,. \tag{2.9}$$

In order to outline the physical nature of the Φ-spinor wave, we start from the following consideration: in the framework of the Special Theory of Relativity, the frequency of a plane monochromatic wave is transformed as

$$\nu = \frac{\nu_0}{\sqrt{1-\mathbf{v}^2/c^2}}\,, \qquad \mathbf{v} = \mathrm{v}_a\,, \tag{2.10}$$

whereas the clock's frequency ν_c is transformed according to

$$\nu_c = \nu_0\sqrt{1-\mathbf{v}^2/c^2}\,. \tag{2.11}$$

If an electron is assumed to contain a rest energy $m_0c^2 = h\nu_0$, it is likened to a small clock of frequency ν_0, so that when moving with velocity $\mathbf{v}$, its frequency ν_c differs from that of the wave which is here noted ν.

In this concept, our main task will consist of showing that the electron is permanently in phase with its associated spinor wave, thus justifying the true nature of Φ that *physically* carries the electron

2.2 The physical nature of the spinor-electron duality

2.2.1 The Planck-Laue relation

We now postulate that the electron possesses a variable proper mass m_0' from which an important useful equation will be inferred.

Let us first write the Lagrange function for an observer who sees the electron of variable proper mass m_0' moving at the 3-velocity $\mathbf{v}$

$$L = -m_0'c^2\sqrt{1-\mathbf{v}^2/c^2} \tag{2.12}$$

so that the least action principle applied to this Lagrangian be still expressed by

$$\delta\int_{t_0}^{t_1} L dt = \delta\int_{t_0}^{t_1}\left(-m_0'c^2\sqrt{1-\mathbf{v}^2/c^2}\right)dt = 0\,. \tag{2.13}$$

From this principle are inferred the equations of motion

$$\frac{d}{dt}\frac{\partial L}{\partial\dot{x}_a} = \frac{\partial L}{\partial x_a} \tag{2.14}$$

with $\dot{x}_a = dx_a/dt$. It leads to

$$\frac{d\boldsymbol{P}'}{dt} = -c^2\sqrt{1-\mathbf{v}^2/c^2}\ \ \mathrm{grad}\,m_0' \tag{2.15}$$

(since m_0' is now variable).

Hence, by differentiating the well know relativistic relation

$$\frac{E'^2}{c^2} = \boldsymbol{P}'^2 + m_0'^2c^2 \tag{2.16}$$

we obtain

$$\frac{dE'}{dt} = c^2\sqrt{1-\mathbf{v}^2/c^2}\,\frac{\partial m_0'}{\partial t}\,. \tag{2.17}$$

Combining (2.15) and (2.17) readily gives

$$\frac{dE'}{dt} - \frac{\mathbf{v}\,d\boldsymbol{P}'}{dt} = c^2\sqrt{1-\mathbf{v}^2/c^2}\,\frac{dm_0'}{dt} \tag{2.18}$$

where

$$\frac{dm_0'}{dt} = \frac{\partial m_0'}{\partial t} + \mathrm{grad}\,m_0'$$

is the variation of the mass in the course of its motion.

On the other hand, we have

$$\frac{d\,(\boldsymbol{P}'\cdot\mathbf{v})}{dt} = \frac{\mathbf{v}\,d\boldsymbol{P}'}{dt} + \frac{m'_0c^2}{\sqrt{1-\mathbf{v}^2/c^2}}\,\frac{\mathbf{v}}{c}\,\frac{d\frac{\mathbf{v}}{c}}{dt} = \\ = \frac{\mathbf{v}\,d\boldsymbol{P}'}{dt} - m'_0c^2\,\frac{d}{dt}\,\sqrt{1-\mathbf{v}^2/c^2} \qquad (2.19)$$

or

$$\frac{d}{dt}\left(m'_0\sqrt{1-\mathbf{v}^2/c^2}\right) = \\ = c^2\,\sqrt{1-\mathbf{v}^2/c^2}\;\frac{dm'_0}{dt} + m'_0c^2\,\frac{d}{dt}\,\sqrt{1-\mathbf{v}^2/c^2}\,.$$

Hence, (2.18) can be written as

$$\frac{d}{dt}\left(E' - \mathbf{v}\cdot\boldsymbol{P}' - m'_0c^2\,\sqrt{1-\mathbf{v}^2/c^2}\right) = 0 \qquad (2.20)$$

which is satisfied when the electron is at rest (that is $\mathbf{v} = 0$, $E'_0 = m'_0c^2$).

Therefore, we must have always

$$E' = \frac{m'_0c^2}{\sqrt{1-\mathbf{v}^2/c^2}} = m'_0c^2\,\sqrt{1-\mathbf{v}^2/c^2} \;+\; \frac{m'_0\,\mathbf{v}^2}{\sqrt{1-\mathbf{v}^2/c^2}}\,. \qquad (2.21)$$

This is known as the Planck-Laue formula which plays a central rôle in our present theory.

2.2.2 Phase identity of the electron and its spinor wave

Let us first recall the relativistic form of the Doppler formula

$$\nu_0 = \nu\,\frac{1-\mathbf{v}/w}{\sqrt{1-\mathbf{v}^2/c^2}}\,, \qquad (2.22)$$

where ν_0 is the wave's frequency in the frame attached to the electron, ν and w are respectively the frequency and phase velocity of the spinor wave in a reference frame where this electron has a velocity $\mathbf{v}$.

With this formula, and taking the classical Planck relation $E = h\nu$ into account, we find

$$E = E_0\,\frac{1-\mathbf{v}^2/c^2}{1-\mathbf{v}/w}\,. \qquad (2.23)$$

However, inspection shows that the usual equation

$$E = \frac{E_0}{\sqrt{1-\mathbf{v}^2/c^2}} \qquad (2.24)$$

holds only if

$$1-\mathbf{v}/w = 1-\mathbf{v}^2/c^2 \qquad (2.25)$$

that implies

$$w\mathbf{v} = c^2. \qquad (2.26)$$

This latter relation is satisfied provided we set up

$$E' = \frac{m'_0c^2}{\sqrt{1-\mathbf{v}^2/c^2}}\,, \qquad (2.27)$$

$$\boldsymbol{P}' = \frac{m'_0\mathbf{v}}{\sqrt{1-\mathbf{v}^2/c^2}}\,. \qquad (2.28)$$

A variable proper mass is then required to insure that the electron as it moves, remains constantly in phase with that of the associated spinor wave. To see this, let us first multiply the Planck-Laue equation by dt

$$\left(\frac{m'_0c^2}{\sqrt{1-\mathbf{v}^2/c^2}} - \frac{m'_0\,\mathbf{v}^2}{\sqrt{1-\mathbf{v}^2/c^2}}\right)dt = m'_0c^2\,\sqrt{1-\mathbf{v}^2/c^2}\;dt. \qquad (2.29)$$

If $\boldsymbol{n}$ is the unit vector normal to the phase surface, we then consider that the electron whose internal frequency is $\nu_0 = m'_0c^2/h$ has travelled a distance $d\boldsymbol{n}$ during a time interval dt, so that its internal phase ϕ_i has been changed by

$$d\phi_i = h\nu_0\,\sqrt{1-\mathbf{v}^2/c^2}\;dt = m'_0c^2\,\sqrt{1-\mathbf{v}^2/c^2}\;dt\,. \qquad (2.30)$$

At the same time, the corresponding spinor wave phase variation is

$$d\phi = \partial_t\phi\,dt + \partial_{\boldsymbol{n}}\phi\,d\boldsymbol{n} = (\partial_t\phi + \mathbf{v}\,\mathrm{grad}\,\phi)\,dt$$

and, by analogy with the classical formulae (2.8) and (2.9), one can write

$$\boldsymbol{P}' = -\,\mathrm{grad}\,\phi = \frac{m'_0\mathbf{v}}{\sqrt{1-\mathbf{v}^2/c^2}}\,,$$

$$E' = \partial_t\phi = \frac{m'_0c^2}{\sqrt{1-\mathbf{v}^2/c^2}}\,,$$

so we find

$$d\phi = \left(\frac{m'_0c^2}{\sqrt{1-\mathbf{v}^2/c^2}} - \frac{m'_0\,\mathbf{v}^2}{\sqrt{1-\mathbf{v}^2/c^2}}\right)dt. \qquad (2.31)$$

Hence, from (2.29) we obtain the fundamental result which states that the internal phase of the electron is identical to that of its associated spinor wave

$$d\phi = d\phi_i\,. \qquad (2.32)$$

With (1.6), there is an obvious *second physical link* between the electron and the spinor wave Φ which clearly *carries* the lepton.

This is what we wanted to show.

Conclusions and outlook

Within the above theory, the electron is guided by its spinor wave which means that it is always in motion. In this case, the electron doesnot apparently comply with atomic quantum stationary states for which the electron is required to have zero velocity. De Broglie et al. [10] thus postulated a vacuum *hidden thermostat* whereby the electron is permanently exchanging energy and momenta. According to the authors this sub-quantum medium would cause the electron to fluctuate in a *Brownian-like* manner so as to exhibit a static situation only at the atomic level. In this way, the wavy-electron would be allowed to undergo perpetual infinitesimal propagation. Our opinion however differs from this hypothesis which we believe, would mark the limitation of the Double Solution theory. Preferably, we suggest that each energy level of an atom be characterized by a stationary limited spinor *wave packet* carrying a dynamical electron: the mean energy of the pair *wavepacket-moving electron* would then represent the quantized energy level of the atom.

"Squeezing" stepwise the wave packet (i.e. increasing the frequency) would mean jumping to a higher energy level and vice versa, which actually could reflect the excited/desexcited states of the atom. This process tends to validate the spectroscopic sharpness of the atomic rays as it is observed. All in all, the exposed theory seems to cope with an electron whose *physical* wave interacts with a *physical* diffraction device, and yet satisfies the established relativistic features of Dirac's theory.

Submitted on July 14, 2016 / Accepted on July 16, 2016

References

1. Davisson C.J., Germer L.H. Reflection of electrons by a crystal of nickel. *Proc. National Acad. of Sciences of the USA*, 1 April 1928, v. 14(4), 317–322.
2. de Broglie L. Thermodynamique Relativiste et Mécanique Ondulatoire. *Ann. Institut Henri Poincaré*, 1968, v. IX, no. 2, 89–108.
3. de Broglie L. Doctorate Thesis (1924). 2nd edition, Masson, Paris, 1963.
4. de Broglie L. Etude du mouvement des particules dans un milieu réfringent. *Ann. Inst. Henri Poincaré*, 1973, v. XVIII, no. 2, 89–98.
5. Dirac P.A.M. The Principles of Quantum Mechanics. PUF, Paris, 1931.
6. Lichnérowicz A. Champ de Dirac, champ du neutrino et transformations C, P, T sur un espace courbe. *Ann. Institut Henri Poincaré Sec. A*, 1964, v. 3, 233–290.
7. Moret-Bailly F. Le Champ Neutrinique en Relativité Générale. *Ann. Institut Henri Poincaré Sec. A*, 1966, v. 4, 301–355.
8. Berestetski V., Lifshitz E., Pitayevski L. Électrodynamique quantique. (Series: Physique théorique, tome 4), 2ème édition, traduit du Russe par V. Kolimeev, Editions de la Paix, Moscou, 1989.
9. Greiner W., Reinhardt J. Field Quantization. Springer (Berlin), 1993, p. 124.
10. Vigier J.P., Bohm D. Model of the causal interpretation of quantum theory in terms of a fluid with irregular fluctuations. *Physical Review*, 1954, v. 96, no. 1, 208–216.

Antigravity and Vacuum Propulsion in the Planck Vacuum Theory

William C. Daywitt

National Institute for Standards and Technology (retired), Boulder, Colorado, USA
E-mail: wcdaywitt@me.com

This paper explores the ideas of antigravity and vacuum propulsion from a fundamental-physics point of view, making use of the Planck vacuum (PV) model of the vacuum state.

1 Introduction

It is shown in a previous paper [1] that free-space gravitational shielding is ineffective, because gravitational waves, the carrier of the gravitational force, propagate within the PV state rather than free space. This result suggests that, as the gravitational waves are interior to the vacuum state, they may be affected by perturbations to that state. The following calculations are focused on that assumption in an attempt to determine if antigravity and vacuum propulsion are viable concepts.

Section 2 examines Newton's gravitational force between the earth (or any other large object), and a much smaller mass, from the viewpoint of the PV theory. The structure of that force is revealed in equations (2) and (3) in terms of n-ratios, which are normalized mass/PV coupling forces between the free space masses and the invisible vacuum state.

2 Newton's gravity

Newton's gravitational force F_{gr} between the two spherical masses $m \ll M$ separated by a distance $r\,(= a + h + A)$ can be expressed as

$$-F_{gr}(r) = \frac{mMG}{r^2} = \frac{(mc^2/r)(Mc^2/r)}{c^4/G} \tag{1}$$

$$= \frac{(mc^2/r)(Mc^2/r)}{m_*c^2/r_*} = n_r(m)n_r(M)\frac{m_*c^2}{r_*} \tag{2}$$

$$= \frac{aA}{r^2}\, n_a(m)\, n_A(M)\, \frac{m_*c^2}{r_*} = \frac{mc^2}{r}\,\frac{An_A(M)}{r} \tag{3}$$

using $G = e_*^2/m_*^2$ and $r_*m_*c^2 = e_*^2$ [2], where a and A are the radii of the masses m and M respectively, and h is the shortest distance between their surfaces. The mass m_* and Compton radius r_* belong to the separate Planck particles making up the degenerate PV state. The n-ratios in (2) and (3) are defined as

$$n_r(m) = \frac{mc^2/r}{m_*c^2/r_*}, \qquad n_r(M) = \frac{Mc^2/r}{m_*c^2/r_*}, \tag{4}$$

and

$$n_a(m) = \frac{mc^2/a}{m_*c^2/r_*}, \qquad n_A(M) = \frac{Mc^2/A}{m_*c^2/r_*}. \tag{5}$$

The coupling forces and the n-ratios are all less that one.

The force $m_*c^2/r_*\,(= c^4/G)$ is the maximum coupling force sustainable by the PV state [3, Fig.1]. Of particular interest to the present paper is $n_a(m)$, which is the normalized coupling force the mass m exerts on the PV at the surface of m. It is noted that the force m_*c^2/r_* normalizing the coupling forces also normalizes the Einstein field equation, and that the n-ratios are at the core of the metrics associated with the Schwarzschild equation [2] [4].

The mass/PV coupling forces in the numerators of (4) and (5) represent gravity-like forces the various free-space masses exert on the PV state. For example

$$\frac{mc^2}{r} = \frac{mc^2G}{r\cdot G} = \frac{mc^2G}{r\cdot e_*^2/m_*^2} = \frac{mm_*^2c^2G}{r\cdot r_*m_*c^2} = \frac{mm_*G}{rr_*} \tag{6}$$

is the force the mass m exerts on the Planck particles within the PV that are at a radius r from the center of m. The other coupling forces in (4) and (5) are similarly interpreted — e.g., $Mc^2/A = Mm_*G/Ar_*$.

Newton's dynamical equations start from his second law of motion ($m\ddot{r} = F_{gr}$) and the final expression in (3). With $dr = dh$ and $\ddot{r} = \ddot{h}$:

$$m\ddot{r} = m\ddot{h} = -\frac{mc^2}{r}\,\frac{An_A(M)}{r} \tag{7}$$

or

$$\ddot{r} = \ddot{h} = -\frac{c^2}{r}\,\frac{An_A(M)}{r} \tag{8}$$

for the acceleration of m toward M. Equation (8) is easily integrated over r via

$$\ddot{r} = \frac{d\dot{r}}{dt} = \dot{r}\,\frac{d\dot{r}}{dr} = \frac{d(\dot{r}^2/2)}{dr} = -\frac{Ac^2}{r^2}\, n_A(M) \tag{9}$$

from $r_0\,(\geqslant r + a)$ to r, and yields

$$\dot{r}^2 - \dot{r}_0^2 = 2c^2\left(\frac{r_0}{r} - 1\right)n_{r_0}(M) = 2c^2\left[n_r(M) - n_{r_0}(M)\right] \tag{10}$$

or

$$\left(\dot{r}^2 - \dot{r}_0^2\right)^{1/2} = -\left\{2c^2\left[n_r(M) - n_{r_0}(M)\right]\right\}^{1/2} \tag{11}$$

which is an equation involving only n-ratios and implying that the gravity dynamic takes place within the vacuum state.

3 PV state

The PV state [2] is assumed to be a degenerate state of negative energy Planck particles $(-e_*, m_*)$. Its degenerate nature implies that the Planck particle eigenstates within the vacuum are fully occupied. Thus the Planck particles are not free to exhibit macroscopic motion. The vacuum is bathed, however, in microscopic zero-point Planck-particle agitation.

Due to this degeneracy, when the PV is perturbed it exhibits percussion-like response waves, much like the waves on the surface of a kettle drum. For example, the free space electron core $(-e_*, m_e)$ perturbs the vacuum with the two-term coupling force "$e_*^2/r^2 - m_e c^2/r$", leading to the Dirac-equation response [5], where that response does not involve macroscopic Planck particle motion.

The previous section outlines the PV response to coupling forces of the form mc^2/r — thus the PV response is of the nature of gravitational percussion waves traveling within the PV between the positions of the free space masses m and M. It is this type of wave motion that is envisioned in the discussion to follow; i.e., wave motion that does not involve macroscopic Planck particle motion.

4 Summary, conclusions, and comments

From a survey of equations (1)–(11), it is clear: that the final expression in (3) is the springboard for the Newtonian dynamics, equations (7)–(11); and that none of the expressions in (2) and (3) show any sign of a direct free-space gravitational force acting between m and M — the force is channeled through the vacuum state. The second conclusion implies that there can be no free-space gravitational shielding [1].

The first expression in (3),

$$F_{gr}(r) = -\frac{aA}{r^2}\, n_a(m)\, n_A(M)\, \frac{m_* c^2}{r_*} \qquad (12)$$

suggests that, if the coupling force mc^2/a in $n_a(m)$ could be masked or eliminated, then $F_{gr} = 0$ and m would experience no gravitational attraction toward the mass M; so the mass m would be effectively weightless. The vanishing of the n-ratio $n_a(m)$ thus leads to a simple explanation for antigravity, once the physical mechanism for nullifying $n_a(m)$ is specified.

It is difficult to find experimental data in the open literature that addresses the preceding theoretical calculations. The one source germane to the present work the author could find is contained in the e-book entitled "What Goes Up..." [6], which is a novel that claims to discuss real experimental data. The principle interest here is the composite electrical coil that is at the heart of a craft that is claimed to exhibit antigravity and vacuum propulsion.

The doughnut shaped coil consists of two current loops each of which supports a separate a.c.-d.c. signal, where the two a.c. signals in the two loops are set at different frequencies. This heuristic description is sketchy due to unavailable details in the coil design. The book claims that the magnetic fields (or the magnetic flux) produced by the coil are the source of antigravity and vacuum propulsion (though the book doesn't use the term "vacuum propulsion"). The a.c. field destroys the gravity force F_{gr}; and the (±) d.c. field causes the craft to move up or down at a high rate of speed. The second paragraph of the present section and the a.c. currents in the coil thus account for antigravity. (The a.c. and d.c. stand for "alternating current" and "direct current" respectively.)

Although much theoretical knowledge concerning the PV state exists [2], there is much still to be learned. The antigravity conundrum was readily resolved with the force equation (12). Even then, details of how the a.c. flux from the coil nullifies the effect of $n_a(m)$ is not fully understood. Concerning vacuum propulsion, things are even worse. For closure sake, then, it will just be stated (assumed) that the ± d.c. flux interacting with the charges $(-e_*)$ of the separate Planck particles within the PV result in the rapid systematic movement of the coil, and hence the space-craft. Reflecting upon the intricacy of the electron spinor field caused by the electron/PV interaction [5], the idea of vacuum propulsion doesn't seem so strange.

Submitted on July 14, 2016 / Accepted on July 17, 2016

References

1. Daywitt W.C. Gravitational shielding as viewed in the Planck Vacuum Theory. *Progress in Physics*, 2016, v. 12, issue 3, 301.
2. Daywitt W.C. The trouble with the equations of modern fundamental physics. *American Journal of Modern Physics*, *Special Issue*: *Physics Without Higgs and Without Supersymmetry*, 2016, v. 5, no. 1-1, 22. See also http://www.planckvacuum.com
3. Daywitt W.C. Limits to the validity of the Einstein field equations and General Relativity from the viewpoint of the negative-energy Planck vacuum state. *Progress in Physics*, 2009, v. 5, issue 3, 27.
4. Daywitt W.C. The Crothers metrics and the black hole metric as viewed from the Planck vacuum perspective. *Galilean Electrodynamics*, 2014, Sept./Oct. 2014, 82.
5. Daywitt W.C. Understanding the Dirac equation and the electron-vacuum system. *Progress in Physics*, 2013, v. 9, issue 4, 78.
6. Stover J.C. What Goes Up... Publish Green, Minneapolis (MN), 2015.

On the Quantum-Relativistic Behavior of Moving Particles

Fernando Ogiba
E-mail: fogiba@gmail.com

The *zitterbewegung* of massless elementary electrical charges consists of two distinct vacuum induced fluctuations. The first, random loops (spin) at the light speed (co-moving frame) [1], is attributed to absorptions and emissions of zero-point radiation at the Compton's rate (stochastic electrodynamics). It will be shown that the second (de Broglie) emerges because such radiation, just passing but tangled for a while (rest mass), doesn't submit to the ordinary motion of bodies; its light speed is ensured by truncations and restoration of the translational motion (inertia). Synchronized with absorption-emission, kinetic energy becomes vibrational energy (x-ray), and vice versa. The implied works are due to back and forth self-stresses (contractions) triggered by imminent violations of the light speed limit (loops at the light speed plus ordinary motion) implicit in the improper de Broglie phase velocity. Time spent to preserve the normal motility of the tangled radiation is observed only in the fixed frame (time dilation).

1 Introduction

Due to permanent interactions with the Planck's vacuum [2–4], massless elementary electrical charges (MEEC) are induced to move along quantum-relativistic paths at the speed of the interacting radiation, independently of the observed ordinary motion of particles, as implicit in the approach originating the concept of *zitterbewegung* [5]. In such approach, it was considered a particle (an electron) of rest mass m_0, which, therefore, must be attributed (respecting the peculiarities of the interaction) to the mass-equivalent of the zero-point energy absorbed (incident momentum) and emitted (reaction momentum) by MEEC. It means that MEEC, on average, retain zero-point radiation; a boson giving the rest mass.

In the particular case of free particles, the argued paths are continual random "jumps" (diffusion of probability) among trajectories belonging to the ensemble dictated by the Dirac equation [6]. Theoretical results indicate that such trajectories are curvilinear, over which particles are found at the light speed, which agrees with experimental facts. Indeed, if they are seen as random loops of electrical current in the co-moving frame (a charge e moving at the light speed c over a spherical shell of average radius r_c), then we find that the corresponding magnetic moment,

$$\mu_z = IA = \frac{ec}{2\pi r_c}\pi r_c^2 = \frac{ecr_c}{2}\,, \tag{1}$$

matches the observed magnetic moment of spin-1/2 particles,

$$\mu_z \approx \frac{e\hbar}{2m_0}\,, \tag{2}$$

if $2\pi r_c = \lambda_c$, where $\lambda_c = h/m_0c$ is the Compton's wavelength.

Alternatively, if an electron can be found over circles at the light speed (co-moving frame), then its momentum components should fluctuate like $p' = m_0\dot{q}' = m_0c\cos(\omega' t' + \phi_{q'})$, where $\phi_{q'}$ are random phases. It implies the coordinates

$$q' = \frac{c}{\omega_c}\sin(\omega' t' + \phi_{q'})\,, \tag{3}$$

where c/ω' is the radius of the loops of current (fluctuations with spherical shape). Inserting the corresponding variances (averaging over random phases),

$$\Delta p'^2 = \frac{1}{2}(m_0c)^2, \quad \Delta q'^2 = \frac{1}{2}\frac{c^2}{\omega'^2}\,, \tag{4}$$

into the minimum uncertainty relation, $\Delta p'\Delta q' = \hbar/2$, yields

$$\omega' = \frac{m_0c^2}{\hbar}\,, \quad r_c = \frac{c}{\omega'} = \frac{\lambda_c}{2\pi}\,, \tag{5}$$

that is, the Compton's angular frequency ($\omega' = \omega_c$).

Considering the center of mass of the fluctuations (vibrations) at the origin of the co-moving frame ($\mathbf{x}' = 0$), it implies that a free particle moving in the x-direction of the fixed frame will be seen as a material wave of wave number $\mathbf{k} = (k, 0, 0)$. Phase invariance, considering special relativity, i.e.

$$\omega' t' - \mathbf{k}'\cdot\mathbf{x}' = \omega t - \mathbf{k}\cdot\mathbf{x}, \tag{6}$$

implies

$$t' = \frac{\omega}{\omega_c}\left(t - \frac{x}{v_p}\right), \quad v_p = \frac{\omega}{k}\,, \tag{7}$$

where v_p is the phase velocity. Comparing the Eq. (7) with the Lorentz transformation

$$t' = \gamma\left(t - \frac{v}{c^2}\,x\right) \tag{8}$$

one gets the parameters of the material wave [7]:

$$\omega = \gamma\frac{m_0c^2}{\hbar}\,, \quad k = \gamma\frac{m_0v}{\hbar}\,, \quad v_p = \frac{\omega}{k} = \frac{c^2}{v}\,, \tag{9}$$

from which we can see that v_p is a violation of the natural speed of electromagnetic waves. This fact makes v_p meaningless in the context of the special relativity, which is reinforced

by the existence of a group velocity (transport of matter) coinciding with the particle velocity, i.e.

$$v_g = \frac{\partial \omega}{\partial k} = \frac{\partial E}{\partial p} = v\,. \tag{10}$$

Technically, the concept of group velocity requires that the resultant material wave be a superposition of waves of different frequencies, which agrees with the successful concept of wave packet [8]. However, a wave packet implies a set of phase velocities. As the phase velocity of the resultant material wave is a violation of the natural speed of radiation, then we should expect that the phase velocities of the constituent waves also are speed violations (at least mostly).

Here, is it wise keep in mind that such speed violations, being in full agreement with the concepts expressed by equations (6), (8) and (10), cannot be meaningless. In effect, notice that an evolution at the phase velocity ($x = v_p t$) implies that time "stops" in the co-moving frame ($t' = 0$). Emphasizing, in this particular situation, time is computed only in the fixed frame. Remarkably, despite of being an improper evolution, it agrees with the ultimate meaning of time dilation.

Until now, we have seen that single frequency (ω_c) fluctuations of spherical shape ($r_c = c/\omega_c$) become multi-frequency fluctuations in the fixed frame [9], which manifest as a wave packet (material wave). The emergence of multiple angular frequencies implies that the translational motion cause a break of the spherical shape of the fluctuations, given that for each emerging angular frequency there must correspond a different radius ($\omega_i r_i = c$, where c is invariant). Coincidentally, this agrees with length contraction, i.e., according to the theory of special relativity, in the fixed frame the fluctuations must present an ellipsoidal shape.

The above argumentation implies that the phase velocity v_p is a statistical quantity; given that all frequencies implied in the wave packet do not exist simultaneously but in the elapsed time of an ordinary measurement (much greater than $2\pi/\omega_c$).

Physically, contractions of the vacuum induced fluctuations requires back and forth forces, whose resultant, at least on average, must be zero. Moreover, these forces — defined only in the fixed frame — do not have the same nature of the electromagnetic forces (from the Planck's vacuum) responsible by the fluctuations in the co-moving frame.

The search for forces triggered by the translational motion must begin noting that the speed violation v_p is dominant in the Lorentz transformations (LT), i.e.

$$x' = \gamma\,(x - vt)\,, \quad t' = \gamma\left(t - \frac{x}{v_p}\right), \quad \gamma = \left(1 - \frac{v}{v_p}\right)^{-\frac{1}{2}}, \tag{11}$$

which suggests that LT — to account for the light speed limit in both reference frames — just consider imminent velocity violations when the linear translational motion takes place. In other words, the emerging vibrations, whose *statistical superposition* gives v_p, must relate to a mechanism ensuring the speed limit of the zero-point radiation (ZPR) tangled for a moment by MEEC (co-moving frame), given that the relative velocity is lower than c.

Let us analyze, heuristically, the complete motion. From the equations (1) to (5) and the presence of the Planck's vacuum, it is implicit that in the co-moving frame MEEC are found over circular trajectories at the speed of the "impregnating" zero-point radiation (ZPR). Therefore, it be expected the occurrence of all sort of violations of the light speed limit when the ordinary translational motion is added. However, resulting velocities for MEEC — imbued with the properties of radiation — either greater or smaller than c are forbidden by the well-known Maxwell's relation $\mu\varepsilon c^2 = 1$. So, it is plausible to think that the vibrations implied in the wave packet — related to radii contraction of the fluctuations — arise to avoid any possible speed violation of the tangled ZPR, which would result from the simple combination of random orbits at light speed with the observed motion of matter.

In the next sections, based on well-known physical facts, it will be presented some evidences that the periodical motion induced by the Planck's vacuum combined with the ordinary motion of particles implies the appearance of periodical back and forth self-stresses, which are imposed by the *normal motility* of the *tangled radiation*. Here, it must be emphasized the following: First, *tangled radiation* is ZPR continually imprisoned during an infinitesimal time (less than $2\pi/\omega_c$) by MEEC. Second, *normal motility* relates to evolutions of free radiation; assumed to be extensible to the *tangled radiation*, given the massless nature of the "host".

2 The need for periodical longitudinal self-stresses

The energy carried by the material wave is the vibrational energy, $E = \hbar\omega$, which must be the energy of the particle, $E = \gamma m_0 c^2$. Therefore,

$$\omega = \frac{m_0 c^2}{\hbar} + \frac{(\gamma - 1) m_0 c^2}{\hbar} = \omega_c + \omega_T, \tag{12}$$

where the Compton's frequency (ω_c) expresses the rate at which zero-point energy is going in and out of the MEEC (on average remaining as rest energy), and ω_T accounts for all vibrations implied in the wave packet; likewise that v_p represents all corresponding phase velocities (one at a time).

Given the statistical nature of the wave packet (in the sense of the quantum superposition), it implies that particles can present, at a given time, only kinetic energy, or only vibrational energy, or a mix of them; all these possibilities occurring, in accordance with energy conservation, at a very high rate (synchronized with ω_c).

Coincidentally, for $v \ll c$, ω_T is the *maximum* frequency emitted by electrons in a x-ray apparatus (Duane-Hunt formula, $\hbar\omega_{max} = eV = m_0 v^2/2$), which does not contradict the fact that electrons can collide presenting frequencies different from ω_{max}. In effect, these other frequencies can be built into

the well-known wavelength spread of x-ray data; the complementary energy (kinetic) simply warm the target.

The above facts suggest that kinetic energy becomes vibrational energy, and vice-versa, but the sum of them, at any time, is $(\gamma - 1)m_0c^2$ or $\hbar\omega_T$, as required by energy conservation. Inexorably, such changes of the kinetic energy imply positive and negative works on the particle. Nonetheless, if one takes into account that the MEEC-ZPR *electromagnetic* interaction is completely resolved, in the sense that it yields well-defined rest energy (mass), spin and Compton's parameters, then there must be another reason for the emergence of vibrations triggered by the translational motion. Only remains to appeal to the dynamics allowed by the tangled ZPR, which, in view of the above, only can be attributed to periodical back and forth self-stresses, whose sole purpose is to ensure its light speed limit; an imposition of the hindmost nature of radiation.

Here, it should be pointed up that these self-stresses — ensuring the normal motility of the tangled radiation — cannot be interpreted in the same sense of Poincaré stresses [10], which were postulated in order to guarantee the stability of the Abraham-Lorentz model for the electron. In effect, the semi-classical electron stability should be understood as an electromagnetic pressure balance involving the Planck's vacuum, as proposed by Casimir [11].

3 The Zitterbewegung and self-stresses

A formal account for the two kind of vacuum induced fluctuations, as exposed elsewhere, can be seen in the quantum-relativistic approach of the *zitterbewegung* [12], although not working the properties of the Planck's vacuum of explicit way; that is, using the recipes of the stochastic electrodynamics. This is possible because Lorentz transformations as well as quantum equations takes into account non-localized statistical features of the wave packet (the ultimate product of the matter-vacuum interaction). Hence, the following results, despite of evidencing the co-moving loops of electrical current (spin), should be interpreted statistically [13].

Inserting the Dirac Hamiltonian, $H = c\alpha_j p_j + \beta m_0 c^2$, into the Heisenberg picture of quantum mechanics and considering that the matrices α_j and β commute with momentum (p_j) and position (x_j) operators, one gets

$$\frac{dp_j}{dt} = \frac{i}{\hbar}\left[H, p_j\right] = 0\,, \quad \frac{dx_j}{dt} = \frac{i}{\hbar}\left[H, x_j\right] = c\alpha_j\,, \qquad (13)$$

where the first implies that H and p_j commute (constants of the motion), and the second, in the full sense of the operation

$$c\alpha_j\psi = \pm c\psi\,, \qquad (14)$$

where ψ represents a four-component spinor, means that "a measurement of a component of the velocity of a free electron is certain to lead to the result $\pm c$" [5, p. 262], which is not the ordinary velocity of free particles, but that of the tangled ZPR.

The result (14) means that — on average, everywhere, in all directions and with equal probability — electrons go forth and back at the light speed; an expected behavior, considering the main properties of the interacting ZPR (homogeneity, isotropy, randomness and Lorentz invariant spectral density).

Whenever the electron is on a permitted Dirac trajectory, despite of being temporarily, it must obey the parameters of such trajectory. As the trajectories are curvilinear, then there are accelerations. In fact, they are given by $\ddot{x}_j = (i/\hbar)[H, \dot{x}_j]$, where $\dot{x}_j = c\alpha_j$, which corresponds to the equations

$$\ddot{x}_j = \frac{2i\left(H\dot{x}_j - c^2 p_j\right)}{\hbar}\,, \quad \ddot{x}_j = \frac{2i\left(c^2 p_j - \dot{x}_j H\right)}{\hbar}\,, \qquad (15)$$

since $Hc\alpha_j + c\alpha_j H = 2cp_j$. Integrating, yields respectively

$$\dot{x}_j = c^2 p_j H^{-1} + \eta_j e^{i2Ht/\hbar}; \quad \dot{x}_j = c^2 p_j H^{-1} + \eta'_j e^{-i2Ht/\hbar}; \qquad (16)$$

where the operators η and η' (constants of integration) must take into account that these *components* must match, periodically, the tangential velocity ($c\alpha_j$), as implicit in Eq. (14), which implies that $\eta = \eta' = c\alpha_j - c^2 p_j H^{-1}$. Moreover, on average the velocity must be the observed one ($c^2 p_j H^{-1}$). Therefore, the velocity operator becomes

$$\dot{x}_j = c^2 p_j H^{-1} + \left(c\alpha_j - c^2 p_j H^{-1}\right)\cos\left(2Ht/\hbar\right)\,, \qquad (17)$$

from which, considering the same above conditions, one gets the position operator

$$x_j(t) = c^2 p_j H^{-1} t + \frac{\left(\hbar c\alpha_j H^{-1} - \hbar c^2 p_j H^{-2}\right)}{2}\sin\left(\frac{2H}{\hbar}t\right). \qquad (18)$$

Notice, for $p_j = 0$ the operators (17) and (18) violate the minimum uncertainty relation ($m_0 \Delta\dot{x}_j \Delta x_j = \hbar/2$) by a factor 2 (the eigenvalues of α_j are unitary and $H \to m_0c^2$). This happens because the Dirac Hamiltonian takes into account matter and antimatter, whose energy gap is $2H$ [14, p. 949]. For only one kind of particle (e.g. free electrons in the two slit experiment, where is not verified the presence of positrons), it suffices to ignore the factor 2 in the equations (15).

Regardless of the comment made in the previous paragraph, the statistical components of the velocity of an electron (moving at the speed of light), as expressed by Eq. (17), show that — in order to maintain the speed imposed by the tangled radiation — the translational velocity $c^2 p_j H^{-1}$ is periodically subtracted and added, depending on the sign of c. Indeed, apart intermediary values, for forward evolutions of the local motion ($+c$), the translational motion is completely subtracted, and for backward evolutions ($-c$), it is completely restored, as can be seen from the allowed values of the cosine and the Eq. (14). Clearly, synchronized with absorptions and emission of zero-point energy (rest energy), the kinetic energy changes at the Compton's rate (considering only one kind of particle). As truncations and restorations of the translational motion behaves as vibrations, then kinetic energy is

being transformed into vibrational energy, and vice versa. These positive and negative works, necessarily, imply back and forth forces (zero, on average). However, as there are no external forces — other than those yielding the well-defined evolutions in the co-moving frame — then such works must be assigned to periodical longitudinal self-stresses (PLSS), which are imposed by the very motility of radiation, as inferred in the preceding paragraph.

From the position operators (18) — statistical coordinates defined in the fixed frame — we can verify the following: First, they do not explicit a set of vibrations composing the wave packet, but the motion of the resulting material wave, whose statistical frequency is $\omega = H/\hbar$. Second, for $p_j = 0$, these coordinates agree with the proposed equations (3); evolutions with spherical shape in the co-moving frame. Third, in the fixed frame ($p_j \neq 0$), the amplitude of the vibration (enclosed difference of operators) suffers a contraction in the direction of the motion; evolutions with ellipsoidal shape.

4 Final remarks

Fluctuations with spherical shape (co-moving frame) becoming fluctuations with ellipsoidal shape (fixed frame) explains the emergence of all vibrations implied in the wave packet, but in the sense that a motion with constant tangential velocity (light speed) over an ellipsoid implies an infinite number of angular frequencies. The wave packet is a statistical concept; it simply expresses the fact that during the time of an ordinary measurement the particle can be found at any position on the ellipsoidal surface; each one corresponding to a given angular frequency (particle states). This is the fundamental feature of quantum superposition.

As "self-impulses", in principle, cannot be observed in the co-moving frame, then the corresponding time intervals also not. From another point of view, the strength of self-stresses depends of the relative velocity, but an observer in the co-moving frame cannot decide about the constant velocity of such frame (principle of relativity); therefore, also cannot decide about self-stresses (and its duration). This is implicit in the LT, as can be seen inserting the improper evolution $x = (c^2/v)t$ (triggering a given self-stress), which gives $t' = 0$. In short, the time spent to preserve the "integrity" of the tangled ZPR is computed only in the fixed frame, which is in full agreement with the cumulative time dilation.

The vibrational energy corresponding to self-stresses only are emitted as radiation under non-uniform decelerations (as in a x-ray apparatus). Contrasting with thermal excitations (external forces), PLSS only imply restrictions to the mobility of vacuum induced fluctuations (without external forces); so, radiationless.

The corresponding back and forth strains (restrictions to the translational motion) explain the non-cumulative length contraction.

Newton's inertia relates to the de Broglie periodicity [15]; that is, the periodicity of the wave packet, whose corresponding vibrations come from PLSS; "opposing forces".

To finalize, truncations of the ordinary motion followed by complete restoration of the kinetic energy, as implicit in the Eq. (17), is in full agreement with the observed energy conservation (first Newton's law).

5 Conclusion

In the light of the foregoing, the quantum relativistic behavior of particles emerge because the ZPR, continually entrapped by MEEC during the time of an absorption-emission of zero-point energy, does not submit to the ordinary motion of bodies. From another point of view, the quantum of the Higgs field (Higgs boson) does not move with the observed velocities of the corresponding particle; its light speed is ensured by conservative periodical truncations and restorations of the ordinary motion, whose momentum dependent strength (amplitude of emerging vibrations) explain why inertia (mass) increases with the particle velocity.

Submitted on July 26, 2016 / Accepted on July 28, 2016

References

1. Huang K. On the Zitterbewegung of the Dirac Electron. *American Journal of Physics*, 1952, v. 20, no. 8, 479–484.
2. Boyer T. Random Electrodynamics: The theory of classical electrodynamics with classical electromagnetic zero-point radiation. *Physical. Review D*, 1975, v. 11, no. 4, 790–808.
3. Milonni P.W. The Quantum Vacuum: An Introduction to Quantum Electrodynamics. Academic Press, Inc, 1994.
4. Ogiba F. Planck's Radiation Law: Thermal excitations of vacuum induced Fluctuations, *Progress in Physics*, 2015, v. 11, no. 2, 145–148.
5. Dirac P. A. M. The Principles of Quantum Mechanics, 4ed. Oxford University Press, 1999.
6. Ogiba F. Addendum to Phenomenological Derivation of the Schrödinger Equation. *Progress in Physics*, 2014, v. 10, no. 2, 108–110.
7. de Broglie L. Ondes et quanta. *Comptes rendus des séances de l'Académie des Sciences*, 1923, v. 177, 507–510.
8. Burkhardt C.E., Leventhal J.J. Foundations of Quantum Physics. Springer, 2008.
9. Dávid G., Cserti J. General theory of Zitterbewegung. *Physical Review B*, 2010, v. 81, 121417-1–121417-4.
10. Poincaré H. Sur la dynamique de l'électron. *Rendiconti del Circolo Matematico di Palermo*, 1906, v. 21, no. 1, 129–175.
11. Puthoff H.E. Casimir Vacuum Energy and the Semiclassical Electron. *International Journal of Theoretical Physics*, 2007, v. 46, no. 12, 3005–3008.
12. Sakurai J.J. Advanced Quantum Mechanics. Addison-Wesley, 1967.
13. Pauli W. The Connection Between Spin and Statistics. *Physical Review*, 1940, v. 58, no. 8, 716–722.
14. Messiah A. Quantum Mechanics. Volume II. North Holland Publishing Company, 1962.
15. Wignall J.W.G. De Broglie waves and the nature of mass. *Foundations of Physics*, 1985, v. 15, no. 2, 207–227.

Type III Spacetime with Closed Timelike Curves

Ahmed Faizuddin
Hindustani Kendriya Vidyalaya, Dinseh Ojha Road, Bhangagarh, Guwahati-05, Assam, India
E-mail: faizuddinahmed15@gmail.com

We present a symmetric spacetime, admitting closed timelike curves (CTCs) which appear after a certain instant of time, *i.e.*, a time-machine spacetime. These closed timelike curves evolve from an initial spacelike hypersurface on the planes $z = constant$ in a causally well-behaved manner. The spacetime discussed here is free from curvature singularities and a 4D generalization of the Misner space in curved spacetime. The matter field is of pure radiation with cosmological constant.

1 Introduction

One of the most intriguing aspects of Einstein's theory of gravitation is that solutions of field equations admit closed timelike curves (CTC). Presence of CTC in a spacetime leads to time-travel which violates the causality condition. The first one being Gödel's spacetime [1] which admits closed timelike curves (CTC) everywhere and an eternal time-machine spacetime. There are a considerable number of spacetimes in literature that admitting closed timelike curves have been constructed. A small sample would be [1–21]. One way of classifying such causality violating spacetimes would be to categorize the metrics as either eternal time-machine in which CTC always exist (in this class would be [1, 2]), or as time-machine spacetimes in which CTC appear after a certain instant of time. In the latter category would be the ones discussed in [18–20]. Many of the models, however, suffer from one or more severe drawbacks. For instance, in some of these solutions, for example [13, 14, 20], the weak energy condition (WEC) is violated indicating unrealistic matter-energy content and some other solutions have singularities.

Among the time-machine spacetimes, we mention two: the first being Ori's compact core [17] which is represented by a vacuum metric locally isometric to pp waves and second, which is more relevant to the present work, the Misner space [22] in 2D. This is essentially a two dimensional metric (hence flat) with peculiar identifications. The Misner space is interesting in the context of CTC as it is a prime example of a spacetime where CTC evolve from causally well-behaved initial conditions.

The metric for the Misner space [22]

$$ds^2_{Misn} = -2\,dt\,dx - t\,dx^2 \tag{1}$$

where $-\infty < t < \infty$ but the co-ordinate x is periodic. The metric (1) is regular everwhere as $\det g = -1$ including at $t = 0$. The curves $t = t_0$, where t_0 is a constant, are closed since x is periodic. The curves $t < 0$ are spacelike, but $t > 0$ are timelike and the null curves $t = t_0 = 0$ form the chronology horizon. The second type of curves, namely, $t = t_0 > 0$ are closed timelike curves (CTC). This metric has been the subject of intense study and quite recently, Levanony and Ori [23], have studied the motion of extended bodies in the 2D Misner space and its flat 4D generalizations. A non-flat 4D spacetime, satisfying all the energy conditions, but with causality violating properties of the Misner space, primarily that CTC evolve smoothly from an initially causally well-behaved stage, would be physically more acceptable as a time-machine spacetime.

In this paper, we shall attempt to show that causality violating curves appear in non-vacuum spacetime with comparatively simple structure. In section 2, we analyze the spacetime; in section 3, the matter distribution and energy condition; in section 4, the spacetime is classified and its kinematical properties discussed; and concluding in section 5.

2 Analysis of the spacetime

Consider the following metric

$$\begin{aligned} ds^2 = {} & 4\,r^2\,dr^2 + e^{2\alpha r^2}\left(dz^2 - t\,d\phi^2 - 2\,dt\,d\phi\right) + \\ & + 4\beta\,z\,r\,e^{-\alpha r^2}\,dr\,d\phi \end{aligned} \tag{2}$$

where ϕ coordinate is assumed periodic $0 \leqslant \phi \leqslant \phi_0$, where α is an integer and $\beta > 0$ is a real number. We have used co-ordinates $x^1 = r$, $x^2 = \phi$, $x^3 = z$ and $x^4 = t$. The ranges of the other co-ordinates are $t, z \in (-\infty, \infty)$ and $0 \leqslant r < \infty$. The metric has signature $(+,+,+,-)$ and the determinant of the corresponding metric tensor $g_{\mu\nu}$, $\det g = -4\,r^2\,e^{6\alpha r^2}$. The non-zero components of the Einstein tensor are

$$\begin{aligned} G^{\mu}_{\mu} &= 3\,\alpha^2, \\ G^{t}_{\phi} &= -\frac{1}{2}\,e^{-6\alpha r^2}\,\beta^2\,. \end{aligned} \tag{3}$$

Consider an azimuthal curve γ defined by $r = r_0$, $z = z_0$ and $t = t_0$, where r_0, z_0, t_0 are constants, then we have from the metric (2)

$$ds^2 = -\,t\,e^{2\alpha r^2}\,d\phi^2. \tag{4}$$

These curves are null for $t = 0$, spacelike throughout for $t = t_0 < 0$, but become timelike for $t = t_0 > 0$, which indicates the presence of closed timelike curves (CTC). Hence CTC form at a definite instant of time satisfy $t = t_0 > 0$.

It is crucial to have analysis that the above CTC evolve from a spacelike $t = constant$ hypersurface (and thus t is a

time coordinate) [17]. This can be ascertained by calculating the norm of the vector $\nabla_\mu t$ (or by determining the sign of the component g^{tt} in the inverse metric tensor $g^{\mu\nu}$ [17]). We find from (2) that

$$g^{tt} = t\, e^{-2\,\alpha\, r^2} + \beta^2\, z^2\, e^{-6\,\alpha\, r^2}\,. \tag{5}$$

A hypersurface $t = constant$ is spacelike provided $g^{tt} < 0$ for $t = t_0 < 0$, but becomes timelike provided $g^{tt} > 0$ for $t = t_0 > 0$. Here we choose the z-planes defined by $z = z_0$, (z_0, a constant equal to zero) such that the above condition is satisfied. Thus the spacelike $t = constant < 0$ hypersurface can be chosen as initial conditions over which the initial may be specified. There is a Cauchy horizon for $t = t_0 = 0$ called Chronology horizon which separates the causal and non-causal parts of the spacetime. Hence the spacetime evolves from a partial Cauchy hypersurface (initial spacelike hypersurface) in a causally well-behaved manner, up to a moment, *i.e.*, a null hypersurface $t = 0$ and CTC form at a definite instant of time on $z = constant$ plane.

Consider the Killing vector $\eta = \partial_\phi$ for metric (2) which has the normal form

$$\eta^\mu = (0, 1, 0, 0)\,. \tag{6}$$

Its co-vector is

$$\eta_\mu = \left(2\,\beta\, z\, r\, e^{-\alpha\, r^2},\ -t\, e^{2\,\alpha\, r^2},\ 0,\ -e^{2\,\alpha\, r^2}\right). \tag{7}$$

The (6) satisfies the Killing equation $\eta_{\mu\,;\,\nu} + \eta_{\nu\,;\,\mu} = 0$. For cyclicly symmetric metric, the norm $\eta_\mu\,\eta^\mu$ of the Killing vector is spacelike, closed orbits [24–28]. We note that

$$\eta^\mu\,\eta_\mu = -t\, e^{2\,\alpha\, r^2} \tag{8}$$

which is spacelike for $t < 0$, closed orbits (ϕ co-ordinate being periodic).

An important note is that the Riemann tensor $R_{\mu\nu\rho\sigma}$ can be expressed in terms of the metric tensor $g_{\mu\nu}$ as

$$R_{\mu\nu\rho\sigma} = k\left(g_{\mu\rho}\, g_{\nu\sigma} - g_{\mu\sigma}\, g_{\nu\rho}\right) \tag{9}$$

where $k = -\alpha^2$ for the spacetime (2).

Another important note is that if we take $\beta = 0$, then the spacetime represented by (2) is maximally symmetric vacuum spacetime and locally isometric anti-de Sitter space in four-dimension. One can easily show by a number of transformations the standard form of locally isometric AdS_4 metric [29]

$$ds^2 = \frac{3}{(-\Lambda)\, x^2}\left(-dt^2 + dx^2 + d\phi^2 + dz^2\right) \tag{10}$$

where one of the co-ordinate ϕ being periodic.

3 Matter distribution of the spacetime and energy condition

Einstein's field equations taking into account the cosmological constant

$$G^{\mu\nu} + \Lambda\, g^{\mu\nu} = T^{\mu\nu}\,, \quad \mu, \nu = 1, 2, 3, 4\,. \tag{11}$$

Consider the energy-momentum tensor of pure radiation field [30]

$$T^{\mu\nu} = \rho\, n^\mu\, n^\nu \tag{12}$$

where n^μ is the null vector defined by

$$n^\mu = (0, 0, 0, 1)\,. \tag{13}$$

The non-zero component of the energy-momentum tensor

$$T^t_\phi = -\rho\, e^{2\,\alpha\, r^2}\,. \tag{14}$$

Equating field equations (11) using (3) and (14), we get

$$\begin{aligned} &\Lambda = -3\,\alpha^2, \\ &\rho = \frac{1}{2}\,\beta^2\, e^{-8\,\alpha\, r^2}, \quad 0 \leqslant r < \infty\,. \end{aligned} \tag{15}$$

The energy-density of pure radiation or null dust decreases exponentially with r and vanish at $r \to \pm\infty$. The matter field pure radiation satisfy the energy condition and the energy density ρ is always positive.

4 Classification and kinematical properties of the spacetime

For classification of the spacetime (2), we can construct the following set of null tetrads $(k, l, m, \bar{m})$ as

$$k_\mu = (0, 1, 0, 0)\,, \tag{16}$$

$$l_\mu = \left(-2\,\beta\, z\, r\, e^{-\alpha\, r^2},\ \frac{t}{2}\, e^{2\,\alpha\, r^2},\ 0,\ e^{2\,\alpha\, r^2}\right), \tag{17}$$

$$m_\mu = \frac{1}{\sqrt{2}}\,(2\, r, 0, i\, e^{\alpha\, r}, 0)\,, \tag{18}$$

$$\bar{m}_\mu = \frac{1}{\sqrt{2}}\left(2\, r, 0, -i\, e^{\alpha\, r^2}, 0\right), \tag{19}$$

where $i = \sqrt{-1}$. The set of null tetrads above are such that the metric tensor for the line element (2) can be expressed as

$$g_{\mu\nu} = -k_\mu\, l_\nu - l_\mu\, k_\nu + m_\mu\, \bar{m}_\nu + \bar{m}_\mu\, m_\nu\,. \tag{20}$$

The vectors (16)–(19) are null vectors and are orthogonal except for $k_\mu\, l^\mu = -1$ and $m_\mu\, \bar{m}^\mu = 1$. Using this null tetrad above, we have calculated the five Weyl scalars

$$\begin{aligned} &\Psi_3 = -\frac{i\,\alpha\,\beta\, e^{-2\,\alpha\, r^2}}{2\,\sqrt{2}}\,, \\ &\Psi_4 = -\frac{1}{4}\,\beta\, e^{-2\,\alpha\, r^2}\left(i + 2\,\alpha\, z\, e^{\alpha\, r^2}\right) \end{aligned} \tag{21}$$

are non-vanishing, while $\Psi_0 = \Psi_1 = \Psi_3 = 0$. The spacetime represented by (2) is of type III in the Petrov classification scheme. Note that the non-zero Weyl scalars Ψ_3 and Ψ_4 are finite at $r \to 0$ and vanish as $r \to \pm\infty$ indicating asymptotic flatness of the spacetime (2). The metric (2) is free

from curvature singularities. The curvature invariant known as Kretchsmann scalar is given by

$$R^{\mu\nu\rho\sigma} R_{\mu\nu\rho\sigma} = 24\,\alpha^4 \tag{22}$$

and the curvature scalar

$$R = -12\,\alpha^2 \tag{23}$$

are constant being non-zero.

Using the null tetrad (16) we have calculated the *Optical* scalars [30] the *expansion*, the *twist* and the *shear* and they are

$$\begin{aligned} \Theta &= \frac{1}{2}\, k^{\mu}_{;\mu} = 0\,, \\ \omega^2 &= \frac{1}{2}\, k_{[\mu\,;\,\nu]}\, k^{\mu\,;\,\nu} = 0\,, \\ \sigma\,\bar{\sigma} &= \frac{1}{2}\, k_{(\mu\,;\,\nu)}\, k^{\mu\,;\,\nu} - \Theta^2 = 0 \end{aligned} \tag{24}$$

and the null vector (16) satisfy the geodesics equation

$$k_{\mu\,;\,\nu}\, k^{\nu} = 0\,. \tag{25}$$

Thus the spacetime represented by (2) is non-diverging, has shear-free null geodesics congruence. One can easily show that for constant r and z, the metric (2) reduces to conformal Misner space in 2D

$$ds^2_{confo} = \Omega\, ds^2_{Misn} \tag{26}$$

where $\Omega = e^{2\,\alpha\, r^2}$ is a constant.

5 Conclusion

Our primary motivation in this paper is to write down a metric for a spacetime that incorporates the Misner space and its causality violating properties and to classify it. The solution presented here is non-vacuum, cyclicly symmetric metric (2) and serves as a model of time-machine spacetime in the sense that CTC appear at a definite instant of time on the z-plane. Most of the CTC spacetimes violate one or more energy conditions or unrealistic matter source and are unphysical. The model discussed here is free from all these problems and matter distribution is of pure radiation field with negative cosmological constant satisfying the energy condition.

Submitted on July 25, 2016 / Accepted on August 9, 2016

References

1. Godel K. An example of a new type of cosmological solutions of Einsteins field equations of gravitation. *Rev. Mod. Phys.*, 1949, v. 21 (3), 447–450.
2. van Stockum W. J. The gravitational field of a distribution of particles rotating about an axis of symmetry. *Proc. R. Soc. Edin.*, 1937, v. 57, 135–154.
3. Tipler F. J. Rotating Cylinders and the Possibility of Global Causality Violation. *Phys. Rev. D*, 1974, v. 9 (8), 2203–2206.
4. Gott J. R. Closed timelike curves produced by pairs of moving cosmic strings: Exact solutions. *Phys. Rev. Lett.*, 1991, v. 66 (9), 1126–1129.
5. Bonnor W. B. An exact, asymptotically flat, vacuum solution of Einstein's equations with closed timelike curves. *Class. Quantum Grav.*, 2002, v. 19, 5951–5957.
6. Bonnor W. B. Closed timelike curves in general relativity. *Int. J. Mod. Phys. D*, 2003, v. 12, 1705–1708.
7. Bonnor W. B., Steadman B. R. Exact solutions of the Einstein Maxwell equations with closed timelike curves. *Gen. Rel. Grav.*, 2005, v. 37 (11), 1833–1844.
8. Kerr R. P. Gravitational Field of a Spinning Mass as an Example of Algebraically Special Metrics. *Phys. Rev. Lett.*, 1963, v. 11 (5), 237–238.
9. Carter B. Global structure of the Kerr family of gravitational fields. *Phys. Rev. D*, 1968, v. 174, 1559–1571.
10. Gürses M., Karasu A., Sarioğlu Ö. Godel-type metrics in various dimensions. *Class. Quantum Grav.*, 2005, v. 22 (9), 1527–1543.
11. Alcubierre M. The warp drive: hyper-fast travel within general relativity. *Class. Quantum Grav.*, 1994, v. 11, L73–L77.
12. Lobo F. S. N., Crawford P. Time, closed timelike curves and causality. The Nature of Time : Geometry, Physics and Perception. NATO Sci. Ser. II, 2003, v. 95, 289–296.
13. Morris M. S., Thorne K. S., Yurtsever U. Time Machines and the Weak Energy Conditions. *Phys. Rev. Lett.* , 1988, v. 61 (13), 1446–1449.
14. Morris M. S., Thorne K. S. Wormholes in space-time and their use for interstellar travel: A tool for teaching general relativity. *Amer. J. Phys.*, 1988, v. 56, 395–412.
15. Krasnikov S. V. Hyper-fast interstellar travel in general relativity. *Phys. Rev. D*, 1998, v. 57 (8), 4760–4766.
16. Everett A. E., Roman T. A. A superluminal subway: the Krasnikov tube. *Phys. Rev. D*, 1997, v. 56, 2100–2108. arXiv: gr-qc/9702049.
17. Ori A. A new time-machine model with compact vacuum core. *Phys. Rev. Lett.* , 2005, v. 95, 021101–021107.
18. Ori A. Formation of closed timelike curves in a composite vacuum/dust asymptotically-flat spacetime. *Phys. Rev. D*, 2007, v. 76, 044002–044015.
19. Ori A. Improved time-machine model. *Phys. Rev. D*, 1996, v. 54 (8), 4858–4861.
20. Ori A. Causality violation and the weak energy condition. *Phys. Rev. D*, 1994, v. 49 (8), 3990–3997.
21. Sarma D., Patgiri M., Ahmed F. U. Pure radiation metric with stable closed timelike curves. *Gen. Rel. Grav.*, 2014, v. 46, 1633–1641.
22. Misner C. W. Taub-NUT Space as a Counterexample to Almost Anything. In Ehlers J., ed. Relativity Theory and Astrophysics 1. Relativity and Cosmology, Am. Math. Soc., Providence, RI, 1967, 160–169.
23. Levanony D., Ori A. Extended time-travelling object in Misner space. *Phys. Rev. D*, 2011, v. 83, 044043. arXiv: gr-qc/1102.0907.
24. Mars M., Senovilla J. M. M. Axial symmetry and conformal Killing vectors. *Class. Quantum Grav.*, 1993, v. 10, 1633–1647.
25. Carter B. The commutation property of a stationary, axisymmetric system. *Commun. Math. Phys.*, 1970, v. 17, 233–238.
26. Branes A. Some restrictions on the symmetry groups of axially symmetric spacetimes. *Class. Quantum Grav.*, 2001, v. 18, 5511–5520.
27. Bičák J., Schmidt B. D. Isometries compatible with gravitational radiation. *J. Math. Phys.*, 1984, v. 25 (3), 600–606.
28. Wald R. M. General Relativity. Cambridge University Press, Cambridge, 1984.
29. Zofka M., Bičák J. Cylindrical spacetimes with $\Lambda \neq 0$ and their sources. *Class. Quantum Grav.*, 2008, v. 25 (1), 015011. arXiv: gr-qc/0712.2144
30. Stephani H., Kramer D., MacCallum M., Hoenselaers C., Herlt E. Exact Solutions to Einstein's Field Equations, Cambridge Univ. Press, 2003.

Experimental and Theoretical Test of Cahill's Detection of Absolute Velocity in Gas-mode Interferometer Experiments

Jay R. Seaver

Energy Matters Foundation, PO BOX 2588, Longmont, CO 80502, USA
E-mail: jay@energy-matters.org

Several papers by Cahill, et al. assert that Michelson-Morley type experiments performed in gas have small but non-null results which, when properly analyzed, show that the absolute speed of the earth was detected. Here we show that Cahill made a fundamental error in his assumptions and that the mathematical analysis upon which he based his conclusions is invalid. We also include a report on an experiment that verifies these mathematical conclusions. The experiment uses water instead of air as the wave medium. The much larger index of refraction of water (1.33 vs. 1.00029) greatly amplifies the effect Cahill predicts and makes the null result of the new experiment dramatically apparent. This confirms both theoretically and experimentally that absolute velocity was not and cannot be detected in Michelson-Morley type experiments regardless of the refractive medium in which they are performed.

1 Introduction

I was intrigued by several papers by Cahill [1–4] that purport to re-evaluate the original Michelson-Morley (MM) and other "gas-mode" interferometer experiments and prove that they actually measured the absolute speed of the earth through space. Cahill shows in these papers that the index of refraction of air caused results that although small were not completely null. He asserts that the absolute velocity of the earth was measured and that absolute space was detected — but was it?

I set out to test Cahill's assertions by designing an experiment capable of getting a larger non-null result. This experiment uses water as the medium through which the light propagates so that the "incomplete cancellation of the geometrical effects" (according to Cahill) would be greatly amplified by the much larger index of refraction. This allows easy detection of the interference-fringe shifts in a low-cost Michelson-type interferometer.

The experiment had a resolution that was more than 10^3 times greater than the effect Cahill's equations predicted. The results of the experiment were unequivocally null. Based on the null results, I set out to reexamine Cahill's assumptions and mathematical derivations. It was through this reexamination that I derived the correct equations and proved that the so-called "cancellation of the geometrical effects" is complete and the results of any MM type experiment must be null whether done in vacuum or in a refractive medium. We show that both the herein derived equations and the results of the present experiment are in complete agreement that absolute space cannot be detected with these types of experiments.

Our derivations (and Cahill's) are based on classical physics. By "classical physics" we mean merely that the equations of the special theory of relativity (SRT) will not be used to transform values between inertial reference frames. All measurements in the derivations are made in the rest frame (or what Cahill calls the "quantum foam" frame) where light-speed is constant and isotropic. But in SRT, light-speed is constant and isotropic in *all* frames. Therefore our derivations will be in complete compliance with the formalism of SRT, while at the same time satisfying Cahill and his followers that they are also valid in Cahill's absolute frame.

The value measured in the experiment is the shift, measured in wavelengths, of the interference pattern of two light beams. Because this measurement is a scalar value, independent of the actual length of the wavelength, it is invariant in all reference frames. This is what allows us to do the entire analysis from the rest frame but make the actual measurement in the laboratory frame — they must agree.

2 Correcting Cahill's derivations

We will use Cahill's equations as derived in [1] for this analysis.

Cahill begins his analysis by making the following (incorrect) assumption regarding the speed of light in the refractive medium of air: "If the gas is moving with respect to the quantum foam, as in an interferometer attached to the earth, then the speed of light relative to the quantum foam is still $V = c/n$ up to corrections due to the Fresnel drag. *But this dragging is a very small effect and is not required in the present analysis*". [emphasis added]) He is correct that Fresnel drag is a very small effect, but as will soon be evident, it is not small compared to the effect he is trying to measure and it cannot be ignored.

The laboratory frame is assumed to have an arbitrary velocity v with respect to the rest frame. We also make the following two assumptions which Cahill made in his analysis and which are entirely consistent with SRT: 1) clocks slow down with velocity and 2) lengths contract with velocity. The

factor by which they slow down is defined as

$$\gamma = \frac{1}{\sqrt{1 - v^2/c^2}}. \quad (1)$$

For convenience, we also make the following definition:

$$\beta = \frac{v}{c} \quad \Rightarrow \quad \gamma = \frac{1}{\sqrt{1 - \beta^2}}. \quad (2)$$

If both arms of the interferometer are of rest-length L and one is aligned parallel to the velocity of the laboratory and the other is aligned at right angles to this velocity, then the length of the orthogonal arm in the rest frame is still L, but the length of the parallel arm experiences a contraction if measured in the rest frame,

$$L_{\|} = L\sqrt{1 - \beta^2} = \frac{L}{\gamma}. \quad (3)$$

Cahill defines n to be the index of refraction of the gas and uses the same value n in both frames. This seems perfectly reasonable, since n is a scalar and therefore invariant. But just because it has the same value in both frames does not mean that it affects the path of the waves in both frames the same way. This will be demonstrated by observing *from within the rest frame* how observers *within the moving frame* measure and define n. It then becomes apparent that in the rest frame the velocity of light in a moving refractive medium is not simply c/n plus the traditional drag term.

Before observing how n is measured, we must first understand how clocks are synchronized using Einstein's method. We will do this by observing from the rest frame as clocks are synchronized in the laboratory frame. Let there be clocks at each end of the arm aligned parallel to the velocity which we designate as clock A and clock B. According to Eq. (3) this distance between the two clocks is L/γ in the rest frame. The procedure for synchronizing the two clocks in the moving frame is as follows:

1. A light wave leaves clock A at time 0 on clock A in the moving frame and also at time 0 in the rest frame.
2. The light beam propagates towards clock B at velocity c in both frames. In the rest frame clock B is moving at velocity v in the same direction as the light beam.
3. The light arrives at B at time t_1 in the rest frame.
4. The total distance the light travels in the rest frame on the outbound path is $c\,t_1$. This can be separated into two distances: 1) the length of the contracted arm L/γ and the distance clock B moved during the time t_1 which is $v\,t_1$. Solving for t_1, we get

$$t_1 = \frac{L}{\gamma\,(c - v)}. \quad (4)$$

5. The light reflects from a mirror at B and returns to A at time t_2 in the rest frame. Since the clock at A was moving towards the light during this leg, the distance that the light traveled before reaching A was $L/\gamma - v\,(t_2 - t_1)$. Using the same logic as above, the time $t_2 - t_1$ to make the return trip as measured in the rest frame is

$$t_2 - t_1 = \frac{L}{\gamma\,(c + v)}. \quad (5)$$

6. Solving for t_2, the total time to make the round trip as measured in the rest frame is

$$t_2 = \frac{L/\gamma}{c + v} + \frac{L/\gamma}{c - v} = \frac{2\,L/\gamma}{c\,(1 - v^2/c^2)} = \frac{2\,L}{c}\gamma. \quad (6)$$

7. The clocks in the moving frame run slower by a factor of γ than the clocks in the rest frame. Therefore, the time on clock A when the light returns is

$$t_A = \frac{t_2}{\gamma} = \frac{2\,L}{c}. \quad (7)$$

8. Using Einstein's method of synchronization, clock B is defined to be synchronized to clock A if at the moment of reflection the time on clock B is set to $t_A/2$.

$$t_B = \frac{L}{c}. \quad (8)$$

As expected, the observers in the laboratory frame measure the speed of light to be c in both directions. But notice that at the moment of reflection of the light from clock B, the time is t_1 in the rest frame and t_B on clock B in the moving frame. But what is the time on clock A at that moment? Since clock A was defined to be 0 at time 0 in the rest frame, and since clock A runs slower by a factor of γ than clocks in the rest frame, the time on clock A must be t_1/γ. But that means that to an observer in the rest frame, there is a bias between clocks A and B,

$$t_{bias} = t_B - \frac{t_1}{\gamma} = \frac{L}{c} - \frac{L}{\gamma^2\,(c - v)} = -\frac{v\,L}{c^2}. \quad (9)$$

Please note that this is in complete agreement with SRT. Position-dependent clock biases are the source of relative simultaneity in SRT. Events are defined to be simultaneous in the moving frame when the clocks at the sites of the two events read the same value. But because of the permanent bias between the clocks (when observed from the rest frame), those same two events are never simultaneous within the rest frame. From this exercise we see that there is nothing mysterious or magical about relative simultaneity — it is simply a byproduct of defining the one-way time of flight of a light wave to be 1/2 of the two-way time of flight.

The bias in Eq. (9) is the same position-dependent bias that occurs in the transformation of time between frames using the Lorentz transformation of SRT. But we have determined its value not by performing this transformation but by simply observing from the rest frame as clocks were synchronized in the moving frame. We have used nothing more than

this definition and classical physics to derive the same bias between the clocks as defined in SRT.

Now that we understand how clocks in the moving frame appear to observers in the rest frame, we are ready to see how the index of refraction, when measured in the laboratory, appears to observers in the rest frame. To measure the index of refraction in the laboratory, a light beam is sent from clock A at time 0 through a refractive material and arrives at clock B at time t_{Bn}, where the n in the subscript indicates time through the refractive material. This is the time of flight of the light beam as measured in the laboratory. The index of refraction is then defined as

$$n = \frac{c\, t_{Bn}}{L}. \tag{10}$$

This corresponds to a velocity of light in the refractive medium of c/n as measured in the laboratory. Let us now look at that same velocity as measured in the rest frame. Because of the bias on clock B, although the time on clock A is 0 when the light is emitted, the observer in the rest frame sees the light wave leave clock A when clock B reads $-v\,L/c^2$. The elapsed time on clock B for the time of flight is therefore

$$\Delta t_{Bn} = t_{Bn} + \frac{v\,L}{c^2}. \tag{11}$$

Using Eq. (10) to substitute for t_{Bn}, and remembering that clocks in the moving frame run slower by a factor of γ, the elapsed time in the rest frame for the time of flight is

$$\Delta t_0 = \frac{L\,(c\,n + v)\,\gamma}{c^2}. \tag{12}$$

We defined the direction from A to B to be the same direction as the velocity of the moving frame. Since lengths contract with velocity, the total distance the light propagated during this time, as measured in the rest frame, is

$$\Delta d_0 = \frac{L}{\gamma} + v\,\Delta t_0 = \frac{L}{\gamma} + \frac{v\,L\,(c\,n + v)\,\gamma}{c^2}. \tag{13}$$

The velocity of the light beam in the refractive material as measured in the rest frame is this distance divided by the propagation time, which simplifies to

$$c_{n0+} = \frac{\Delta d_0}{\Delta t_0} = \frac{c\,(c + n\,v)}{c\,n + v}. \tag{14}$$

Notice that this can be put in the following form:

$$c_{n0+} = \frac{c/n + v}{1 + \dfrac{(c/n)\,v}{c^2}}. \tag{15}$$

In this form it is very obvious that we have derived the velocity addition formula of SRT where the two velocities are c/n and v. This shows that there is nothing mysterious about the velocity addition formula of SRT. It is easily derived using classical physics if one acknowledges that clocks and lengths change with velocity. The only mystery is what causes velocity-dependent lengths and clock-rates in the first place. But that is a topic for a separate paper.

We can also write this equation in a different form,

$$c_{n0+} = \frac{c}{n} + \left(\frac{n^2 - 1}{n^2}\right)\left(\frac{n}{n + \beta}\right)v. \tag{16}$$

In this form, we can clearly see that the Fresnel drag coefficient is simply a consequence of the velocity addition formula. They are not separate phenomena. Prior to Lorentz and Einstein, it was thought that the Fresnel drag term consisted only of the $\dfrac{n^2 - 1}{n^2}v$ term. The $\dfrac{n}{n + \beta}$ term is so close to 1 that except for extremely high velocities it was unobservable.

What we have shown in this derivation is that the Fresnel drag term is automatically included in our derivation once we acknowledge that lengths and times change with velocity. In fact, Fresnel drag is proof that lengths and times really do change with velocity.

When the light is sent in the opposite direction through the refractive medium, the sign of the laboratory's velocity v in equation (14) is inverted resulting in a reverse speed of

$$c_{n0-} = \frac{c\,(c - n\,v)}{c\,n - v}. \tag{17}$$

Summing the times of propagation for these out and back velocities, we can calculate the total time for a round trip on the parallel arm in the rest frame if the light is passing through a moving refractive medium with an index of refraction n:

$$\Delta t_{\|0} = \frac{L}{\gamma\,(c_{n0+} - v)} + \frac{L}{\gamma\,(c_{n0-} + v)} = 2\frac{L}{c/n}\gamma. \tag{18}$$

Not surprisingly, this is the same value we would have calculated if we had simply used the Lorentz transforms of SRT to transform the time on clock A into the rest frame for a round trip of length $2\,L$ at velocity c/n. Be we have derived it using nothing but classical physics and the two assumptions regarding length contraction and the slowing of clocks with velocity.

We will now look at the time for the round trip on the orthogonal arm. In the laboratory frame, n has the same value in all directions.* Therefore, as measured in the laboratory frame, the round-trip time in the orthogonal direction is

$$\Delta t_{\perp} = \frac{2\,L}{c/n} = \frac{2\,L\,n}{c}. \tag{19}$$

With the arm oriented orthogonal to the velocity, the light-propagation times for the outbound and return trips are equal in the rest frame so there is no bias between clocks A and B. Since clocks in the moving frame run slower when observed

*This is proven in Section 4.2 where the velocity of light in a moving refractive medium is derived for any arbitrary direction.

from the stationary frame, this same time in the stationary frame is simply the elapsed time in the rest frame multiplied by γ,

$$\Delta t_{\perp 0} = 2\frac{L}{c/n}\gamma. \tag{20}$$

We see that this is exactly the same as the time for the parallel path given in equation (18) so the MM experiment is doomed to give null results regardless of the index of refraction of the medium.

3 Comparing to Cahill's results

We now compare these results to Cahill's results (we use subscript C for Cahill's times), which come from his equations (7) and (10) in [1]:

$$\left.\begin{aligned} \Delta t_{\parallel C} &= \frac{2L}{\gamma\frac{c}{n}\left(1-\frac{v^2}{c^2}n^2\right)} = \frac{2L\gamma}{c/n}\left(\frac{1}{\gamma^2\left(1-n^2\beta^2\right)}\right) \\ \Delta t_{\perp C} &= \frac{2L}{\sqrt{\frac{c^2}{n^2}-v^2}} = \frac{2L\gamma}{(c/n)}\left(\frac{1}{\gamma\sqrt{1-n^2\beta^2}}\right) \end{aligned}\right\}. \tag{21}$$

The right-most terms in parenthesis are the error factors Cahill introduced by ignoring the "drag" effect. Without these terms, the times are identical. Notice that both of these error terms are very close to 1. In fact for a velocity of 360 km/sec and $n = 1.00029$ (which are the approximate values Cahill used in his paper), the two terms in parenthesis are $(1 + 8 \times 10^{-10})$ and $(1 + 4 \times 10^{-10})$, respectively. It is easy to see why Cahill thought they could be ignored and simply set to 1.

The difference between equations (21) is Cahill's measured time difference between the parallel and orthogonal orientations. It can be shown that for $v/c = \beta << 1$ this difference can be approximated by

$$\Delta t_{\parallel C} - \Delta t_{\perp C} = \frac{Ln}{\gamma c}\left(\frac{\left(n^2-1\right)\beta^2}{1-n^2\beta^2}\right). \tag{22}$$

In the original MM experiment, $L = 11$ and $n \approx 1.00029$. The absolute velocity that Cahill calculated was on the order of 360 km/sec, which results in $\beta \approx 0.0012$. Substituting these into equation (22) results in a measured time difference of

$$\Delta t_{\parallel C} - \Delta t_{\perp C} \approx 3.1 \times 10^{-17}. \tag{23}$$

This confirms Cahill's estimate of a difference on the order of 10^{-17} sec. The wavelength of light used in the original experiment was approximately 600 nm which for a velocity of c has a temporal period of about 2.0×10^{-15} sec. Since there is one spatial period (wavelength) for each temporal period, the fringe shift in wavelengths is the total time delay of Eq. (23) divided by the temporal period of the light wave:

$$\Delta\lambda = \frac{3.1 \times 10^{-17}}{2.0 \times 10^{-15}}\lambda \approx 0.016\lambda. \tag{24}$$

This represents a predicted fringe shift of about 1.6% of a wavelength in the original experiment. It is this value that Cahill used to predict the non-null results.

We conclude that Cahill made a fatal mistake when he assumed he could ignore the Fresnel drag effects. It is precisely the ignoring of Fresnel drag that creates the 1.6% difference in phase. Quoting Cahill, "Of course experimental evidence is the final arbiter in this conflict of theories." In that spirit, we will present the design and results of an experiment that proves that an index of refraction greater than 1 does not give non-null results in Michelson-interferometer experiments as Cahill asserts.

Cahill's analysis of the raw data from the original MM experiment shows a non-null result which is sidereal in nature and which agrees, according to Cahill, with his above calculations. It is beyond the scope of this paper to address the source of the non-null, sidereal effect found in the raw data. But one paper that has addressed this issue shows that the very large drift in the experiment combined with an improper statistical analysis is entirely responsible for the apparent non-null result [5].

4 Design of the new experiment

The analysis of the experiment to test Cahill's results is again done as if we are an observer in a rest frame where light speed is isotropic. Since we are constrained to make all of the actual measurements in the moving frame of our laboratory, we define the results of the experiment in terms of an invariant scalar value that will have the same value in all frames. This is done by measuring the shift of an interference pattern in units of wavelengths. This is a scalar value that must be the same in all frames and allows us to make measurements in the moving frame that are in full agreement with those same measurements made in the hypothetical rest frame.

As mentioned above, the non-null result that Cahill predicted is less than 2% of a wavelength. This is much too small to be measured in an inexpensive, home-built interferometer. To increase the sensitivity of the experiment, the index of refraction was increased from 1.00029 of air to 1.33 of water. Of course, the experiment cannot be done completely submerged in water, so a refractive block containing water was introduced into one of the paths.

Figure 1 shows the physical layout of the experiment. A laser emits a beam that is split into two separate beams. One beam travels exclusively through air on its path to the detector. The other beam travels the same distance, but part of this path passes through a block of refractive material of length L that slows the wave down. When it exits the refractive block (RB), it then continues at the normal speed of light until it is recombined with its sister beam at the detector. Distilled water with an index of refraction of 1.33 is used for the refractive block. Unfortunately, using a refractive block is not the same as performing the entire experiment while im-

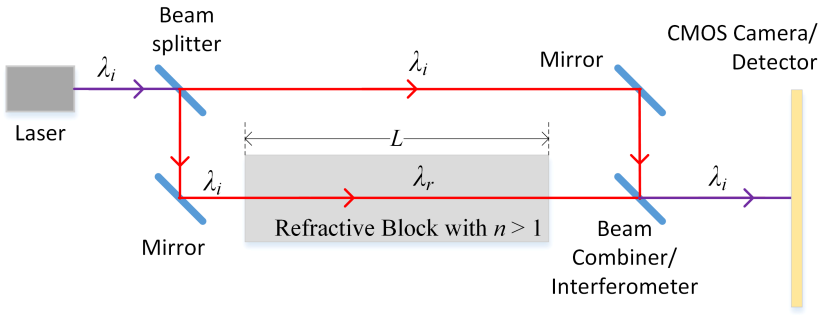

Fig. 1: Layout of experiment.

mersed in a high-refractive medium. Specifically, it complicates the mathematics by introducing refraction in the beam as it passes through the boundary between the air and the water. But the complication is worth it because it allows a large enough fringe shift (according to Cahill's equations) that even our inexpensive interferometer is sensitive enough to measure it.

The wavelength that is emitted from the laser after taking into account the velocity-dependent slowing of the clocks and the Doppler shift, is designated as the incident wavelength λ_i. At the first beam splitter, one wave goes straight along an unrefracted path. The other beam gets reflected downward (in the figure) before reflecting off a second mirror that puts it on a trajectory that is parallel to the first beam but which passes through the refractive block. The two beams recombine at the beam combiner and propagate together to the camera detector. The phase and frequency shifts due to the reflection of the mirrors and beam splitters are exactly the same for the two paths and exactly cancel one another so they can be ignored. The wavelength leaving the laser and arriving at the phase detector is also the same for both paths.

It is the phase relationship between the two beams at the detector that we are interested in. Since the entire path is identical for both beams except for the length L of the RB, we only need to calculate the phase shift that occurs through the RB and compare it to the phase change that occurs over this same distance in the other path to account for the entire phase shift at the detector. All other effects will be identical on both paths and cannot alter the phase difference caused by the delay through the RB. By rotating the experiment 90 degrees we can measure the phase shift in each direction. Any difference between the two directions is a measure of absolute velocity through space — which Cahill predicts will be non-zero.

4.1 Velocity and the path of the beam

In this analysis, we are only going to look at the two cases where the velocity of the laboratory is orthogonal to the beam and parallel to the beam, respectively. We will be discussing multiple angles in this analysis. To keep these angles straight, the following definitions will be used:

1. The symbol φ will be used for the angle between the velocity vector of the refractive medium (laboratory) and the light wave path within the medium. It will have no subscript in the moving frame and a 0 subscript in the rest frame.
2. The symbol θ_i will be used for the incident angle of the wave path at the surface of the refractive block. It is defined as the angle between the light wave path and the normal to the refractive surface, which is the standard definition from geometric optics. It will have a subscript 0 when measured in the rest frame and no additional subscript in the moving frame.
3. The symbol θ_r will be used for the refracted angle of the wave path within the refractive block. It is defined as the angle between the light wave path in the RB and the line that is normal to the refractive surface, which is again the standard definition from geometric optics. It will have a subscript 0 when measured in the rest frame and no additional subscript in the moving frame.
4. In the case where the velocity is parallel to the line that is normal to the refractive surface, the θ angles will have an additional $\|$ symbol in the subscript. If the velocity is orthogonal to the normal a $\perp$ symbol will be used. Since the φ angles are by definition between the light path and the velocity, no subscript is necessary to indicate velocity direction.

Figure 2 shows a laser diode with a highly divergent beam that is collimated using an aperture. In actual lasers, a collimating lens is used instead of an aperture because a lens can capture most of the light. Obviously the aperture loses all of the light that doesn't pass through it. But for our purposes the math and visualization is easier with the aperture and the principle is the same. The view in Figure 2 is for a laser that is stationary with respect to the observer.

Figure 3 shows what happens to the path of the beam if the laser is moving up (orthogonal to beam) in this figure at velocity v. The laser and aperture position are shown at time t for an emission that occurred at time 0. Notice that during the time that a wave front in the beam travels a distance ct (in vacuum), the aperture and laser move a distance vt. This

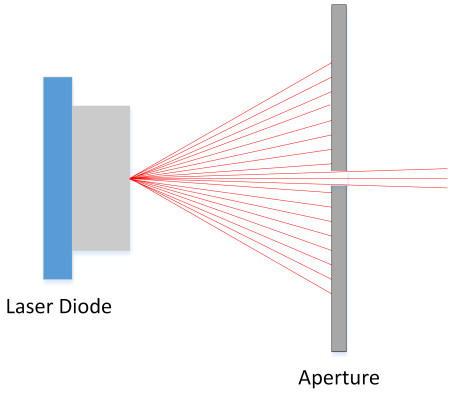

Fig. 2: Laser collimation using an aperture.

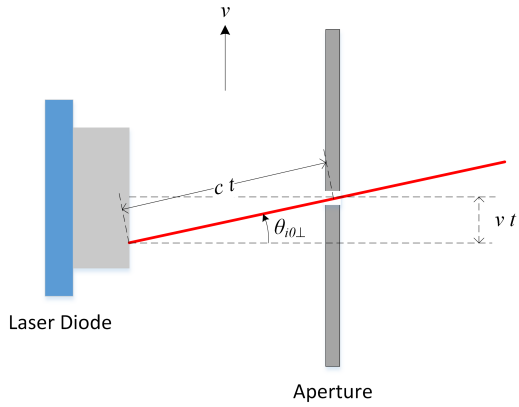

Fig. 3: Path of a single wavelet/photon for orthogonal direction.

means that only waves that left the laser at an angle of $\theta_{i0\perp}$ (in the rest frame) make it through the aperture — hence we have only shown one path in the figure. This angle assures that the orthogonal component of the velocity of the wave is exactly v and the parallel velocity of the wave is $\sqrt{c^2 - v^2}$.

Since every wave leaving the laser that makes it through the aperture follows a similar path, the resulting beam, which is made up of all of these individual wavelets, appears to remain perfectly aligned with the laser and with the aperture. The solid red line in Figure 3 shows the path of an individual wavelet from its emission at the laser surface to its exit from the aperture. Although the wavelet moves at an angle , the beam one would see at any instant in time is the collection of all of the wavelets that have left the laser. A "snapshot" of the positions of several of these wavelets, each on its own unique path, is shown in Figure 4 . Notice that the three wavelets that have been propagating for times t_1, t_2 and t_3 each remain perfectly aligned with each other and with the center of the laser because the aperature assures that their velocity component in the orthogonal direction is exactly v. Any wavelets with different orthogonal velocities are blocked by the aperture.

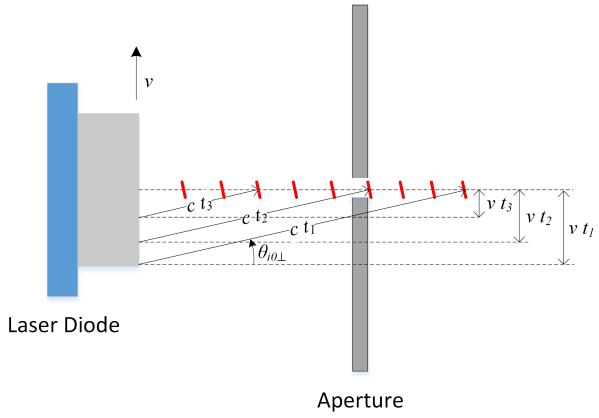

Fig. 4: Snapshot of laser beam for orthogonal direction.

We see that Mother Nature has conspired with light so that an observer in any frame sees a straight, horizontal beam going from the center of the laser through the center of the aperture and arriving at a distant target still centered — just as it appears when the system is stationary. This assures that the path of the composite beam relative to the laboratory is independent of the velocity of the laboratory even though the individual wavelets are moving at a velocity-dependent angle.

Since the index of refraction of air is so close to 1 and since the effect of the index of refraction of the refractive block is so much larger, we are going to simplify the math by treating the air as if the index of refraction were exactly 1. From Figure 3, we can see that the sine and cosine of $\theta_{i0\perp}$ are given by

$$\left.\begin{aligned} \sin\theta_{i0\perp} &= \frac{v}{c} = \beta \\ \cos\theta_{i0\perp} &= \sqrt{1-\sin^2\theta_{i0\perp}} = \sqrt{1-\beta^2} = \frac{1}{\gamma} \end{aligned}\right\}. \qquad (25)$$

4.2 Velocity of light in a moving medium at arbitrary angle

In the orthogonal direction, we can see that the wavelets enter the refractive block at an angle. This means that the wavelet angle will be refracted upon passing through the surface of the RB. The angle of refraction of a moving block cannot be determined by Snell's law alone – it is much more complicated.

Before calculating exactly how a beam refracts in a moving medium, we will first derive the general term for the velocity of light in a moving medium where the angle between the wavelet path and the velocity of the medium is an arbitrary angle between 0 and π.

In the rest frame of the medium, the geometry is as shown in Figure 5. The path AB is that of a laser beam propagating a distance L in a medium with an index of refraction of n. The source A and destination B are on opposite ends of an arm

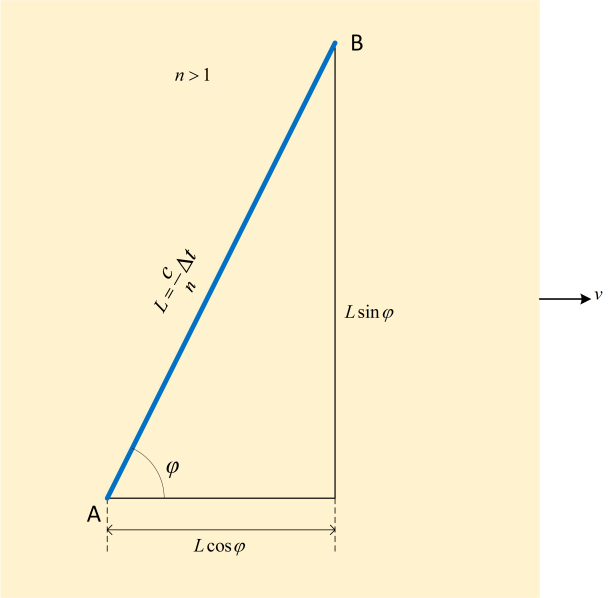

Fig. 5: Beam path at arbitrary angle in rest frame of medium.

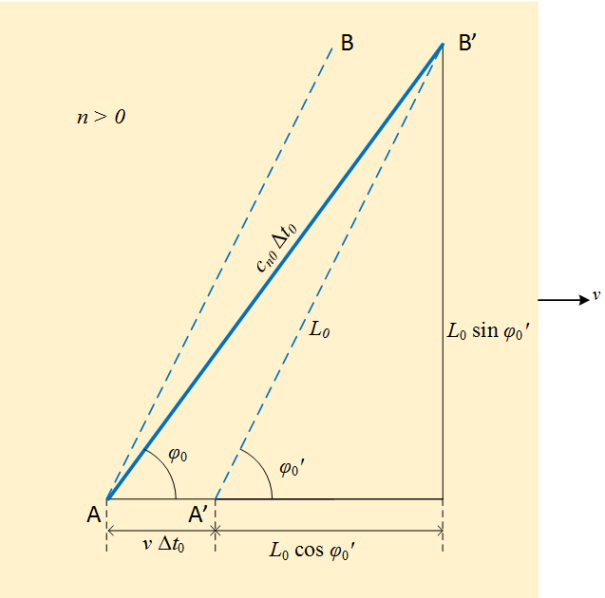

Fig. 6: Wavelet path at arbitrary angle in absolute frame.

of the experiment. The arm and the medium are both moving in the direction shown at velocity v with respect to the rest frame. The values given in the figure are for measurements made by an observer within the moving frame. In this frame, the time for a wavelet in the beam to travel from the source to the destination is by definition of the index of refraction n,

$$\Delta t = \frac{L\,n}{c}. \tag{26}$$

Figure 6 shows the path of the same wavelet if the beam is observed from the rest frame. The dotted lines show the instantaneous positions of the ensemble of wavelets that make up the beam at two different times. And the angle φ_0' is the angle that the visible composite beam makes with the velocity. The bold solid line shows the path that an individual wavelet takes.

In the moving frame, the clocks at A and B are assumed to have been synchronized using Einstein's method. As we derived earlier, synchronizing the clocks in the moving frame will create a bias between the clocks when observed from the rest frame:

$$t_{0bias} = \frac{v\,L\,\cos\varphi}{c^2}. \tag{27}$$

Taking this into account and also accounting for the fact that clocks run slower in the moving frame, the time for a wavelet to propagate from A to B′ in the rest frame is

$$\Delta t_0 = (\Delta t - t_{0bias})\,\gamma = \left(\frac{L\,n}{c} + \frac{v\,L\,\cos\varphi}{c^2}\right)\gamma. \tag{28}$$

Length contraction in the direction of the velocity causes the angle φ in the moving frame to increase to φ_0' in the rest frame (beam and wavelet path are the same within the moving frame). The length of the arm L will decrease in the rest frame to L_0:

$$L_0 = L\sqrt{\frac{\cos^2\varphi}{\gamma^2} + \sin^2\varphi}. \tag{29}$$

Since lengths do not contract in directions orthogonal to the velocity,

$$L\,\sin\varphi = L_0\,\sin\varphi_0'. \tag{30}$$

From the right triangle with hypotenuse AB′ in Figure 6, we get the following relationship for angle φ_0:

$$\sin\varphi_0 = \frac{L\,\sin\varphi}{c_{n0}\,\Delta t_0}. \tag{31}$$

Pythagorean's Theorem requires that

$$(c_{n0}\Delta t_0)^2 = \left(v\,\Delta t_0 + L_0\sin\varphi_0'\right)^2 + \left(L_0\sin\varphi_0'\right)^2. \tag{32}$$

Using equations (30), (31) and (32) we can solve for c_{n0} and $\sin\varphi_0$:

$$c_{n0} = \sqrt{\frac{L_0^2}{\Delta t_0^2} + v^2 \pm \frac{2\sqrt{\left(L_0^2 - L^2\sin^2\varphi\right)v^2}}{\Delta t_0}}, \tag{33}$$

$$\sin\varphi_0 = \frac{L\sin\varphi}{\sqrt{\frac{L_0^2}{\Delta t_0^2} + v^2 \pm \frac{2\sqrt{\left(L_0^2 - L^2\sin^2\varphi\right)v^2}}{\Delta t_0}}}. \tag{34}$$

Substituting equations (28) and (29) into these equations, results in solutions involving only the angle φ in the rest frame of the medium:

$$c_{n0} = c\sqrt{1 - \frac{n^2 - 1}{\gamma^2 (n + \beta\cos\varphi)^2}}\,, \tag{35}$$

$$\sin\varphi_0 = \frac{\sin\varphi}{\sqrt{\gamma^2 (n + \beta\cos\varphi)^2 - n^2 + 1}}\,. \tag{36}$$

From which we can also calculate the cosine:

$$\cos\varphi_0 = \sqrt{1 - \frac{\sin^2\varphi}{\gamma^2 (n + \beta\cos\varphi)^2 - n^2 + 1}}\,. \tag{37}$$

Equation (35) is the speed of an individual wavelet as measured in the rest frame when the medium (i.e. laboratory) is moving at velocity $v = c\beta$. It demonstrates that there is not a unique index of refraction $n_0 = c/c_{n0}$ for a moving medium. The speed of light through the medium is a function of both the velocity of the medium and the angle which the beam makes with that velocity. Cahill ignored the "drag" component and assumed the velocity in the moving medium was the same c/n as in the stationary medium. This is what introduced his error.

The angle φ is the angle as measured in the moving frame between the velocity of the frame and the direction of the light waves. Equations (36) and (37) describe the angle φ_0 at which the light waves are moving in the rest frame in terms of φ in the moving frame.

The velocity of the light wavelets can be separated into two components, one parallel to the laboratory velocity and one orthogonal to the laboratory velocity. In Figure 6, these two components are

$$\left.\begin{aligned} c_{n0\perp} &= c_{n0}\sin\varphi_0, \\ c_{n0\parallel} &= c_{n0}\cos\varphi_0 \end{aligned}\right\}. \tag{38}$$

Substituting equations (35), (36) and (37) into these equations gives us the expressions for the parallel and orthogonal components of wavelet velocity in the rest frame:

$$\left.\begin{aligned} c_{n0\perp} &= \frac{c}{n}\left(\frac{\sin\varphi}{\gamma\left(1 + \frac{\beta}{n}\cos\varphi\right)}\right) \\ c_{n0\parallel} &= \frac{c}{n}\left(\frac{\cos\varphi + \beta n}{1 + \frac{\beta}{n}\cos\varphi}\right) \end{aligned}\right\}. \tag{39}$$

With the parallel and orthogonal components of the velocity, we know everything about the velocity and direction of the wavelets within the moving medium. We are now ready to investigate how this affects the refraction of a beam that is entering a moving medium as observed from the rest frame.

4.3 Refraction of light entering a moving refractive medium

For our analysis of refraction, we will refer to Figure 7 where we have added the incident and refracted angles. This figure again shows a moving refractive medium with index of refraction n as measured in the moving frame. A laser source is attached to and moving along with the refractive medium. Both the medium and the laser are moving at velocity v in the rest frame in the direction shown, which is orthogonal to the line which is normal to the refractive surface. The line normal to the refractive surface will be referred to as the normal line. The medium is shown at two different positions separated in time. The laser source is shown at three different times.

The dotted lines leaving the laser again show the location of the ensemble of wavelets that make up the composite visible laser beam at these times. This is the apparent path of the laser beam. The bold line shows the path that is actually taken by an individual wavelet or photon within the beam in propagating from the source to A and then through the medium to B′.

It is readily apparent that the relationship between the angles is

$$\theta_{r0\perp} = \frac{\pi}{2} - \varphi_0. \tag{40}$$

This can be expressed as

$$\left.\begin{aligned} \sin\varphi_0 &= \cos\theta_{r0\perp} \\ \cos\varphi_0 &= \sin\theta_{r0\perp} \end{aligned}\right\}. \tag{41}$$

These angles as measured in the moving frame will have a similar relationship:

$$\left.\begin{aligned} \sin\varphi &= \cos\theta_{r\perp} \\ \cos\varphi &= \sin\theta_{r\perp} \end{aligned}\right\}. \tag{42}$$

From Snell's law, the incident and refracted angles in the moving frame (i.e. in the rest frame of the RB) are related by

$$\sin\theta_{i\perp} = n\,\sin\theta_{r\perp}. \tag{43}$$

Substituting this into equations (42) results in

$$\left.\begin{aligned} \sin\varphi &= \sqrt{1 - \frac{\sin^2\theta_{i\perp}}{n^2}} \\ \cos\varphi &= \frac{\sin\theta_{i\perp}}{n} \end{aligned}\right\}. \tag{44}$$

Substituting these into equations (39) gives us the parallel and orthogonal components of the wave velocity in the rest frame as a function of the incident angle in the moving frame:

$$c_{n0\parallel} = \frac{c}{n}\left(\frac{\sin\theta_{i\perp} + \beta n^2}{n + \frac{\beta}{n}\sin\theta_{i\perp}}\right) \tag{45}$$

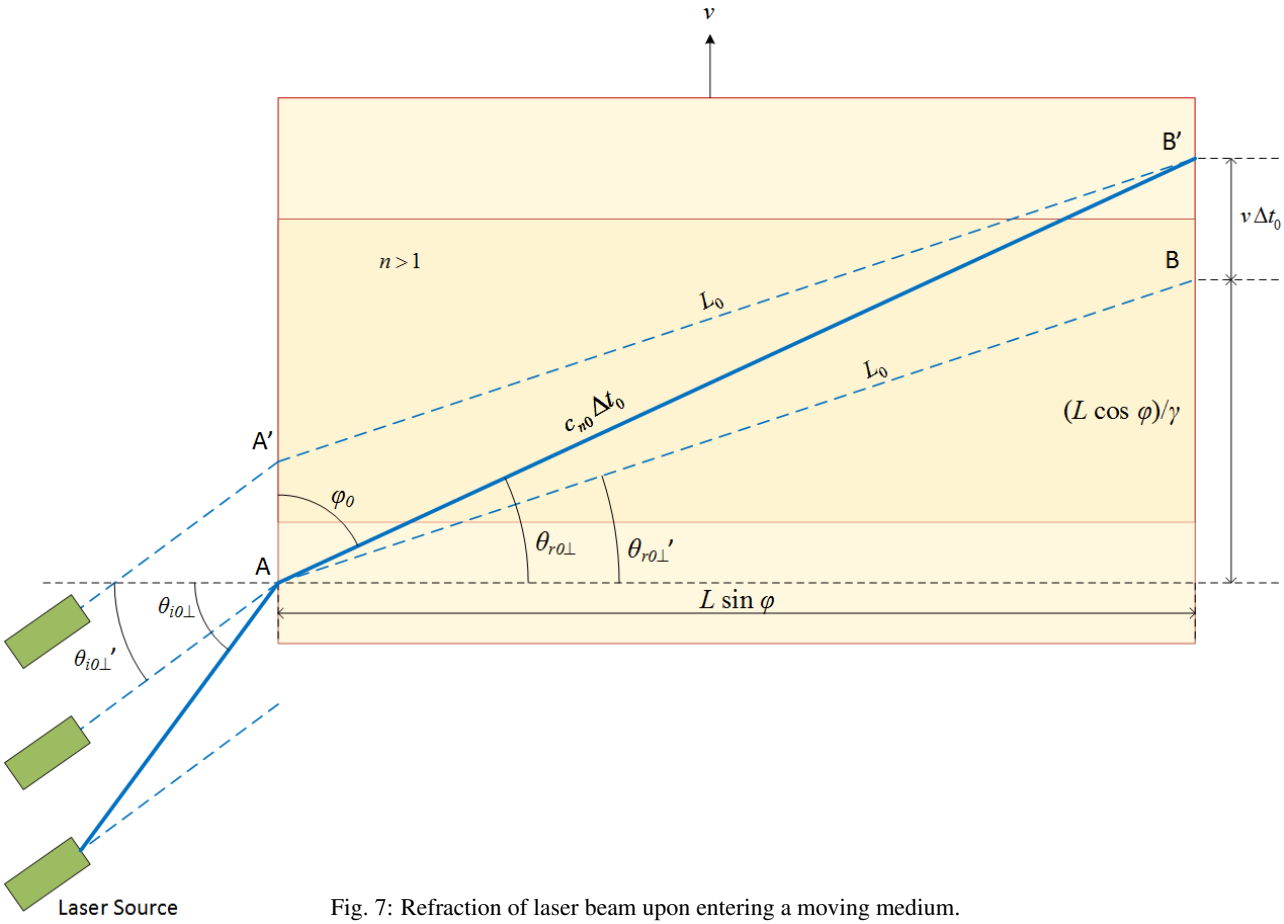

Fig. 7: Refraction of laser beam upon entering a moving medium.

$$c_{n0\perp} = \frac{c}{n}\left[\frac{n\sqrt{1-\dfrac{\sin^2\theta_{i\perp}}{n^2}}}{\gamma\left(n+\dfrac{\beta}{n}\sin\theta_{i\perp}\right)}\right]. \tag{46}$$

A similar set of equations can be obtained when the velocity is parallel to the normal line. Although the parallel case is not shown in the figure, it is easy to see that in this case the refracted angle is equal to φ_0 so that

$$\left.\begin{aligned}\sin\varphi = \sin\theta_{r\parallel} &= \frac{\sin\theta_{i\parallel}}{n}\\ \cos\varphi = \cos\theta_{r\parallel} &= \sqrt{1-\frac{\sin^2\theta_{i\parallel}}{n^2}}\end{aligned}\right\}. \tag{47}$$

Substituting these into equation (39) gives the orthogonal and parallel components of the wave velocity for the parallel orientation:

$$c_{n0\parallel} = \left(\frac{c}{n}\right)\frac{\left(n\beta+\sqrt{1-\dfrac{\sin^2\theta_{i\parallel}}{n^2}}\right)}{1+\dfrac{\beta}{n}\sqrt{1-\dfrac{\sin^2\theta_{i\parallel}}{n^2}}}, \tag{48}$$

$$c_{n0\perp} = \left(\frac{c}{n}\right)\frac{\sin\theta_{i\parallel}}{\gamma\left(n+\beta\sqrt{1-\dfrac{\sin^2\theta_{i\parallel}}{n^2}}\right)}. \tag{49}$$

We now have a complete description of how an incident wave is refracted when it enters a moving refractive medium. Equations (45) and (46) govern the refraction if the medium is moving orthogonal to the normal line. Equations (48) and (49) govern when the medium is moving parallel to the normal line.

4.4 Refraction with $\theta_i = 0$ and velocity orthogonal to beam

With the general equations derived, we are now ready to analyze the specific situation of this experiment. The incident angle, as measured in the moving frame (i.e. rest frame of the medium) is zero whether the direction is orthogonal or parallel:

$$\theta_{i\parallel} = \theta_{i\perp} = 0. \tag{50}$$

Substituting these into the expressions for the wave velocity components when the velocity is orthogonal to the normal

line (Equations (45) and (46)), we get

$$c_{n0\parallel} = \frac{c}{n}\left(\frac{\beta n^2}{n}\right) = v, \tag{51}$$

$$c_{n0\perp} = \frac{c}{n}\left[\frac{n\sqrt{1}}{\gamma(n)}\right] = \frac{c}{n\gamma}. \tag{52}$$

And for the case when the velocity is parallel to the normal line (Equations (48) and (49)), we have

$$c_{n0\parallel} = \left(\frac{c}{n}\right)\frac{(n\beta+1)}{1+\frac{\beta}{n}} = \frac{c+cn\beta}{n+\beta} = \frac{c(c+nv)}{cn+v}, \tag{53}$$

$$c_{n0\perp} = 0. \tag{54}$$

We already derived this expression for the parallel case in equation (14). We repeat it here to show that equations (48) and (49) are consistent with the earlier derivation.

The angle of propagation in the parallel case is 0, but in the orthogonal case it is defined by

$$\sin\varphi_0 = \frac{c_{n0\parallel}}{\sqrt{{c_{n0\parallel}}^2 + {c_{n0\perp}}^2}} = \frac{v}{\sqrt{v^2 + \dfrac{c^2}{n\gamma^2}}}. \tag{55}$$

Equations (51) and (52) are quite remarkable. Equation (51) shows that the velocity component of the wave velocity that is parallel to the medium velocity v is always exactly equal to v. It is completely independent of the index of refraction n. This is what guarantees that the path that a wave takes through the medium will not change relative to the medium no matter how fast the source and medium are moving or no matter what the index of refraction is. This is why observers in the medium cannot detect any change in the trajectory of the waves when their velocity changes.

Equation (52) gives the component of wave speed that is orthogonal to the velocity of the medium. This is the term that guarantees that the time measured for the wave to pass through the medium is always measured to be c/n in the moving frame (the rest frame of the medium). For example, if the laboratory is at rest the velocity of a wave is c/n, and the time to pass through a block that is of length L is Ln/c. If the laboratory is then accelerated to a velocity of v in the orthogonal direction, the clocks in that frame slow so that the time Ln/c becomes $Ln\gamma/c$. But from equation (52) we see that the orthongonal component of the wave speed slows down by the same factor of γ so that the time measured in the laboratory to traverse length L remains at Ln/c.

5 Calculating time delays and phase shifts

Knowing the incident wavelengths, velocities and directions, we can calculate the change in phase shift that occurs with velocity. The only place that the phase can be different between the two paths is when the beam is passing through the refractive block. The distance that the unrefracted beam races ahead of the refracted wave while the refracted wave is slowed down by the RB is proportional to the phase difference between the two paths.

We will begin by analyzing the parallel direction where the velocity of the medium and velocity of the light beam are aligned.

5.1 Time delay and phase shift with light beam parallel to velocity

In this case, the laboratory is moving at velocity v with the light beam parallel to the velocity. The length of the RB will contract to

$$L_{0\parallel} = \frac{L}{\gamma}. \tag{56}$$

The velocity of the light within the refractive material, with respect to the rest frame, is given by equations (53) and (54):

$$\left.\begin{aligned} c_{n0\parallel} &= \frac{c}{n}\left(\frac{1+\beta n}{1+\dfrac{\beta}{n}}\right) = \frac{c(c+nv)}{cn+v} \\ c_{n0\perp} &= 0 \end{aligned}\right\}. \tag{57}$$

The refractive block itself is moving at velocity v, so the effective velocity of the light with respect to the RB is

$$c_{n0\parallel e} = c_{n0\parallel} - v = \frac{c(c+nv)}{cn+v} - v = \frac{c}{\gamma^2}\left(\frac{1}{n+\beta}\right). \tag{58}$$

At this relative velocity, the total time it takes a wave to propagate through the RB is

$$\Delta t_{0\parallel} = \frac{L_{0\parallel}}{c_{n0\parallel e}} = \frac{L}{\gamma\dfrac{c}{\gamma^2}\left(\dfrac{1}{n+\beta}\right)} = \frac{L(n+\beta)\gamma}{c}. \tag{59}$$

The total distance a wavelet propagates in the parallel direction while inside the RB is measured in the rest frame to be

$$\Delta x_{0\parallel} = \frac{L}{\gamma} + v\,\Delta t_{0\parallel} = \frac{L}{\gamma} + L\beta(n+\beta)\gamma = L\gamma(1+n\beta). \tag{60}$$

The total distance the unrefracted beam propagates in this same time is

$$\Delta x_{0u\parallel} = c\,\Delta t_{0\parallel} = L(n+\beta)\gamma. \tag{61}$$

The difference between these two distances for the refracted and unrefracted paths is the spatial phase shift that occurred between the two waves as a result of the path through the RB:

$$\Delta x_{\parallel} = \Delta x_{0\parallel} - \Delta x_{0u\parallel} = L\gamma(n-1)(1-\beta). \tag{62}$$

Dividing this difference by the wavelength of the incident wave gives the phase shift in wavelengths in the parallel orientation:

$$k_{\parallel} = \frac{L}{\lambda_{i0\parallel}}\,\gamma\,(n-1)\,(1-\beta)\,. \tag{63}$$

This is a scalar value. Like the number of marbles in a bowl, it is the same for all observers in all frames. It represents the phase difference between the refracted path and the unrefracted path in the parallel direction as measured in wavelengths.

Since it is an invariant, we should be able to verify that it is the same value as measured in the moving frame. The phase shift in that frame that would be expected is

$$k_{\parallel} = \left(c - \frac{c}{n}\right)\frac{\Delta t}{\lambda_i} = \left(c - \frac{c}{n}\right)\left(\frac{L\,n}{\lambda_i\,c}\right) = \frac{L}{\lambda_i}\,(n-1)\,. \tag{64}$$

To show that equations (63) and (64) are, in fact, the same scalar value, we note that the frequency of the laser source will be reduced in the rest frame and there will also be a Doppler shift of the wavelength in that frame. Thus, the wavelength of the incident wave in the rest frame is

$$\lambda_{i0\parallel} = \lambda_i\,\gamma\,(1-\beta) = \lambda_i\sqrt{\frac{(1-\beta)^2}{(1+\beta)\,(1-\beta)}} = \lambda_i\sqrt{\frac{1-\beta}{1+\beta}}. \tag{65}$$

Substituting this into equation (63) gives the total phase shift in wavelengths between the two paths in the parallel orientation:

$$k_{\parallel} = \frac{L}{\lambda_i}\sqrt{\frac{1+\beta}{1-\beta}}\,\gamma\,(n-1)\,(1-\beta) = \frac{L}{\lambda_i}\,(n-1)\,. \tag{66}$$

This is, of course, the same scalar value measured in the moving frame in equation (64). The interesting thing about this number is that it is completely independent of the velocity of the medium. That is just another way of saying that no matter what the velocity of the frame, all observers will always measure exactly the same phase shift.

Notice that k is a very large number since L is measured in meters and the wavelength is measured in hundreds of nanometers. This number is not measurable by the interferometer. It is only able to measure *differences* in phase. Fortunately it is the difference between the orthogonal and parallel phase shifts that we are interested in. We will now repeat the above procedure to determine the phase shift for the orthogonal direction.

5.2 Time delay and phase with the light beam orthogonal to velocity

When the light beam is orthogonal to the velocity of the laboratory, no contraction occurs and the length of the RB remains at its rest length of L. Since the individual wavelets are moving through the RB at an angle, the time that it takes for an individual wavelet to travel through the block is determined by the component of its velocity that is parallel to the normal line.

This is obtained from equation (52):

$$c_{n0\,\perp} = \frac{c}{n\,\gamma}. \tag{67}$$

Of course, it propagates a distance L in this direction at this speed. Since the velocity of the laboratory is orthogonal to the RB, this is also the velocity of a wave relative to the RB. The total time for a wave to propagate through the RB is

$$\Delta t_{0\perp} = \frac{L}{c_{n0\perp}} = \frac{L\,n\,\gamma}{c}. \tag{68}$$

During this same time, the unrefracted beam is propagating at speed c but not exactly orthogonal. It's velocity in the orthogonal direction is also given by equation (52), but with $n = 1$, since it is moving through vacuum:

$$c_{n0u\perp} = \frac{c}{\gamma}. \tag{69}$$

The distance that the unrefracted beam travels in this time is

$$\Delta x_{0u\perp} = \frac{c}{\gamma}\,\Delta t_{0\perp} = \frac{c}{\gamma}\,\frac{L\,n\,\gamma}{c} = L\,n. \tag{70}$$

The difference between the two distances is

$$\Delta x_{\perp} = \Delta x_{0u\perp} - \Delta x_{0\perp} = n\,L - L = L\,(n-1)\,. \tag{71}$$

We divide this by the wavelength in the orthogonal direction to get the total phase shift:

$$k_{\perp} = \frac{L}{\lambda_{i0\perp}}\,(n-1)\,. \tag{72}$$

For calculating $\lambda_{i0\perp}$ we must again account for the longer wavelength due to the slowing of the frequency source. While there is no Doppler shift orthogonal to a moving source, we must consider the change in wavelength due to the angle at which it is propagating in the rest frame. So

$$\lambda_{i\,0\perp} = \lambda_i\,\gamma\,\cos\theta_{i\,0\perp}. \tag{73}$$

Since this wavelength is measured in vacuum while the wave is moving at velocity c, from equation (69), we see that

$$\cos\theta_{i\,0\perp} = \frac{c/\gamma}{c} = \frac{1}{\gamma}. \tag{74}$$

Thus, $\lambda_{0_{\perp}} = \lambda_i$ and the total phase shift in wavelengths from equation (72) becomes

$$k_{\perp} = \frac{L}{\lambda_i}\,(n-1)\,. \tag{75}$$

Comparing this to the phase shift for the parallel case in equation (66), we see that they are identical. We have now proven mathematically that regardless of whether or not the experiment is performed in vacuum or in a refractive medium there is no difference in phase between the two orientations — it will always be a null experiment.

6 Numerical values of Cahill's predictions

Cahill, on the other hand, predicted that there will be a measurable phase difference. Cahill predicts in his equation (11) in [1] that the time difference between the two paths will approximate to his equation (12). Again using a "C" in the subscripts to indicate Cahill's predictions, his time difference is

$$\Delta t_C \approx L n \left(n^2 - 1\right)\left(\frac{\beta^2}{c}\right). \tag{76}$$

But this is for a two-way experiment. Our experiment is a one-way measurement. Cahill's one-way time in the parallel direction through the refractive block is derived from his equations (1) and (2):

$$\Delta t_{0\parallel C} = \frac{L n}{c}\left(\frac{1}{\gamma\,(1 - n\beta)}\right). \tag{77}$$

His time in the orthogonal direction is given in his equation (8) in [1]:

$$\Delta t_{0\perp C} = \frac{L n}{c}\left(\frac{1}{\sqrt{1 - n^2\,\beta^2}}\right). \tag{78}$$

Both of these times are as measured in the rest reference frame and represent the total time between a wavelet entering the refractive block until it exits.

According to Cahill, the speed of light in the refractive material is approximately c/n in both cases and Fresnel drag is insignificant. In the orthogonal case, from his Figure 1 (b) this requires that the direction of the wave is actually at an angle that satisfies the equations

$$\left.\begin{aligned} \sin\theta_{r0\perp C} &= \frac{v\,n}{c} \\ \cos\theta_{r0\perp C} &= \sqrt{1 - \left(\frac{v\,n}{c}\right)^2} = \sqrt{1 - n^2\,\beta^2} \end{aligned}\right\}. \tag{79}$$

Therefore the distances traveled in the parallel and orthogonal directions during the times of equations (77) and (78) are respectively

$$\left.\begin{aligned} \Delta x_{0\parallel C} &= \frac{c}{n}\Delta t_{0\parallel} = \frac{L}{\gamma\,(1 - n\beta)} \\ \Delta x_{0\perp C} &= \frac{c}{n}\,\Delta t_{0\perp}\cos\theta_{r0\perp} \\ &= L\left(\frac{1}{\sqrt{1 - n^2\beta^2}}\right)\sqrt{1 - n^2\,\beta^2} = L \end{aligned}\right\}. \tag{80}$$

On the other hand, the distances traveled by the light in the unrefracted paths in these times are

$$\left.\begin{aligned} \Delta x_{0u\parallel C} &= c\,\Delta t_{0\parallel} = \frac{L n}{\gamma\,(1 - n\beta)} \\ \Delta x_{0u\perp C} &= c\,\Delta t_{0\perp}\cos\theta_{i0\perp} = \frac{L n}{\gamma}\left(\frac{1}{\sqrt{1 - n^2\,\beta^2}}\right) \end{aligned}\right\}. \tag{81}$$

For each direction, respectively, the differences between the refracted and unrefracted lengths are

$$\left.\begin{aligned} \Delta x_{\parallel C} &= \Delta x_{0u\parallel C} - \Delta x_{0\parallel C} = \frac{L}{\gamma\,(1 - n\beta)}\,(n - 1) \\ \Delta x_{\perp C} &= \Delta x_{0u\perp C} - \Delta x_{0\perp C} = L\left(\frac{n}{\gamma\,\sqrt{1 - n^2\beta^2}} - 1\right) \end{aligned}\right\}. \tag{82}$$

Using equation (65) for the parallel incident wavelength (orthogonal incident wavelength is unchanged), we can convert these distances to wavelengths:

$$\left.\begin{aligned} k_{\parallel C} &= \frac{\Delta x_{\parallel C}}{\lambda_{i0\,\parallel C}} = \frac{L}{\gamma\,\lambda_i\,(1 - n\beta)}\,(n - 1)\,\sqrt{\frac{1 + \beta}{1 - \beta}} \\ k_{\perp C} &= \frac{\Delta x_{\perp C}}{\lambda_{i0\,\perp C}} = \frac{L}{\lambda_i}\left(\frac{n}{\gamma\,\sqrt{1 - n^2\beta^2}} - 1\right) \end{aligned}\right\}. \tag{83}$$

The total phase shift predicted by Cahill's equations is the difference between these two values, which simplifies to

$$\Delta k_C = \frac{L}{\lambda_i\,(1 - n\beta)}\left(n - \beta - \frac{n}{\gamma}\sqrt{\frac{1 - n\beta}{1 + n\beta}}\right). \tag{84}$$

In this experiment

$$L = 1\text{ m} \qquad n = 1.33 \qquad \lambda_i = 650\text{ nm}. \tag{85}$$

Cahill claims that the original MM experiment measured a velocity of about 360 km/sec. Thus,

$$v = 3.6 \times 10^5 \qquad \Rightarrow \qquad \beta = 0.0012. \tag{86}$$

Substituting all these values into equation (84) gives us the phase shift that Cahill predicts for this experiment:

$$\Delta k_C = 1421\text{ wavelengths}. \tag{87}$$

This is an enormous phase difference which would easily be detected by this experiment if it existed.

7 Results of experiment

The present experiment is capable of measuring phase differences with a resolution of about 0.1 wavelengths. The phase shift was measured between a north-south orientation and an east-west orientation each hour for 12 hours. Had there been any significant velocity difference in any direction, one or more of these measurements would have been able to detect it.

The peak phase difference (after averaging) was measured to be 0.1 wavelengths at 10 a.m. This is within the error tolerance of the experiment and is therefore not statistically different from zero. After averaging the 10 measurements at each time, the measured phase shifts in wavelengths are graphed in Figure 8.

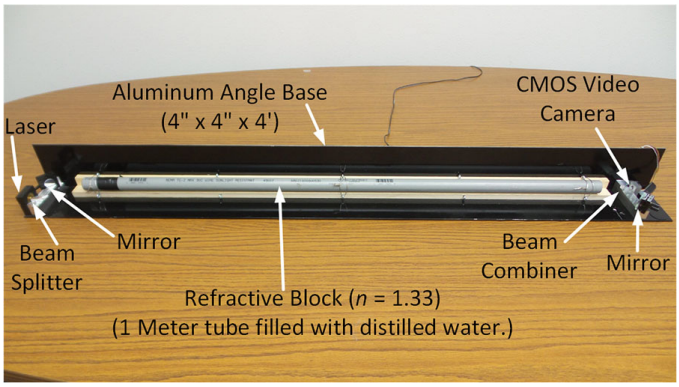

Fig. 9: Overview of interferometer system.

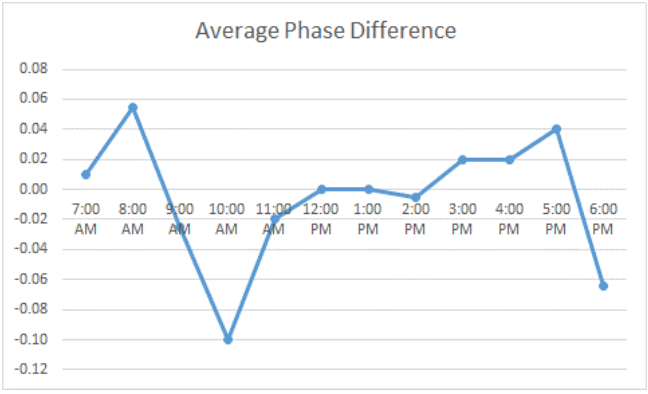

Fig. 8: Measured phase shift.

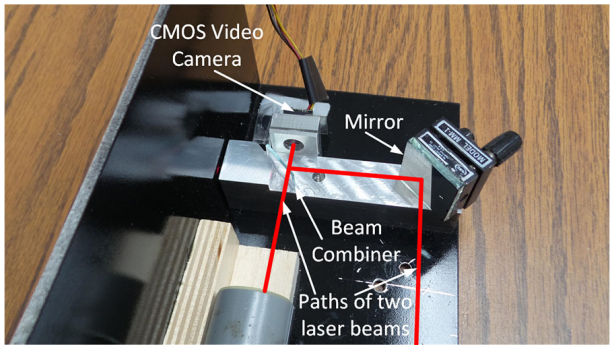

Fig. 10: Closeup of camera/detector end.

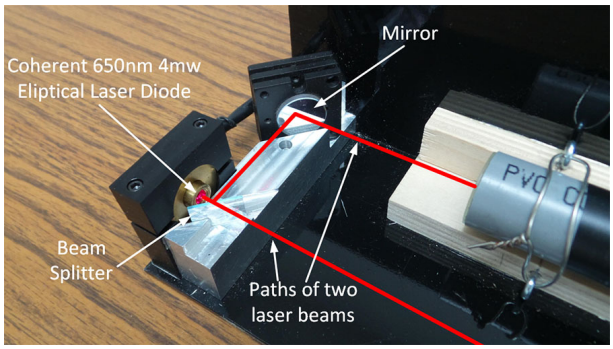

Fig. 11: Closeup of laser diode end.

The results of this experiment are the "final arbiter" and clearly rule in favor of the derivation in this paper and against Cahill's derivation. The measured phase shifts are 4 orders of magnitude less than those predicted by Cahill and they are within the measurement tolerances of the null prediction of this paper. We can conclude that the mathematical derivations in this paper are correct and that it is impossible to detect the absolute velocity of the earth using MM type experiments regardless of the index of refraction of the medium used.

8 Description and procedures of experiment

Figures 9, 10 and 11 show actual annotated photographs of the interferometer system used in the experiment. It is arranged according to the layout shown in Figure 1. Not shown in these pictures are two polarizers — one at the output of the laser and one at the input to the camera. These were rotated relative to one another to attenuate the light to just the right brightness so that the camera image was optimized for visualization of the fringe pattern. Without them the image was too bright and the camera's CMOS detector bloomed to an all-white image.

8.1 Measurement considerations

The fringe shifts are measured by displaying the output of the camera on a computer monitor. Figure 12 shows the camera output plus two drafting triangles that were placed on the monitor as references to assist in measuring fringe movement.

The entire system is mounted on a 4-foot (1.22 m) aluminum base that is painted black. The thermal expansion coefficient of aluminum causes it to expand about 29 μm per degree C. That is 45 wavelengths of light per degree C or about one half wavelength for each hundredth of a degree C.

Fig. 12: Fringe pattern output from camera.

An even larger sensitivity occurs due to the fluctuations in barometric pressure which change the index of refraction of the air. Because of this extreme sensitivity to temperature and pressure, there is a constant drifting of the fringe patterns that must be taken out of the measurement.

To minimize the thermal drift, the following mitigating techniques were employed:

1. The entire interferometer was placed inside a cardboard tubular shipping container and sealed on both ends.
2. The system was allowed to warm up and reach a stable temperature prior to making any measurements.
3. The measurements were taken inside a room with no outside walls or windows.
4. The heating and air conditioning system was turned off so that only slow, convection heating from outside the building could affect the temperature inside the room.
5. A 4 foot wooden dowel was used to rotate the system so that human body temperature was kept away from the system.
6. The system was rotated very slowly (about 30 seconds for a 90 degree rotation) to minimize the cooling and pressure effects of the air flow.

By doing all of these things, the drift was reduced to significantly less than 1 fringe per minute (probably mostly due to barometric pressure drift), which was easy to remove from the measurements.

Mechanical disturbances were minimized by placing the system on pillows and attaching it to a rotatable platform with a bungee cord pressing it into the pillows. The platform is made from an aluminum trailer hitch-mounted cargo carrier with the hitch attachment removed. The platform was mounted to the base of a rotating office chair (after removing the seat) so that it could be rotated very smoothly and with little effort. The pillows prevented any residual vibrations of the platform from propagating to the interferometer. The result is that almost no vibrations affected the fringes so they were very easy to follow as they drifted slowly across the screen.

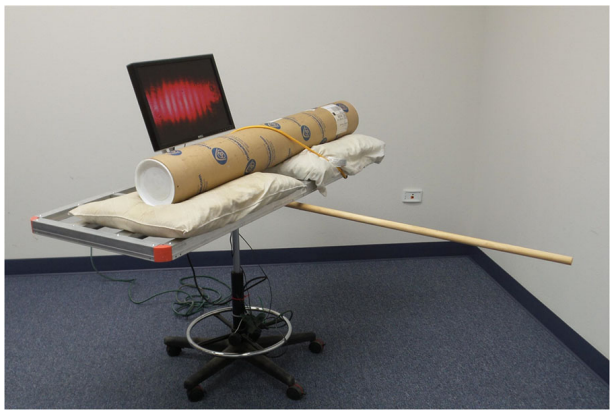

Fig. 13: Complete system with vibrational and thermal mitigation.

Figure 13 shows the system after employing these temperature and vibration mitigating techniques. The interferometer is sealed inside the tubular cardboard shipping container with the camera output coming through a small hole in the back of the container into the monitor.

8.2 Measurement procedure

To improve accuracy and resolution, 10 measurements were made at 1 hour intervals for 12 hours – which corresponds to 10 measurements every 15 degrees of earth's rotation for 180 degrees total rotation. The measurements were performed in Longmont, Colorado between 7 am and 6 pm on September 22 and 23, 2015. The following procedure was used:

1. Turn on the system and let it warm up for 2 hours.
2. At the top of each hour, position the system in a north-south orientation.
3. Place the edge of a triangle in the middle of the fringe nearest to the center of the screen.
4. Very slowly rotate the system clockwise 90 degrees until it reaches an east-west orientation. (about 30 seconds)
5. Estimate the movement of the fringe to the nearest 0.1 wavelength – including any drift that occurred. Record this as phase 1.
6. Reposition the edge of the triangle in the middle of the center fringe.
7. Very slowly rotate the system counterclockwise to return to the north-south orientation.
8. Estimate the movement of the fringe to the nearest 0.1 wavelength – including any drift that occurred. Record this as phase 2.
9. Repeat steps 2 to 8 until 10 pairs of phase 1 and phase 2 measurements have been recorded.
10. Wait until the top of the next hour and repeat steps 2 to 9 until data for 12 hours have been recorded.

After all data were recorded, the phase shift of each measurement was calculated as

$$PhaseShift = \frac{1}{2}\,(Phase1 - Phase2)\,. \tag{88}$$

This removes any drift from the measurement because it will be constant in both phases.* For example, suppose *Phase1* includes a real shift of k and a drift of d. Then when returning, *Phase2* will measure a real shift of $-k$ and the same drift d. The phase shift recorded will be

$$PhaseShiftR = \frac{(k+d)-(-k+d)}{2} = k. \tag{89}$$

This was done for each of the 10 measurements at each hour. The 10 measurements for each hour were averaged. This improves the resolution of the final answer and averages out drift errors due to each "slow" rotation not being exactly the same amount of time. These results are tabulated in Table 1 and were graphed earlier in Figure 8.

Time	Average Phase Shift
7:00	0.01
8:00	0.06
9:00	−0.03
10:00	−0.10
11:00	−0.10
12:00	0.00
13:00	0.00
14:00	−0.01
15:00	0.02
16:00	0.02
17:00	0.04
18:00	−0.06

Table 1: Measured phase shifts.

9 Conclusions

We have now shown both mathematically and experimentally that Michelson-Morely-type interferometer experiments cannot detect the absolute speed of the earth through space regardless of the medium through which the light is propagating. This experiment and the accompanying mathematical analysis show that the conspiracy between Mother Nature and light is complete. They have conspired to make it impossible to detect our absolute speed using light signals.

Acknowledgements

I am sincerely grateful to Doug Klingbeil for his insight and suggestions regarding the optical components. He also designed and machined the aluminum blocks upon which the optical components are mounted. Special thanks also goes to my daughter Lindsea Seaver for her assistance in precisely assembling the apparatus.

Submitted on August 16, 2016 / Accepted on September 4, 2016

References

1. Cahill R.T., Kitto K. Michelson-Morley Experiments Revisited and the Cosmic Background Radiation Preferred Frame. *Apeiron*, April 2003, v. 10(2), 104–117.
2. Cahill R.T. The Michelson and Morley 1887 Experiment and the Discovery of Absolute Motion. *Progress in Physics*, 2005, v. 1(3), 25–29.
3. Cahill R.T. A New Light-Speed Anisotropy Experiment: Absolute Motion and Gravitational Waves Detected. *Progress in Physics*, 2006, v. 2(4), 73–92.
4. Cahill R.T. Absolute Motion and Gravitational Effects. *Apeiron*, 2004, v. 11(1), 53–111.
5. Roberts T.J. An Explanation of Dayton Miller's Anomalous "Ether Drift" Result. arXiv: physics/0608238.

*The rate of change of the temperature and the pressure are assumed to be nearly constant over the 1 minute required to take each measurement.

Dark Matter, the Correction to Newton's Law in a Disk

Yuri Heymann

3 rue Chandieu, 1202 Geneva, Switzerland. E-mail: y.heymann@yahoo.com

The dark matter problem in the context of spiral galaxies refers to the discrepancy between the galactic mass estimated from luminosity measurements of galaxies with a given mass-to-luminosity ratio and the galactic mass measured from the rotational speed of stars using the Newton's law. Newton's law fails when applied to a star in a spiral galaxy. The problem stems from the fact that Newton's law is applicable to masses represented as points by their barycenter. As spiral galaxies have shapes similar to a disk, we shall correct Newton's law accordingly. We found that the Newton's force exerted by the interior mass of a disk on an adjacent mass shall be multiplied by the coefficient η_{disk} estimated to be 7.44 ± 0.83 at a 99% confidence level. The corrective coefficient for the gravitational force exerted by a homogeneous sphere at it's surface is 1.00 ± 0.01 at a 99% confidence level, meaning that Newton's law is not modified for a spherical geometry. This result was proven a long time ago by Newton in the shell theorem.

1 Introduction

Dark matter is an hypothetical type of matter, which refers to the missing mass of galaxies, obtained from the difference between the mass measured from the rotational speed of stars using the Newton's law and the visual mass. The visual mass is estimated based on luminosity measurements of galaxies with a given mass-to-luminosity ratio.

The problem of galaxy rotational curves was discovered by Vera Rubin in the 1970s [1–3], with the assistance of the instrument maker Kent Ford. In Figure 1, we show the rotational velocity curve of stars versus the expected rotational velocity curve from visible mass as a function of the radius of a typical spiral galaxy. According to [4], the estimated dark matter to visible matter ratio in the universe is about 5.5.

It has been hypothesized that dark matter is made of invisible particles which do not interact with electromagnetic radiations. The hunt for the dark matter particle has already begun. The Xenon dark matter experiment [5] is taking place in a former gold mine nearly a mile underground in South Dakota. The idea is to find hypothetical dark matter particles underneath the earth to avoid particule interference from the surface.

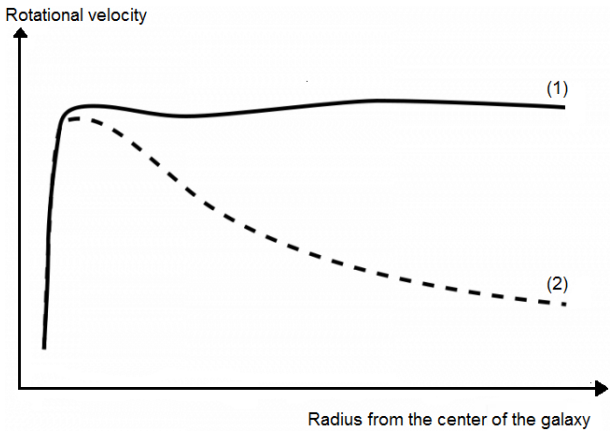

Fig. 1: The problem of galaxy rotational curves, where (1) is the actual rotational velocity curve of stars; and (2) the expected rotational velocity curve from the visible disk.

Other experiments seek dark matter in space. In 2011, NASA lauched the AMS (Alpha Magnetic Spectrometer) experiment, a particle detector mounted on the ISS (International Space Station) aimed at measuring antimatter in cosmic rays and search for evidence of dark matter. In December 2015, the Chinese Academy of Sciences lauched the DAMPE (Dark Matter Particle Explorer), a satellite hosting a poweful space telescope for cosmic ray detection and investigating particles in space and hypothetical dark matter.

An investigation of the amount of planetary-mass dark matter detected via gravitational microlensing concluded that these objects only represent a small portion of the total dark matter halo [6]. The study of the distribution of dark matter in galaxies led to the development of two models of the dark matter halo. These models are known as the dark matter halo profile of Navarro, Frenk and White [7], and the Burkert dark matter halo profile [8, 9].

Dark matter is a hot topic in particle physics, and has led to the development of various theories. According to [10], the favoured candidates for dark matter are axions, supersymmetric particles, and to some extent massive neutrinos. The Majorana fermion has also been proposed as a candidate for dark matter [11, 12]. Other candidates for dark matter would be dark pions, a set of pseudo-Goldstone bosons [13]. Many alternatives have been proposed including modified Newtonian gravity. Mordehai Milgrom proposed the MOND theory, according to which Newton's law is modified for large distances [14, 15]. Moffat proposed a modified gravity theory based on the action principle using field theory [16, 17]. James Feng and Charles Gallo proposed to model galaxy ro-

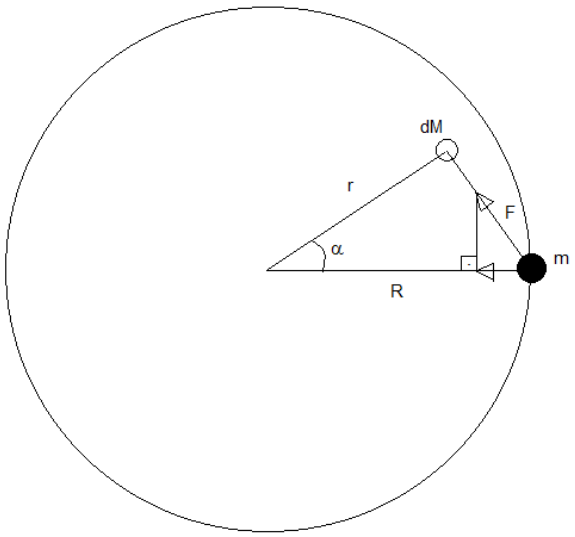

Fig. 2: Force exerted by an infinitesimal mass dM of the disk on a mass m located at the edge of the disk using polar coordinates. The radius of the disk is R. Let the mass dM be at a distance r from the center of the disk. Let α be the angle between the two axis passing by the center of the disk in the direction of the two masses dM and m.

tational curves by applying Newtonian dynamics to a rotating thin disk [18, 19]. Their approach is similar to the route we undertake in the current work, although the latter was done independently.

According to Pavel Kroupa, the dark matter crisis is a major problem for cosmology [20]. In addition, he states that the hypothesis that exotic dark matter exists must be rejected [21]. In the present study we find that dark matter is mainly a problem of geometry because Newton's law is applicable to masses which can be approximated by a point in space. Below, we compute the corrective coefficient to Newton's law in a disk and in a sphere.

2 Calculation of the gravitational force in a disk

The Newton's law states that the gravitational force between two bodies is expressed as follows:

$$F_{\text{Newton}} = \frac{G\,M\,m}{R^2}\,, \tag{1}$$

where G is the gravitational constant, M and m the respective masses of the two bodies in interaction, and R the distance between the barycenters of the two masses.

The shape of spiral galaxies allows us to use the gravitational force computed for a disk. Let us assume a homogeneous disk of surface density ρ_s, and radius R. A mass m is located at the edge of this disk at a distance R from the center of the disk.

In Figure 2, we represent the force exerted by an infinitesimal mass dM of the disk on the mass m using polar coordinates. Because of the symmetry of the disk with respect to

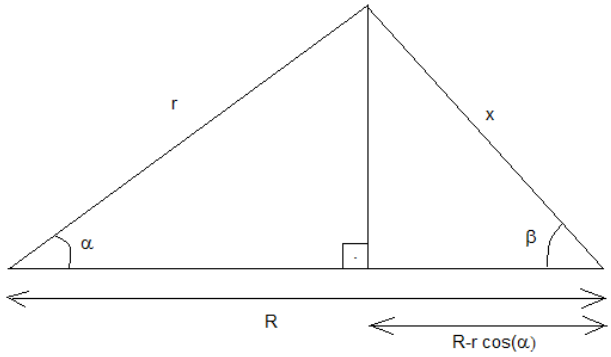

Fig. 3: Triangle to compute the projection of the force exerted by the infinitesimal mass dM on mass m on the axis passing by the center of the disk to the mass m

the axis passing between its center and the mass m, we need to compute the projection of the force exerted by the infinitesimal mass dM on this axis. For this purpose we apply basic trigonometric rules (see figure 3). For convenience, we consider the polar coordinates (r, α) to describe the position of dM, where r is the radial distance, and α the angle between the mass dM and an arbitrary direction as viewed from the center of the disk.

Let us say x is the distance between the mass dM and m. From trigonometry we calculate x as follows:

$$x^2 = r^2 \sin^2\alpha + (R - r\cos\alpha)^2\,. \tag{2}$$

Hence, we get:

$$x^2 = r^2 + R^2 - 2Rr\cos\alpha\,. \tag{3}$$

Let β be the angle between the center of the disk and the mass dM as viewed from the mass m. The angle β is calculated as follows:

$$\cos\beta = \frac{R - r\cos\alpha}{x}\,. \tag{4}$$

By Newton's law, the infinitesimal force exerted by dM on m projected on the axis passing through the center of the disk and the mass m is as follows:

$$dF = \frac{G\,m\,dM}{x^2}\cos\beta\,. \tag{5}$$

Combining (4) and (5), we get:

$$dF = \frac{G\,m\,dM}{x^3}\,(R - r\cos\alpha)\,. \tag{6}$$

Combining (3) and (6), we get:

$$dF = \frac{G\,m\,dM\;(R - r\cos\alpha)}{(r^2 + R^2 - 2Rr\cos\alpha)^{\frac{3}{2}}}\,. \tag{7}$$

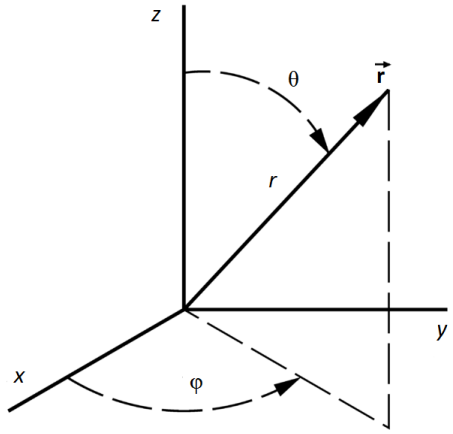

Fig. 4: Spherical coordinate system, where r is the radial distance, θ the polar angle, and φ the azimutal angle.

Because we are using polar coordinates, the surface element dA is as follows:

$$dA = r\,dr\,d\alpha\,. \tag{8}$$

To obtain the infinitesimal mass dM, we multiply the infinitesimal surface dA by the surface density ρ_s; hence, we get:

$$dM = \rho_s\, r\,dr\,d\alpha\,. \tag{9}$$

Therefore, the infinitesimal force dF is as follows:

$$dF = \frac{\rho_s\, G\, m\left(Rr - r^2\cos\alpha\right)}{\left(r^2 + R^2 - 2Rr\cos\alpha\right)^{\frac{3}{2}}}\,dr\,d\alpha\,. \tag{10}$$

Because the total mass of the disk is $M = \rho_s\,\pi\,R^2$, we get:

$$dF = \frac{G\,M\,m}{\pi\,R^2}\,\frac{\left(Rr - r^2\cos\alpha\right)}{\left(r^2 + R^2 - 2Rr\cos\alpha\right)^{\frac{3}{2}}}\,dr\,d\alpha\,. \tag{11}$$

The total force F exerted by the disk on the mass m is obtained by the following integral:

$$F = \frac{G\,M\,m}{\pi\,R^2}\int_{r=0}^{R}\int_{\alpha=0}^{2\pi}\frac{\left(Rr - r^2\cos\alpha\right)}{\left(r^2 + R^2 - 2Rr\cos\alpha\right)^{\frac{3}{2}}}\,dr\,d\alpha\,. \tag{12}$$

We rearrange the terms in the integral to obtain:

$$F = \frac{G\,M\,m}{\pi\,R^2}\times \times\int_{r=0}^{R}\int_{\alpha=0}^{2\pi}\frac{R^2\left(\frac{r}{R} - \left(\frac{r}{R}\right)^2\cos\alpha\right)}{R^3\left(\left(\frac{r}{R}\right)^2 + 1 - 2\left(\frac{r}{R}\right)\cos\alpha\right)^{\frac{3}{2}}}\,dr\,d\alpha\,. \tag{13}$$

Hence:

$$F = \frac{G\,M\,m}{\pi\,R^3}\times \times\int_{r=0}^{R}\int_{\alpha=0}^{2\pi}\frac{\left(\frac{r}{R} - \left(\frac{r}{R}\right)^2\cos\alpha\right)}{\left(\left(\frac{r}{R}\right)^2 + 1 - 2\left(\frac{r}{R}\right)\cos\alpha\right)^{\frac{3}{2}}}\,dr\,d\alpha\,. \tag{14}$$

We apply the change of variable $u = \frac{r}{R}$, hence $dr = R\,du$. Therefore, we get:

$$F = \frac{G\,M\,m}{\pi\,R^2}\int_{u=0}^{1}\int_{\alpha=0}^{2\pi}\frac{\left(u - u^2\cos\alpha\right)}{\left(u^2 + 1 - 2u\cos\alpha\right)^{\frac{3}{2}}}\,du\,d\alpha\,. \tag{15}$$

From (15), we see that in a disk, Newton's force $F_{\text{Newton}} = \frac{G\,M\,m}{R^2}$ needs to be multiplied by the following coefficient:

$$\eta_{disk} = \frac{1}{\pi}\int_{u=0}^{1}\int_{\alpha=0}^{2\pi}\frac{\left(u - u^2\cos\alpha\right)}{\left(u^2 + 1 - 2u\cos\alpha\right)^{\frac{3}{2}}}\,du\,d\alpha\,. \tag{16}$$

3 Calculation of the gravitational force in a sphere

Let us consider a homogeneous sphere of radius R and average mass density ρ. We consider an infinitesimal mass dM of the sphere represented by its spherical coordinates (r, θ, φ), where r is the radial distance, θ the polar angle, and φ the azimuthal angle (see Figure 4). Let the volume of the sphere be defined by the following boundaries: $r \in [0, R]$, $\theta \in [0, \pi]$, and $\varphi \in [0, 2\pi]$. We assume that a mass m is located at the surface of this sphere on the x-axis.

In Cartesian coordinates we have $x = r\sin\theta\,cos\varphi$, $y = r\sin\theta\,sin\varphi$ and $z = r\cos\theta$. Hence, the distance x between the mass dM and m is as follows:

$$x = \sqrt{(R - r\sin\theta\,\cos\varphi)^2 + r^2\sin^2\theta\,\sin^2\varphi + r^2\cos^2\theta}. \tag{17}$$

Let β be the angle as viewed from the mass m between the direction of the center of the sphere and the mass dM. Hence, we get:

$$\cos\beta = \frac{R - r\sin\theta\cos\varphi}{x}\,. \tag{18}$$

The volume element in spherical coordinates is as follows:

$$dV = r^2\sin\theta\,d\theta\,d\varphi\,dr\,. \tag{19}$$

Therefore, the infinitesimal force exerted by dM on m projected in the axis passing through m and the center of the sphere is as follows:

$$dF = \frac{G\,m\,\rho\,r^2\sin\theta\,\cos\beta}{x^2}\,d\theta\,d\varphi\,dr = \frac{G\,m\,\rho\,r^2\sin\theta\,(R - r\sin\theta\cos\varphi)}{x^3}\,d\theta\,d\varphi\,dr\,. \tag{20}$$

Let $M = \rho\frac{4}{3}\pi R^3$ be the total mass of the sphere, hence:

$$F = G\,m\,M\frac{3}{4\pi R^3}\int_{r=0}^{R}\int_{\theta=0}^{\pi}\int_{\varphi=0}^{2\pi}\frac{r^2\sin\theta\,(R - r\sin\theta\,\cos\varphi)}{\left(R^2 + r^2\sin^2\theta\,\cos^2\varphi - 2Rr\sin\theta\,\cos\varphi + r^2\sin^2\theta\,\sin^2\varphi + r^2\cos^2\theta\right)^{\frac{3}{2}}}\,d\theta\,d\varphi\,dr\,. \tag{21}$$

We rearrange the terms in the integral to obtain a function of ratios of r/R, and apply the substition $u = \frac{r}{R}$; hence, we get:

$$F = \frac{G\,m\,M}{R^2}\frac{3}{4\pi}\int_{u=0}^{1}\int_{\theta=0}^{\pi}\int_{\varphi=0}^{2\pi}\frac{u^2\sin\theta\,(1 - u\sin\theta\cos\varphi)}{\left(1 + u^2\sin^2\theta\,\cos^2\varphi - 2u\sin\theta\,\cos\varphi + u^2\sin^2\theta\,\sin^2\varphi + u^2\cos^2\theta\right)^{\frac{3}{2}}}\,d\theta\,d\varphi\,dr\,. \tag{22}$$

Therefore, the corrective coefficient to Newton's law in a sphere is as follows:

$$\eta_{sphere} = \frac{3}{4\pi}\int_{u=0}^{1}\int_{\theta=0}^{\pi}\int_{\varphi=0}^{2\pi}\frac{u^2\sin\theta\,(1 - u\sin\theta\,\cos\varphi)}{\left(1 + u^2\sin^2\theta\,\cos^2\varphi - 2u\sin\theta\,\cos\varphi + u^2\sin^2\theta\,\sin^2\varphi + u^2\cos^2\theta\right)^{\frac{3}{2}}}\,d\theta\,d\varphi\,dr\,. \tag{23}$$

4 Numerical evaluation of the gravitational corrective coefficients

Because the integrals in (16) and (23) do not have a known closed-form solution, we need to evaluate them numerically. Monte Carlo simulation is an appropriate method for computing multidimentional integrals. Using Monte Carlo simulation we can compute both an estimate of the integral and its standard deviation.

4.1 Numerical evaluation of the double integral over the disk

Let us consider the integration of a function $f(r,\alpha)$ over a disk of radius R in polar coordinates, where r is the radius and α an angle from a reference direction. The integral to evaluate is expressed as follows:

$$\int_0^{2\pi}\int_0^{R} f(r,\alpha)\,r\,dr\,d\alpha\,. \tag{24}$$

We shall apply the following change of variables:

$$\alpha = 2\pi u_1\,, \tag{25}$$

and

$$r = R\sqrt{u_2}\,, \tag{26}$$

where u_1 and u_2 are two independent random variables of uniform distribution over [0, 1]. This change of variables gives a uniform distribution on the disk of radius R.

Let N be the number of times we generate the random set (u_1, u_2). Hence, the integral of $f(r,\alpha)$ over the disk converges towards the following estimate for N large:

$$I = \pi R^2\frac{\sum_1^N f_i}{N}\,, \tag{27}$$

where f_i is the function $f(r,\alpha)$ evaluated for each draw of the random set (u_1, u_2) with the change of variables (25) and (26).

Because the variance of a random variable X is given by $Var(X) = E[X^2] - (E[X])^2$ and the variance of the sample mean is $Var(\bar{X}) = \frac{Var(X)}{N}$, the variance of the estimate is computed as follows:

$$\mathrm{Var}(I) = \frac{\pi^2R^4\frac{\sum_1^N f_i^2}{N} - \left(\pi R^2\frac{\sum_1^N f_i}{N}\right)^2}{N}\,. \tag{28}$$

The standard deviation of the estimate of η_{disk} is equal to the square root of the variance of the estimate of the double integral on the disk divided by π. To evaluate the integral in (16), we used the Mersenne Twister pseudo-random number generator [22] with N= 1.2×10^{10}. We obtained $\eta_{disk} = 7.44$ with standard deviation of 0.320.

4.2 Numerical evaluation of the triple integral over the sphere

As for the disk, let us use Monte Carlo simulation to evaluate the triple integral of $f(r,\theta,\varphi)$ over the sphere of radius R in the spherical coordinate system. The integral to evaluate is expressed as follows:

$$\int_0^{R}\int_0^{\pi}\int_0^{2\pi} f(r,\theta,\varphi)\,r^2\,\sin\theta\,d\varphi\,d\theta dr\,. \tag{29}$$

For this pupose we generate a set of three independent random variables (u_1, u_2, u_3), each with a uniform distribution over the interval [0, 1]. We apply the following change of variables, which gives a uniform distribution over the sphere:

$$\theta = 2\arcsin\left(\sqrt{u_1}\right)\,, \tag{30}$$

and

$$\varphi = 2\pi u_2 \,, \tag{31}$$

and

$$r = R\, u_3^{\frac{1}{3}} \,. \tag{32}$$

Let N be the number of time we generate the random set (u_1, u_2, u_3). Hence, the triple integral over the sphere converges towards the following estimate for N large:

$$I = \frac{4\pi R^3}{3} \frac{\sum_1^N f_i}{N} \,, \tag{33}$$

where f_i is the function $f(r, \theta, \varphi)$ evaluated for each draw of the random set (u_1, u_2, u_3) using the change of variables (30), (31) and (32).

The variance of the estimate is computed as follows:

$$\mathrm{Var}(I) = \frac{\left(\frac{4\pi R^3}{3}\right)^2 \frac{\sum_1^N f_i^2}{N} - \frac{4\pi R^3}{3}\left(\frac{\sum_1^N f_i}{N}\right)^2}{N} \,. \tag{34}$$

The standard deviation of the estimate of η_{sphere} is equal to the square root of the variance of the estimate of the triple integral on the sphere multiplied by $\frac{3}{4\pi}$. To evaluate the integral in (23), we used the Mersenne Twister pseudo-random number generator with N= $1{\times}10^8$. We obtained $\eta_{sphere} = 1.00$ with standard deviation of $3.85{\times}10^{-3}$.

5 Interpretation

In the present study, we have solved the dark matter puzzle in the context of spiral galaxies by considering the geometry of massive bodies. Dark matter is a hypothetical mass introduced to fill the discrepancy between galaxy mass as measured from the rotational speed of stars and visible mass. Isaac Newton proved the shell theorem [23], which applies to objects of spherical geometry. The shell theorem states that:

1. A spherical body affects external objects gravitationally as though all of its mass were concentrated in a point at its barycenter.
2. For a spherical body, no net gravitational force is exerted by the external shell on any object inside the sphere, regardless of the position.

Because spiral galaxies have shapes which can be approximated by a disk, the distribution of matter will directly affect the perceived gravitational force for a mass rotating on such a disk, and the shell theorem does not apply. By considering an interior mass distributed in space according to an idealised homogeneous disk, we found that Newton's law is corrected by a multiplicative coefficient. This coefficient is estimated to be about 7.44 based on our calculations above of the dark matter to visible mass ratio of 5.5. This coefficient can be interpreted as if the mass of the disk was excentered towards the object perceiving it. In our calculations, we only considered the interior mass of the disk for radii below the position of the object. For an object located on the disk, the outer mass of the disk for radii above of the position of the object may also exert a gravitational force of opposite direction on the object, mitigating the gravitational force exerted by the interior of the disk. This effect which was not quantified should create the asymptotic behavior for galaxy rotational curves when moving far away from the galaxy's central bulge.

Furthermore, for a spiral galaxy, the mass density may increase as we move closer to the center of the disk, causing a departure from the idealised homogeneous disk. In addition, the closer we move towards the central supermassive black hole, which is spherical, the more the interior mass tends towards a sphere and the gravitational corrective coefficient converges towards unity. The shift in the gravitational corrective coefficient at different radii on the galactic disk ought to explain the observed shape of galaxy rotational curves.

Let us illustrate the impact of the gravitational coefficient we found on the mass of the Milky Way. The centripetal force of a star in orbit is expressed as $F_c = \frac{mv^2}{R}$, where m is the mass of the star, v the tangential velocity and R the radius to the center of the galaxy. Hence, the interior mass of the galaxy for a given star is expressed as $M = \frac{Rv^2}{\eta G}$, where $v = wR$ with w the angular velocity, η the gravitational coefficient, and G the gravitational constant. The apparent mass of the Milky Way was estimated to be around $6.82{\times}10^{11}\ M_\odot$ [24]. Let us approximate the Milky Way by a homogeneous disk; therefore, the gravitational coefficient at the periphery of the disk is about $\eta = 7.44$. This leads to an intrinsic mass of the Milky Way of $9.17{\times}10^{10} M_\odot$.

6 Conclusion

To address the discrepancy between galaxy mass estimated from the rotational velocity of stars and visual mass estimated from luminosity measurements, the existence of dark matter was hypothesized. A number of approaches have taken to hunt for both the dark matter particle and modified gravity. For instance, Milgrom proposed that Newton's law should be modified for large distances. Dark matter remains an unresolved problem challenging cosmology and particle physics.

In the present study, we propose a geometrical approach as Newton's law applies to masses that can be approximated by a point in space corresponding to their barycenter. As spiral galaxies have shapes close to a disk, we derived the corrective coefficient to Newton's law in an idealised disk of homogeneous mass distribution. We found that the Newton's law in a homogeneous disk shall be multiplied by the coefficient η_{disk} estimated to be 7.44 ± 0.83 at a 99% confidence level, which fills the dark matter gap in galaxy haloes. We conclude that dark matter in spiral galaxies is a problem of geometry, and that Newton's law needs to be corrected to account for the geometry of the mass. For a spherical geometry, we found that the corrective gravitational coefficient η_{sphere} is

1.00 ± 0.01 at a 99% confidence level.

This means that the Newton's law is not modified for spherical geometry, which was proven a long time ago by Newton.

Submitted on September 5, 2016 / Accepted on September 7, 2016

References

1. Rubin V.C., Ford W.K. Jr. Rotation of the Andromeda Nebula from a Spectroscopic Survey of Emission Regions *The Astrophysical Journal*, 1970, v. 159, 379–403.
2. Rubin V.C., Thonnard N., Ford W.K. Jr. Rotational properties of 21 SC galaxies with a large range of luminosities and radii, from NGC 4605 /R = 4kpc/ to UGC 2885 /R = 122 kpc/ *The Astrophysical Journal*, 1980, v. 238, 471–487.
3. Rubin V.C., Burstein D., Ford W.K. Jr., and Thonnard N. Rotation velocities of 16 SA galaxies and a comparison of Sa, Sb, and SC rotation properties *The Astrophysical Journal*, 1985, v. 289, 81–104.
4. Planck collaboration. Planck 2013 results. I. Overview of products and scientific results. *Astronomy and Astrophysics*, 2014, v. 571, Table 10.
5. Aprile E., Alfonsi M., Arisaka K., Arneodo F., Balan C., Baudis L., Behrens A., Beltrame P., Bokeloh K., Brown E., Bruno G., Budnik R., Cardoso J.M.R., Chen W.-T., Choi B., Cline D.B., Contreras H., Cussonneau J.P., Decowski M.P., Duchovni E., Fattori S., Ferella A.D., Fulgione W., Gao F., Garbini M., Giboni K.-L., Goetzke L.W., Grignon C., Gross E., Hampel W., Kish A., Lamblin J., Landsman H., Lang R.F., Le Calloch M., Levy C., Lim K.E., Lin Q., Lindemann S., Lindner M., Lopes J.A.M., Lung K., Marrodán Undagoitia T., Massoli F.V., Mei Y., Melgarejo Fernandez A.J., Meng Y., Molinario A., Nativ E., Ni K., Oberlack U., Orrigo S.E.A., Pantic E., Persiani R., Plante G., Priel N., Rizzo A., Rosendahl S., dos Santos J.M.F., Sartorelli G., Schreiner J., Schumann M., Scotto Lavina L., Scovell P.R., Selvi M., Shagin P., Simgen H., Teymourian A., Thers D., Vitells O., Wang H., Weber M., and Weinheimer C. Analysis of the XENON100 Dark Matter Search Data *Astroparticle Physics*, 2014, v. 54, 11–24.
6. EROS Collaboration and MACHO Collaboration. EROS and MACHO Combined Limits on Planetary Mass Dark Matter in the Galactic Halo. arXiv: astro-ph/9803082.
7. Navarro J.F., Frenk C.S., and White S.D.M. A universal density profile from hierarchical clustering. *The Astrophysical Journal*, 1997, v. 490, 493–508.
8. Salucci P., Walter F., and Borriello A. ΛCDM and the distribution of dark matter in galaxies: A constant-density halo around DDO 47. *Astronomy and Astrophysics*, 2003, v. 409, 53–56.
9. Burkert A. The Structure of Dark Matter Halos in Dwarf Galaxies. *The Astrophysical Journal Letters*, 1995, v. 447, L25.
10. Bergstrom L. Non-Baryonic Dark Matter arXiv: astro-ph/9712179.
11. Ho C.M. and Scherrer R.J. Anapole Dark Matter. arXiv: 1211.0503.
12. Jacques T., Katz A., Morgante E., Racco D., Rameez M., and Riotto A. Complementarity of DM Searches in a Consistent Simplified Model: the Case of Z. arXiv: 1605.06513.
13. Bhattacharya S., Melic B., and Wudka J. Dark Matter Pions. *Acta Physica Polonica Series B*, 2013, v. 44, no. 11, 2359–2366.
14. Milgrom M. A modification of the Newtonian dynamics as a possible alternative to the hidden mass hypothesis *Astrophysical Journal* , 1983, v. 270, 365–370.
15. Milgrom M. A modification of the Newtonian dynamics — Implications for galaxies. *Astrophysical Journal* , 1983, v. 270, 371–389.
16. Brownstein J.R. and Moffat J.W. Galaxy Rotation Curves Without Non-Baryonic Dark Matter. *The Astrophysical Journal*, 2006, v. 636, 721–741.
17. Moffat J.W. Nonsymmetric Gravitational Theory. *Journal of Mathematical Physics*, 1995, v. 36, 3722.
18. Feng J.Q. and Gallo C.F. Modeling the Newtonian dynamics for rotation curve analysis of thin-disk galaxies. *Research in Astronomy and Astrophysics*, 2011, v. 11, 1429–1448.
19. Feng J.Q. and Gallo C.F. Mass distribution in rotating thin-disk galaxies according to Newtonian dynamics. arXiv: 1212.5317.
20. Kroupa P. The Dark Matter Crisis: Falsification of the Current Standard Model of Cosmology. *Publications of the Astronomical Society of Australia*, 2012, v. 29, 395–433.
21. Kroupa P. Lessons from the Local Group (and beyond) on dark matter. arXiv: 1409.6302.
22. Matsumoto M., and Nishimura T. Mersenne Twister: a 623 dimensionally equidistributed uniform pseudo-random number generator. *ACM Transactions on Modeling and Computer Simulation — Special issue on uniform random number generation*, 1998, v. 8, 3–30.
23. Newton I. Philosophiae Naturalis Principia Mathematica. London, 1687, Theorem XXXI.
24. Eadie G. M. and Harris W. E. Bayesian Mass Estimates of the Milky Way II: The Dark and Light Sides of Parameter assumptions. arXiv: 1608.04757.

Principle of Spacetime Black Hole Equivalence

T. X. Zhang

Department of Physics, Alabama A & M University, Normal, Alabama 35762. E-mail: tianxi.zhang@aamu.edu

A new principle of spacetime black hole equivalence (SBHEP) is proposed. In addition to Einstein's general relativity and the cosmological principle, the SBHEP principle provides the third base for the black hole universe model that was recently developed by the author in attempt to model the universe, explain existing observations, and overcome cosmic problems and difficulties without relying on a set of hypothetical entities. A black hole universe does not have the horizon and flatness problems so that an inflation epoch is not required. Its origin from starlike and supermassive black holes removes the initial big bang singularity and magnetic monopole problems. A black hole or spacetime is static or in equilibrium when it does not accrete or merge with others, otherwise it becomes dynamic, expands, and emits. Gamma ray bursts, X-ray flares from galactic centers, and quasars can be self-consistently explained as emissions of dynamic starlike, massive, and supermassive black holes. Cosmic microwave background radiations are blackbody radiations of the black hole universe, an ideal blackbody. A black hole universe can accelerate if it accretes matter in an increasing rate, so that an explanation of the supernova measurements does not need dark energy.

1 Introduction

Cosmology is the study of the origin and development of the universe. The currently accepted standard big bang model of the universe (BBU) stands on two bases, which are (1) Einstein's general relativity (GR) that describes the effect of matter on spacetime and (2) the cosmological principle (CP) of spacetime isotropy and homogeneity that generates the Friedmann-Lemaître-Robertson-Walker (FLRW) metric of spacetime [1–4]. The Einstein field equation given in GR along with the FLRW metric of spacetime derived from CP produces the Friedmann equation (FE) that governs the development and dynamics of the universe. Although the big bang theory has made incredible successes in explaining the universe, there still exists innumerable problems and difficulties. Solutions of these problems and difficulties severely rely on an increasing number of hypothetical entities (HEs) such as dark matter, dark energy, inflation, big bang, and so on [5]. Therefore, the BBU consists of GR, CP, and innumerable HEs, *i.e.* BBU = {GR, CP, HE, HE, HE,....} (see the blue part of Fig. 1). Although it has only two bases (GR and CP), the BBU severely relies on an increasing number of HEs that have not yet been and may never be tested or falsifiable.

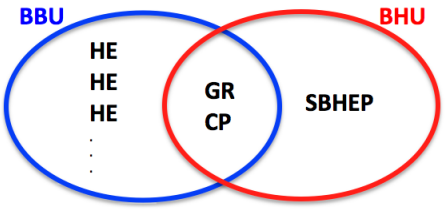

Fig. 1: The comparison of fundamentals between BBU and BHU (see Section 1 for details).

Describing the universe without relying on a set of HEs to explain observations and overcome cosmic problems and difficulties is essential to developing a physical cosmology. Recently, the author has developed a new physical cosmology called black hole universe (BHU) [6–7]. Instead of making many those HEs as the BBU did, the BHU proposes a new principle to the cosmology – the Principle of Spacetime Black Hole Equivalence (SBHEP) – in an attempt to explain all the existing observations of the universe and overcome all the existing problems and difficulties [8–12]. Standing on the three bases (GR, CP, and SBHEP), the new cosmological theory – BHU = {GR, CP, SBHEP} (see the red part of Fig. 1) – can fully explain the universe in various aspects as well as to conquer all the cosmic problems according to the well-developed physics without making any other HEs and including any other unsolved difficulties. GR and CP are common to both BBU and BHU. The BBU stands on two legs unstably so that needs many crutches for support, while the BHU stands on three legs stably without needing any other props. In the BHU, a single SBHEP removes all of innumerable HEs made in the BBU. This paper describes how this new black hole universe model explains the universe and conquers the cosmic difficulties with the principle of spacetime black hole equivalence.

2 Equivalence between spacetime and black hole

The effect of matter on spacetime can be obtained by solving Einstein's field equation provided in GR [13],

$$G_{\mu\nu} = \frac{8\pi G}{c^4} T_{\mu\nu} \tag{1}$$

where the subscripts μ and ν are the four-dimensional (4D) spacetime coordinate indices running through 0–3. $G_{\mu\nu}$ is

Einstein's curvature tensor, G is the gravitational constant, c is the speed of light in free space, and $T_{\mu\nu}$ is the 4D energy-momentum tensor. Adding a term of $\Lambda g_{\mu\nu}$ to the left hand side of (1), Einstein developed a static cosmology [14] and de Sitter developed a dynamic cosmology [15]. Here Λ is the cosmological constant and $g_{\mu\nu}$ is the metric of spacetime,

According to the cosmological principle, the universe, if it is viewed on a scale that is sufficient large, is homogeneous and isotropic. This principle implies that there is no special location and direction in the universe. The properties of the universe are the same for all observers in the universe. More strongly, physical laws are all universal. If a physical law is applicable to the Earth, then it can be applied to everywhere. The isotropic and homogeneous spacetime can be described by the FLRW metric [1–4],

$$\begin{aligned} ds^2 &= -g_{\mu\nu}dx^\mu dx^\nu \\ &= c^2dt^2 - R^2(t)\left[\frac{dr^2}{1-kr^2} + r^2\left(d\theta^2 + \sin^2\theta d\phi^2\right)\right], \end{aligned} \tag{2}$$

where $R(t)$ is the radius of curvature of the space and k is the curvature constant of the space.

Substituting the FLRW metric of spacetime into the Einstein field equation of general relativity, one can have the Friedmann equation [16],

$$H^2(t) \equiv \frac{\dot{R}^2(t)}{R^2(t)} = \frac{8\pi G\rho(t)}{3} - \frac{kc^2}{R^2(t)}, \tag{3}$$

where $H(t)$ is the Hubble parameter or the expansion rate of the universe and ρ is the density of matter. The dot sign refers to the derivative of the quantity with respect to time, $\dot{R}(t) \equiv dR(t)/dt$. Including the cosmological constant, (3) has a term of $\Lambda/3$ on the right hand side.

According to the Schwarzschild field solution of (1) [17], the metric of spacetime surrounding a spherical body with mass M appears to be singular at the Schwarzschild radius $r_g = 2GM/c^2$, which divides the space into two disconnected patches. This indicates that a region of space, where matter accumulates up to a critical level such that the mass-radius (M-R) ratio reaches up to $M/R = c^2/(2G) \simeq 6.67 \times 10^{26}$ kg/m, forms a black hole and constructs its own spacetime, which is singular in space and non-causal in time to the outside. Therefore, it is reasonable to suggest or postulate that a black hole once formed constructs its own spacetime and a spacetime encloses its own unique black hole [6–7]. In other words, spacetime and black hole are equivalent. This postulate of the equivalence between spacetime and black hole plays a fundamental role in the modeling of the universe; therefore, we raise it as a new principle of the cosmology [18]. Without matter, a physical spacetime cannot be formed; without a spacetime, matter cannot become into existence. As a moral idea or belief, we cannot prove its correctness mathematically, but the truth for the principle of spacetime black hole equivalence can be justified and validated through explaining various observations of the universe, such as CMB and supernova measurements, *etc.*, and overcoming cosmic problems, such as dark energy and inflation problems, *etc.*, in accordance with the black hole model of the universe that is developed on the basis of this principle. In the following sections, we will demonstrate how the black hole model of the universe developed on the basis of this new principle to explain the observations of the universe and overcome the cosmic problems and difficulties.

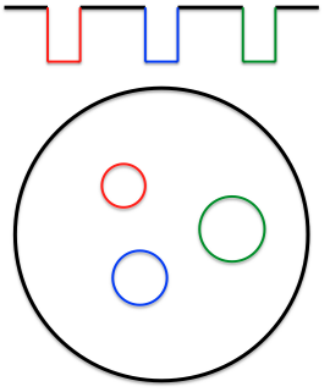

Fig. 2: The hierarchically layered structure of black hole universe. Inside our spacetime or black hole universe (the region represented or circled by the solid black lines), there are a number of subspacetimes (the regions represented or circled by the solid color lines), which are the observed star-like, massive, and supermassive black holes.

3 Black hole universe

From this principle of spacetime black hole equivalence, we understand that our universe, because it is constructed in a 4D spacetime, is or wraps a black hole, which is extremely supermassive and fully expanded. Its big radius and enormous mass can be determined in terms of the measurement of matter density of the universe as detailed below in the subsection 3.1. The inside observed star-like, massive, and supermassive black holes can be considered as subspacetimes (or called child universes) of our black hole universe (see Fig. 2). This hierarchically layered structure of spacetimes and subspacetimes genuinely overcomes the horizon problem, which was identified to exist in the big bang model of the universe primarily by Charles Misner in 1960s [19–20] and solved by Alan Guth in 1980s with the hypothesis of cosmic inflation [21] according to a field that does not correspond to any physical field. Therefore, in the black hole model of the universe, there does not exist the horizon problem at all.

3.1 Mass-radius relation and spacetime equilibrium

The boundary of a spacetime or black hole is determined, according to the Schwarzschild solution, by

$$\frac{2GM}{c^2R} = 1, \tag{4}$$

which is also the relation of the effective mass and radius of the universe according to Mach's principle [22–24] as well as

the relation of the observable mass and radius of the universe according to observations. The mass and radius of a spacetime or black hole satisfy this Mach-Schwarzschild M-R relation. The space curvature constant of a closed spacetime or black hole is positive, *i.e.*

$$k = 1. \tag{5}$$

It is noted here that the big bang model suggests that the spacetime of the universe is flat (*i.e.* $k = 0$).

The cosmological principle expresses the matter inside a spacetime or black hole to be uniformly (*i.e.* isotropically and homogeneously) distributed in a scale which is sufficiently large (*i.e.* comparable rather than too small) in comparison with respect to the size of the spacetime. Then, the density of matter in a spacetime or black hole is given by

$$\rho \equiv \frac{M}{V} = \frac{3c^2}{8\pi GR^2} = \frac{3c^6}{32\pi G^3M^2}, \tag{6}$$

which is inversely proportional to the square of radius or the square of mass. This square-law density expression (ρR^2 = constant or ρM^2 = constant) naturally removes the flatness problem of the universe, which was first pointed out by Robert Dicke in the BBU [25–26].

Therefore, the flatness (or fine-tuning) problem does not exist in the black hole model of the universe. Furthermore, by measuring the density, we can determine both the radius and mass of the universe. For the density of the present universe to be about the critical density $\rho_0 \sim \rho_c \equiv 3H_0^2/(8\pi G)$, we have the mass and radius of the present universe to be $M_0 \sim 8.8\times10^{52}$ kg (about a half hundred sextillions of solar masses) and $R_0 \sim 1.32 \times 10^{26}$ m (about forty-three hundred Mpc or one Hubble length). Here, according to measurements [27–30], the Hubble constant is chosen as $H_0 = 70$ km/s/Mpc. Therefore, the present universe is an extremely supermassive and fully expanded black hole with extremely low density and weak gravity. The gravitational field at its surface is $g_0 = GM_0/R_0^2 \sim 3 \times 10^{-10}$ m/s^2 and thus a 100-kg object at the surface or inside only weighs 3×10^{-8} N or less.

The big bang universe is an isolated system and the total energy or mass (though unknown) is a constant, so that the density is inversely proportional to the cube of radius (*i.e.* ρR^3 = constant). Fig. 3 plots the density of a black hole as a function of its radius in the unit of kilometers (the solid line) or a function of the mass in the unit of 0.337 solar masses (the same line). The dashed line plots the density of the big bang universe as a function of its radius with mass equal to M_0 (for a bigger mass, the line is shifted to a larger radius). The dotted line marks the density of the present universe (ρ_0) and its intersection with the solid line shows the mass (M_0), density (ρ_0), and radius (R_0) of the present universe. Three circles along the solid line represent a star-like black hole with three solar masses, a supermassive black hole with three billion solar masses, and the present black hole universe with mass M_0. The black hole universe is not an isolated system because its mass increases as it expands. The density decreases inversely proportional to the square of the radius (or the mass) of the black hole universe. Considering that matter can enter but cannot exit a black hole, we can suggest that the black hole universe is a semi-open system surrounded by outer space and matter. The entire space is infinite, existed forever, and isolated. It contains everything without outside and edge. Inside the entire space, any universe has outside space and matter and thus cannot be isolated.

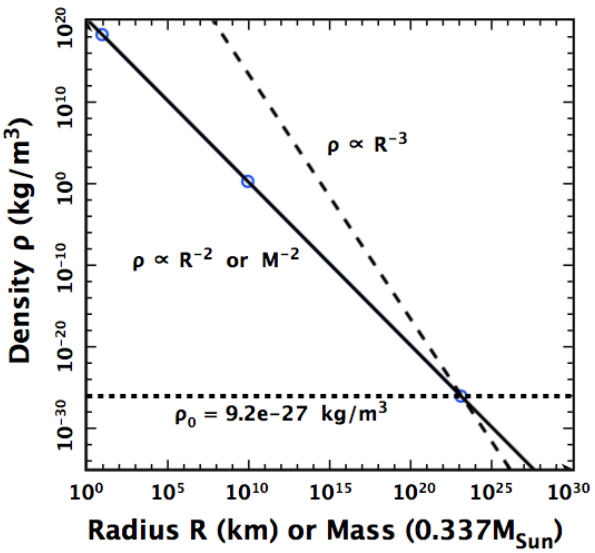

Fig. 3: The density of the black hole universe versus its mass and radius (the solid line). The dotted line refers to $\rho = \rho_0$, so that the intersection of the solid and dotted lines represents the density, radius, and mass of the present universe. The dashed line plots the density of the big bang universe, if it has mass M_0, as a function of the radius.

In the black hole universe model, we have that the effective and observable radii are the actual radius of the universe at all time, so that the black hole universe is always all observable and Mach's principle holds forever. In the big bang theory, the ratio between the effective radius and the radius of the universe increases as the universe expands and will reach the unity at a point, which is the present time if the universe has mass M_0. Before the point, the effective radius is less than the radius of the universe. While, after the point, the effective radius will be greater than the radius of the universe, at which Mach's principle does not hold, so that other physical laws neither hold.

According to GR and the stellar physics, a star with 20 or more solar masses, at the end of its life, will form a black hole after a supernova explosion [31]. Therefore, the black hole model of the universe does not need a big bang. The universe can be considered to originate from a star-like black hole (child universe) with several solar masses, which grows through a supermassive black hole with billion solar masses to the present universe with hundred-sextillion solar masses

by accreting ambient matter and merging with other black holes. Which one was the first or initial black hole that the universe has grown up from is not critical or important to the present universe because the mass of the original one only takes one part of a sextillion in the present universe. This origin of the universe from black holes not only overcomes the fine-tuning problem but also conquer the difficulty of banging the universe out from nothing that violates the law of conservation of energy. This resolves the big bang singularity problem. In addition, if the universe originated from a star-like black hole, it would not be hot enough to create a magnetic monopole in any time period, thus solving the magnetic monopole problem. The recent discovery of gravitational waves confirms the existence and merger of black holes [32] and thus support this black hole model of the universe.

Substituting the Mach-Schwarzschild M-R relation (4) (or density (6)) and positive space curvature constant (5) into the Friedmann equation (3), we have $\dot{R} = 0$ and $\dot{M} = 0$ – a zero rate of change in radius or mass. This indicates that a spacetime or black hole is static [7,33] when it neither accretes matter from the outside nor merges with other black holes. In the static state, the spacetime reaches equilibrium because the positive curvature balances the gravity entirely. A spacetime with the curvature radius R can hold the matter with mass equal to $c^2R/(2G)$ in equilibrium. Hawking [34] theorized the surface radiation of a static black hole with the quantum effect. For a star-like or more massive black hole, the Hawking radiation is negligibly weak and ultra-cold, which leads to the entropy of a static black hole to be 20 orders higher than its massive parent star. Including the cosmological constant, (3) determines Λ in the static state as $\Lambda = 3H^2$, which is $\sim 1.55 \times 10^{-35}$ s^{-2}.

3.2 Expansion and acceleration of spacetime

When a spacetime or black hole accretes its ambient matter or merges with other black holes, it becomes dynamic and expands. The rate of expansion or Hubble parameter is given by

$$H = \frac{\dot{R}}{R} = \frac{\dot{M}}{M}, \tag{7}$$

and the deceleration parameter is given by

$$q = -\frac{R\ddot{R}}{\dot{R}^2} = -\frac{M\ddot{M}}{\dot{M}^2}. \tag{8}$$

Here, the double dot symbol refers to the second order derivative of the parameter with respect to time. A spacetime or black hole expands if it gains matter, *i.e.* $\dot{M} > 0$, and accelerates if it gains matter in an increasing rate, *i.e.* $\ddot{M} > 0$. The expansion of spacetime is physical and outward without violating Einstein's light-speed upper limit and conservation of energy. A spacetime or black hole grows its space as it accretes matter by taking the outside space rather than by stretching the space of itself geometrically.

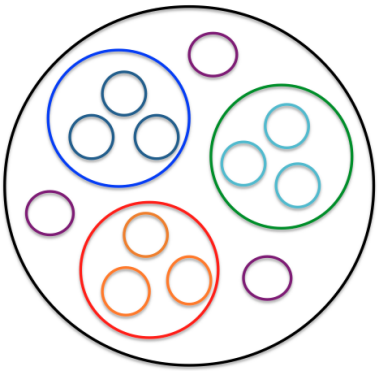

Fig. 4: A simple sketch of the innermost three layers of the entire space that is structured hierarchically. The black circle represents the mother universe. Our black hole universe is coded as red, in which three child universes (*i.e.* star-like or supermassive black holes) were drawn. Parallel to our universe, there are sister universes. Here two adult sister universes (blue and green circles) and three little sister universes (brown circles). The adult sister universes have also their child or baby universes, but the little sister universes are too young to have their babies.

For a spacetime or black hole including our black hole universe to expand, it must have an outside, where matter is available for accretion. The black hole model of the universe suggests that the entire space is structured with layers, hierarchically and family-like. Fig. 4 sketches the innermost three layers of the black hole universe including the mother universe (black circle), our universe itself (red circle), and child or baby universes (*i.e.* star-like or supermassive black holes). We have only drawn three child universes (yellow circles). We have also drawn two adult sister universes (blue and green circles) and three little sister universes (brown circles), which are universes parallel to our black hole universe. The adult sister universes have also their child universes. There should have a number of child universes and may also have many sister universes. A child universe grows by accreting material from its outside or by merging with other child universes. This universe grows up by accreting material from the mother universe or by merging with sister universes. The mother universe will also grow up if it has outside; otherwise, it is static. If the whole space is finite, then the number of layers is finite. Otherwise, it has infinite layers and the outermost layer corresponds to the limit of zero Kelvin for the absolute temperature, zero for the density, and infinite for the radius and mass.

From the data of type Ia supernova measurements, Daly et al. obtained the deceleration parameter of the present universe to be $q_0 \sim -0.48$ for the flat spacetime (for a closed spacetime, q_0 is smaller, *e.g.* $q_0 = -0.6$) [35]. Riess et al. and Perlmutter et al. explained the acceleration of the universe by suggesting the big bang universe to be dominated by dark energy up to about $\sim 73\%$ [36–37]. In the black hole universe model, however, the universe accelerates because it inhales the outside matter in an increasing rate, *i.e.* a positive $\ddot{M} > 0$. To have $q_0 = -0.48$, the present black hole universe

only needs to inhale the outside matter in an increasing rate at $\ddot{M}_0 = -q_0 M_0 H_0^2 \sim 2.2 \times 10^{17}$ kg/s^2 (or about 220 solar masses per year square).

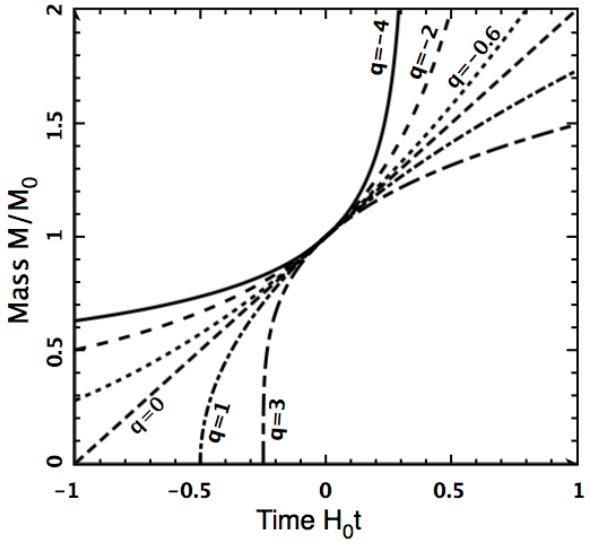

Fig. 5: Mass of black hole universe versus time with various deceleration parameters $q = -4, -2, -0.6, 0, 1, 3$.

For a constant acceleration expansion universe, the time-dependent mass can be analytically solved from (8) as [10],

$$\frac{M}{M_0} = [(q+1)H_0 t + 1]^{1/(q+1)}. \tag{9}$$

To quantitatively see how the mass $M(t)$ varies with time and depends on the deceleration parameter q, we plot in Fig. 5 according to (9) the mass as a function of time with various values of $q = -4, -2, -0.6, 0, 1, 3$. The lines with negative q are concave upward, which show that the mass increases in an increasing rate and the universe accelerates. The lines with positive q are concave downward, which show that the mass increases in a decreasing rate and the universe decelerates. For $q = 0$, the black hole universe accretes matter or increases its mass in a constant rate and thus expands uniformly.

The cosmological redshift of light from a source in an expanding spacetime is determined by

$$1 + Z = \frac{R_0}{R} = \frac{M_0}{M}. \tag{10}$$

The luminosity distance of the light source depends on the redshift as [10,38–39],

$$\begin{aligned} d_L &= (1+Z)M_0 \sin\left[\int_t^0 \frac{cdt}{M}\right] \\ &= (1+Z)R_0 \sin\left[\frac{c^3}{2GM_0H_0}\frac{1-(1+Z)^{-q}}{q}\right]. \end{aligned} \tag{11}$$

Here we have applied (9) and (10) to complete the integration. Eq. (11) reduces to the Hubble law, $H_0 d_L = cZ$, at $Z \ll 1$ [40] and perfectly explains the type Ia supernova measurements if the universe accretes matter in an increasing rate of $q = -0.6$ [34]) or $\ddot{M} \sim 3 \times 10^{17}$ kg/s^2 in average [10].

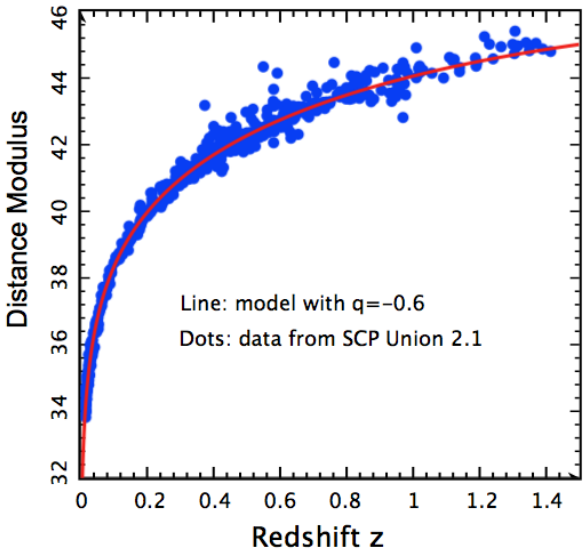

Fig. 6: Luminosity distance-redshift relation of type Ia supernovae. Blue dots are measurements credited by the Union2 compilation of 580 SNeIa data from Supernova Cosmology Project [41–42]. Red line is analytical results from this study with $q = -0.6$. The distance modulus is plotted as a function of the cosmological redshift.

Fig. 6 plots the luminosity distance-redshift relation (red line) along with the type Ia supernova measurements (blue dots), which are credited by the Union 2.1 compilation of 580 SNIA data from Supernova Cosmology Project [41–42]. In this plot the Hubble constant is chosen to be $H_0 = 70$ km/s/Mpc and the deceleration parameter is chosen to be $q = -0.6$. The distance modulus, which is defined by $\mu = 5 \log_{10} d_{\rm L} - 5$ with $d_{\rm L}$ in parsecs, is plotted as a function of redshift. The chi-square statistic is very close to unity [10]. Therefore, the black hole universe model can perfectly explain the measurements of type Ia supernovae without dark energy, which is needed to take $\sim 73\%$ in the big bang universe [36–37].

3.3 Temperature of spacetime and background radiation

The temperature inside a spacetime or black hole depends on the state and density of matter enclosed and hence depends on the radius or mass. The stellar physics has shown that a neutron star can reach trillions of Kelvin at the moment of its birth and then quickly cools down to hundred millions of Kelvin due to strong radiation and neutrino emissions. Since it is compact as a neutron star, a star-like black hole should also initially reach trillions of Kelvin but statically holds this hotness due to lack of significant emissions to the outside (the Hawking radiation is negligible). The thermal radiation inside a spacetime or black hole is the blackbody radiation

governed by the Planck law, from which one can derive the total energy of blackbody radiation inside a spacetime or black hole with radius R and temperature T to be

$$U_\gamma = \alpha R^3 T^4. \tag{12}$$

Here, the constant α is given by, $\alpha \equiv 32\pi^6 k^4/(45h^3c^3) \sim 3.2\times^{-15}$ J/m^3/K^4, with k the Boltzmann constant and h the Planck constant.

When a spacetime or black hole accretes matter and radiation from its outside, it becomes dynamic and expands. Considering that the gain of matter and radiation inside is equal to the loss of matter and radiation outside, we have [8]

$$\frac{dT}{dR} = -\frac{3T}{4R}\left[1 - \left(\frac{T_p}{T}\right)^4\right], \tag{13}$$

where T is the temperature inside and T_p is the temperature outside. This equation governs the thermal history of the black hole universe from its origin as a star-like black hole with several solar masses and growing through a supermassive black hole with billions of solar masses to the present state with hundred sextillions of solar masses. Since the temperature outside is always less than that inside, $T_p < T$, the temperature of a spacetime or black hole decreases with its radius. As the black hole universe grows in size from a star-like black hole to the present state, its temperature decreases from trillions of Kelvin to about 3 K [8]. The cosmic microwave background radiation (CMB) is explained as the blackbody radiation of the black hole universe – an ideal blackbody – rather than the fireball leftover of the big bang universe.

Considering the black hole universe to decrease its relative temperature in a rate slightly faster than the mother universe, we have [8]

$$T_p = aT^b, \quad \text{or} \quad T_p/T = aT^{b-1} \tag{14}$$

Here b is a constant slightly less than 1 and a can be derived from b according to the temperature and radius of the present universe (T_0 and R_0). Then, (13) can be analytically solved as

$$T = R^{-3/4}\left(a^4 R^{3-3b} + T_s^{4-4b} R_s^{3-3b}\right)^{1/(4-4b)}, \tag{15}$$

where the constant a is given by

$$a = \left[T_0^{4-4b} - \left(\frac{R_s}{R_0}\right)^{3-3b}\right]^{1/4}. \tag{16}$$

Choosing b appropriately (or slightly less than 1), we can completely determine the thermal history of the black hole universe that evolved from a hot star-like black hole with temperature T_s and radius R_s to the present universe with temperature T_0 and radius R_0. In Fig. 7, the temperature of the black hole universe is plotted as a function of the universe radius with $b = 0.93$. Here we have chosen $T_0 = 2.725$ K, $R_0 = 1.32 \times 10^{26}$ m, $R_s = 8.9$ km, and $T_s = 10^{12}$ K.

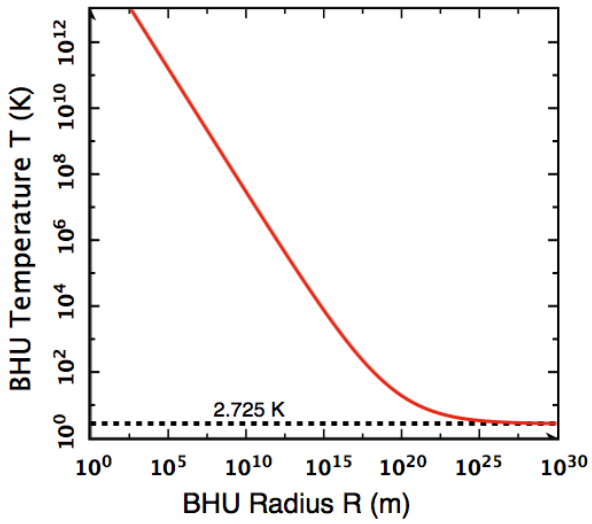

Fig. 7: The possible thermal history of the black hole universe. A hot star-like black hole with $T_s = 10^{12}$ K expands to the size of the present universe and cools down to ~ 2.725 K. The temperature line is curved by concaving upward and approaches ~ 2.725 K at the present time as the black hole universe expands to the present size.

It is seen that the temperature line is concave upward and approaches ~ 2.725 K as the black hole universe expands to the present size. The initial temperature of the star-like black hole T_s is not critical to the present universe. The reason is because most matter and radiation are from the mother universe. This reason also explains why all other physical properties of the star-like black hole, including its size (or mass), angular momentum, and charge, and the evolution of the early universe are not critical to the present universe. Furthermore, the early process of material accretion and black hole mergers do not have significant leftover in the present universe.

The above explanation of the CMB of this universe requires a decreasing temperature outside, *i.e.* an expanding mother universe. To have an expanding mother universe and explain its CMB with a decreasing temperature, there needs an expanding grandmother universe, and so forth. Therefore, the entire space is eternal and infinite, containing everything with infinite layers (Fig. 8). Nothing can be outside the entire space. The star-like or supermassive black holes called child universes belong to the innermost layer. They are subspacetimes of our black hole universe (the second innermost layer) that we live in. Our black hole universe is a subspacetime of the mother universe (the third innermost layer). The mother universe may contain a great number of child universes that are parallel to (and hence sisters of) our black hole universe. Mathematically, we can use an infinite large family tree that contains infinite generations or an infinite large set that contains infinite subsets to represent the relationships among different generations of black hole universes. The outermost layer called grand universe is infinitely large in size, mass, and entropy but has zero limits for both the density and

absolute temperature.

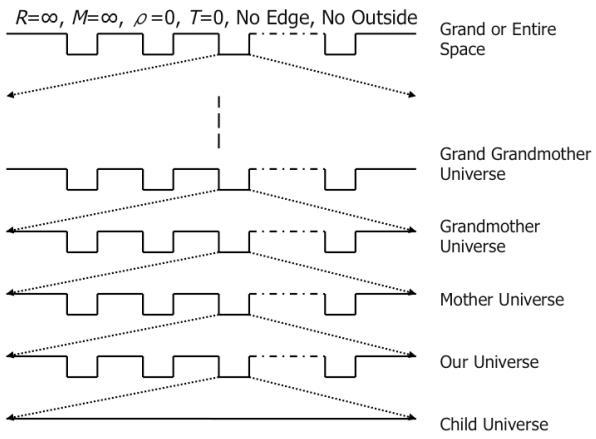

Fig. 8: The entire space with infinite layers or subspacetimess [8]. The bottom layer is a child universe or an empty spacetime. The child universe is a subspacetime of the universe in which we live in. Similarly, our universe is a subspacetime of the mother universe, and so on. The top layer is the entire space of all subspacetimes.

Each layer or black hole universe tends to absorb its outside matter and radiation and takes its outside space and expands outward. When our black hole universe expands to be one as large as the mother universe, the inside star-like and supermassive black holes will have merged and grown up into a black hole universe that is similar to the present one. This process is irreversible with neither a beginning nor an end. The evolution of black hole universe is iterative – beginningless and endless. When one black hole universe is expanded out, a new similar black hole universe is formed from inside child universes [7]. The black hole model of the universe is complete because it can address our universe not only at the present as well as its inside, but also in the past and future as well as its outside.

The total radiation energy inside the black hole universe is plotted in Fig. 9 as a function of the radius. It is seen that a young black hole universe with radius less than 10^{15} m or mass less than some hundred billions of solar masses remains the total radiation energy as a constant. This characteristic allows us to explain the activities and emissions of dynamic star-like and supermassive black holes observed in the universe.

3.4 Emissions of dynamic black holes

For a star-like black hole with several solar masses to grow through a supermassive black hole with billion solar masses, the temperature outside is negligibly lower than the temperature inside, *i.e.* $T_p \ll T$. In this case, (13) can be solved as

$$R^3T^4 = \text{Constant}, \tag{17}$$

which implies that the total radiation energy inside a spacetime or black hole with mass about billions of solar masses or

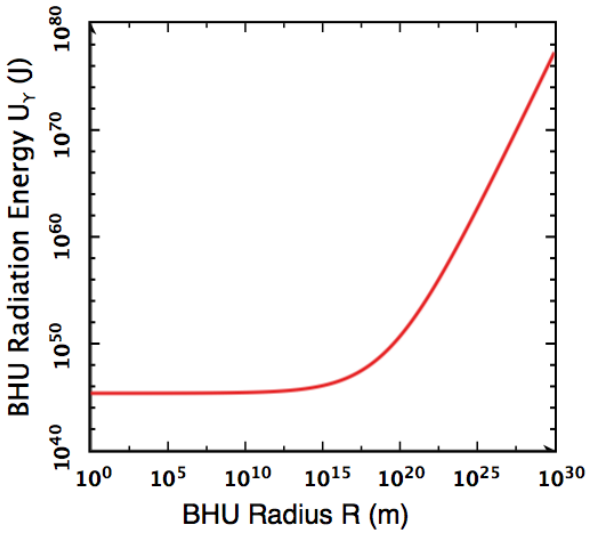

Fig. 9: Radiation energy of the black hole universe. As a hot star-like black hole with $T_s = 10^{12}$ K expands to the size of the present universe and cools down to ~ 2.725 K, its radiation energy first remains as a constant and then rapidly increases with radius when it grows into a supermassive black hole with radius greater than about thousand billions of kilometers or mass greater than about hundred billions of solar masses.

less remains the same amount as shown in Fig. 9. Therefore, accreting outside matter and radiation or merging with other black holes into a single one, a black hole not only becomes dynamic and expands but also intensively emits its inside hot and hence high-frequency blackbody radiation out of its horizon, which has been disturbed or broken by the accretion or merger in order for the total energy of its inside radiation to remain as a constant.

This emission mechanism of dynamic black holes can self-consistently explain the observed gamma ray bursts, X-ray flares from galactic centers, and quasar emissions as emissions of dynamic star-like, massive, and supermassive black holes, respectively (the details on these have been described in [9,11–12]). Dynamic star-like black holes with trillions of Kelvin radiate gamma rays and produce gamma ray bursts, while dynamic massive or supermassive black holes with millions to billions of Kelvin radiate X-rays such as X-ray emissions from quasars and X-ray flares from Sgr A* (a massive black hole at the Milky Way center). The energetic events associated with black holes are activities of child universes. The author has shown that a child universe with radius $R \gtrsim 10^{18}$ m or mass $M \gtrsim 3 \times 10^{14}$ solar masses does not emit [9], but can strongly attract and accrete its ambient matter including galaxies, which may help us to understand great attractors observed with thousand trillions of solar masses, *e.g.* the Norma Cluster. On the other hand, quasars if electrically charged may have a significant electric redshift as illustrated by [43]. The merger of star-like black holes if missing mass may release significant gravitational waves as recently detected by LIGO [32].

4 Discussion and conclusions

In addition to above issues that have been addressed in details in the early papers [7–12,39], the black hole model of the universe can also self-consistently illustrate various other problems of the universe such as why the redshifts of galaxies are quantized, how the galaxies and clusters are formed, why the expansion of the universe can be anisotropic, how the elements are synthesized, why the universe increases its entropy extremely without significantly increasing its disorder, how the heavy-ion enriched objects are formed in extremely deep fields or the young universe, what the great attractor is, why the voids exist, and so on. Preliminary results on some of them have been presented in a sequence of AAS (213^{rd}-215^{th}, 217^{th}, 219^{th}-224^{th}, 228^{th}) meetings and the details on all these problems will be addressed in future in full length papers.

The BHU stands on three bases, which are (1) GR of describing matter effect on spacetime, (2) CP of spacetime homogeneity and isotropy, and (3) SBHEP of spacetime black hole equivalence. We have not yet explored the quantum effect on this model to pop up baby universes and holes. In this model, baby or child universes are star-like and supermassive black holes, which are formed from stars and galaxies. To appropriately explain CMB, the entire space is favored to be infinite and eternal and includes infinite universes, which are layered hierarchically and evolved iteratively. Due to gravity and Jeans collapse criterion, matter forms stars, which then, if massive, end as black holes or child universes. A black hole, once formed, will grow and expand by accreting its ambient matter and merging with other black holes. A galaxy (usually including a massive black hole at its center), once most stars run out their fuels and died as dwarfs, neutron stars, and black holes, will eventually form a supermassive black hole (or quasar) by accreting all galactic matter and objects, and merging all stellar black holes into the massive black hole at the center. LIGO recently discovered the gravitational wave that confirms the existence of black holes and their merger [32]. A black hole universe can be considered to be originated or born from a star-like black hole (or child universe) without a big bang singularity, flatness, horizon, and magnetic monopole problems. It gradually grows or expands by accreting outside matter or merging with other black holes without dark energy and inflation problems. Each star-like black hole or supermassive black hole is usually rotating with significant angular momentum. But when many randomly rotating black holes merge to form a large universe like our present universe, the net angular velocity may be negligibly small. Inside a fully expanded or grown universe, objects formed from the collapse of matter (*e.g.* planets, stars, galaxies, clusters, *etc.*) can rotate globally. Gamow speculated that the rotations of these objects might be due to the cosmic rotation [44] and Godel obtained a cosmological solution of Einstein's field equation for rotating universes [45]. The black hole model of the universe is a model with multiverses (infinite or uncountable), which are hierarchically layered. It is different from other models of multiverse such that the many-world (or universes) interpretation of quantum physics proposed by [46] and the branes model of multiverse that suggested the visible 4D spacetime universe to be restricted inside a higher-dimensional space [47].

The three bases of BHU (GR, CP, and SBHEP) with well-developed physics theories and laws such as the conservation of energy, Planck's radiation, and so on can derive some laws or regularities of the BHU such as the spacetime equilibrium, the spacetime expansion and acceleration, the conservation of blackbody radiation, the increase of entropy, and so on that regulate and govern the development and dynamics of black hole universes. These laws or regularities can help us to explain and describe the origin, structure, expansion, evolution, acceleration of the universe, CMB, quasar, Sgr A* X-ray flare, *etc.* and meantime to overcome problems such as the horizon, flatness, monopole, dark matter, dark energy, low initial entropy, redshift quantization, big bang, old objects in the young universe, entropy, and so on. The BHU does not have unknowns. Both the charge and angular momentum are zero ($Q = 0$ and $J = 0$). The mass M is the only or key parameter. The radius or scale factor R, the temperature T, and the entropy S are derived from M according to the relations given by (4), (13), and entropy equations of thermodynamics. Measuring density tells us the radius R, and thus T and S. Measuring the Hubble parameter H tells the rate of change in $\dot{M}$, and thus $\dot{R}$, $\dot{T}$, $\dot{S}$. Measuring the deceleration parameter q tells us the double rate of change in mass $\ddot{M}$, and thus radius $\ddot{R}$, temperature $\ddot{T}$, entropy $\ddot{S}$. Measuring CMB, supernovae, *etc.* also tells us R and thus M, T, S, so that finds how the universe expands, *e.g.* acceleration or not.

As a consequence, installing one more leg (or fundamental) – the Principle of Spacetime Black Hole Equivalence – to the cosmology, we can attempt to fully explain the universe and simply overcome the difficulties according to the well-developed physics without needing to make other hypotheses such as inflation, dark energy, and so on. The black hole model of the universe is robust by only needing one stroke (the single postulate or principle SBHEP) rather than relying on an increasing number of hypothetical entities (HEs) as done in the big bang model [5] to explain the universe and solve the cosmic problems.

Acknowledgements

This work was partially supported by the NSF HBCU-UP, REU (PHY-1263253), and AAMU Title III programs.

Submitted on August 1, 2016 / Accepted on September 9, 2016

References

1. Friedmann A. Über die Krümmung des Raumes. *Zeitschrift für Physik*, 1922, v. 10, 377–386.

2. Lemaître G. Expansion of the universe, A homogeneous universe of constant mass and increasing radius accounting for the radial velocity of extra-galactic nebulae. *Monthly Notices of the Royal Astronomical Society*, 1931, v. 91, 483–490.
3. Robertson H. P. Kinematics and world-structure. *Astrophysical Journal*, 1935, v. 82, 284–301.
4. Walker A. G. On Milne's theory of world-structure. *Proceedings of the London Mathematical Society*, 1937, v. 42, 90–127.
5. Arp H. et al. An open letter to the scientific community - signed by scientists/engineers/researchers. *New Scientist*, 2004, May, 22.
6. Zhang T. X. A new cosmological model: Black hole universe. *American Astronomical Society 211st Meeting*, 2007, Abstract #152.04.
7. Zhang T.X. A new cosmological model: Black hole universe. *Progress in Physics*, 2009, v. 5 (2), 3–11.
8. Zhang T. X. Cosmic microwave background radiation of black hole universe. *Astrophysics and Space Science*, 2010, v. 330, 157–165.
9. Zhang T. X. Quasar formation and energy emission in black hole universe. *Progress in Physics*, 2012, v. 8 (3), 48–53.
10. Zhang T. X., Frederick C. Acceleration of black hole universe. *Astrophysics and Space Science*, 2014, v. 349, 567–573.
11. Zhang T. X. Gamma ray bursts and blak hole universe. *Astrophysics and Space Science*, 2015, v. 358., article.id. #14, DOI 10.1007/s10509-015-2409-1, 8 pp.
12. Zhang T. X., Wilson C. and Schamschula M. P. X-ray flares from Sagittarius A* and black hole universe, *Progress in Physics,*, 2016, v. 12 (1), 61–67.
13. Einstein A. Die grundlage der allgemeinen relativitatstheorie. *Annalen der Physik*, 1916, v. 354, 769–822.
14. Einstein A. Kosmologische betrachtungen zur allgemeinen relativitatstheorie. *Sitz. Preu. Akad. Wiss. (Berlin)*, 1917, Part 1, 142–152.
15. de Sitter W. Einstein's theory of gravitation and its astronomical consequence. *Monthly Notices of the Royal Astronomical Society*, 1917, v. 78, 3–28.
16. Friedmann A. Über die Möglichkeit einer Welt mit konstanter negativer Krümmung des Raumes. 1924, *Zeitschrift für Physik*, v. 21, 326–332.
17. Schwarzschild K. Ober das gravitationsfeld eines massenpunktes nach der Einsteinschen theorie. *Sitz. Pruess. Akad. Wiss.*, 1916, v. 1, 189–196.
18. Zhang T. X. Principle of spacetime and black hole equivalence. *American Astronomical Society 228th Meeting*, 2016, Abstract #403.08.
19. Misner C. W. Coley A. A., Ellis G. F. R., Hancock M. The isotropy of the universe. *The Astrophysical Journal*, 1968, v. 151, 431–457.
20. Misner C. W. Thorne K. S., Wheeler J. A. *Gravitation*, 1973, San Francisco: W.H. Freeman and Co., ISBN 0-7167-0344-0.
21. Guth A. H. Inflationary universe: A possible solution to the horizon and flatness problems. *Physical Review D*, 1981, v. 23, 347–356.
22. Brans C. H., Dicke R. H. Mach's principle and a relativistic theory of gravitation. *Physical Review*, 1961, v. 124, 925–935.
23. Sciama D. W. On the origin of inertia. *Monthly Notices of the Royal Astronomical Society*, 1953, v. 113, 34–42.
24. Davidson W. General relativity and Mach's principle. *Monthly Notices of the Royal Astronomical Society*, 1957, v. 117, 212–224.
25. Dicke R. H. Remarks on gravitation and cosmology. *Proceedings of the International Symposium for Theoretical Physics*, 1969, v. 1, 507–510.
26. Dicke R. H., Peebles P J. E. The big bang cosmology - enigmas and nostrums. *General Relativity*, 1979, 504–517.
27. Hughes J. P., Birkinshaw M. A. A measurement of the Hubble constant from the X-ray properties and the Sunyaev-Zeldovich rffect of CL 0016+16, *The Astrophysical Journal*, 1998, v. 501, 1–14.
28. Mauskopf P. D. *et al*. A determination of the Hubble constant using measurements of X-ray emission and the Sunyaev-Zeldovich effect at millimeter wavelengths in the cluster Abell 1835. *The Astrophysical Journal*, 2000, v. 538, 505–516.
29. Sandage A., Tammann G. A., Saha A., Reindl B., Macchetto F. D., Panagia N. The Hubble constant: A summary of the Hubble Space Telescope Program for the luminosity calibration of type Ia supernovae by means of Cepheids. *The Astrophysical Journal*, 2006, v. 653, 843–860.
30. Suyu S. H. *et al*. Dissecting the gravitational lens B1608+656. II. Precision measurements of the Hubble constant, spatial curvature, and the dark energy equation of state. *The Astrophysical Journal*, 2010, v. 711, 201–221.
31. Carroll S. M. Spacetime and geometry. An introduction to general relativity. San Francisco, CA, USA: Addison Wesley, 2004, ISBN 0-8053-8732-3.
32. Abbott B. P. *et al*. Observation of gravitational waves from a binary black hole merger. Physical Review Letters, 2016, v. 116, id.061102
33. Carter B. Black hole equilibrium states, in B. S. DeWitt and C. DeWitt, Black Holes (Les Astres Occlus), 1973, 57–214.
34. Hawking S. Black hole explosions? *Nature*, 1974, v. 248, 30–31.
35. Daly R. A. *et al*. Improved constraints on the acceleration history of the universe and the properties of the dark energy *The Astrophysical Journal*, 2008, v. 677, 1–11.
36. Riess A. G. *et al*. Observational evidence from supernovae for an accelerating universe and a cosmological constant. *Astronomical Journal*, 1998, v. 116, 1009–1038.
37. Perlmutter S. *et al*. Measurements of Omega and Lambda from 42 high-redshift supernovae. *Astrophysical Journal*, 1999, v. 517, 565–586.
38. Weinberg S. *Gravitation and Cosmology*, Wiley: New York, NY, USA, 1980.
39. Zhang T. X. Key to the mystery of dark energy: Corrected relationship between luminosity distance and redshift. *Progress in Physics*, 2013, v. 5, 1–6.
40. Hubble E. P. A relation between distance and radial velocity among extra-galactic nebulae. *Proceedings of the National Academy of Sciences of the United States of America*, 1929, v. 15, 168–173.
41. Amanullah R. *et al*. Spectra and Hubble Space Telescope light curves of six type Ia supernovae at $0.511 < z < 1.12$ and the Union2 compilation, *The Astrophysical Journal*, 2010, v. 716, 712–738.
42. Suzuki N. *et al*. The Hubble Space Telescope Cluster Supernova survey. V. Improving the dark-energy constraints above z ¿ 1 and building an early-type-hosted supernova sample, *The Astrophysical Journal*, 2012, v. 746, article id. 85, 24 pp.
43. Zhang T. X. Electric redshift and quasar. *The Astrophysical Journal Letters*, 2006, v. 636, L61–L63.
44. Gamow G. Rotating universe? *Nature*, 1946, v. 158, 549–549.
45. Godel K. An example of a new type of cosmological solutions of Einstein's field equations of gravitation. *Reviews of Modern Physics*, 1949, v. 21, 447–450.
46. Everett H. Relative state formulation of quantum mechanics, *Reviews pf Modern Physics*, 1957, v. 29, 454–462.
47. Rubakov V. A., Shaposhnikov M. E. Do we live inside a domain wall? *Physics Letters B*, 1983, v. 125, 136–138.

Attempt to Replicate Cahill's Quantum Gravity Experiment to Measure Absolute Velocity

Jay R. Seaver

Energy Matters Foundation, PO BOX 2588, Longmont, CO 80502, USA
E-mail:jay@energy-matters.org

In December 2015 in a laboratory in Longmont, Colorado, USA, I attempted to repeat the experiments of Reginald T. Cahill for detecting dynamical space by using reverse biased Zener diodes as quantum tunnelling devices whose tunnelling currents are modulated by the motion of dynamical space relative to the earth. I successfully produced the correlated signals of the same frequency and amplitude as Cahill has produced in his laboratory in Adelaide, Australia. But I determined that rather than being disturbances in space, these signals were merely transient responses to local electromagnetic disturbances which appeared to be correlated due to the identical natural frequencies of the two detectors. This paper is a report on those experiments.

1 Introduction

Recent papers by Cahill [1–3] discuss gravity wave detection using reverse-biased Zener diodes as "quantum gravitational wave detectors". In December 2015, in Longmont, Colorado, I built these quantum wave detectors using the identical parts and schematic as Cahill in order to confirm his measurements. I consulted with Cahill via email to make sure they were exactly as he designed them.

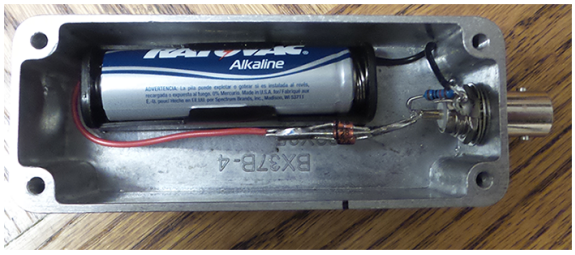

Fig. 1: Inside of Quantum Detector used in experiment.

Figure 1 shows a photograph of the inside one of the quantum detectors used in the experiment. It consists of a parallel connected array of three 3.0 V 1N4728 Zener diodes serially connected to a 1.5 V battery and a 10 kOhm sense resistor. The voltage across the sense resistor goes through a BNC connector and a 3 ft. RG58 coax cable to the AC-coupled input of a LeCroy 1 GHz bandwidth Digital Sampling Oscilloscope (DSO). The schematic and a picture of the inside of Cahill's detector can be seen in Figure 1 of [1].

Figure 2 shows the detector after it has been sealed up inside an aluminum case and connected to the coax cable that goes to the DSO input.

In my correspondence with Cahill in December 2015, he was kind enough to take some additional measurements and send me the oscilloscope pictures of the correlated quantum waves he is detecting in his laboratory in Adalaide, Australia.

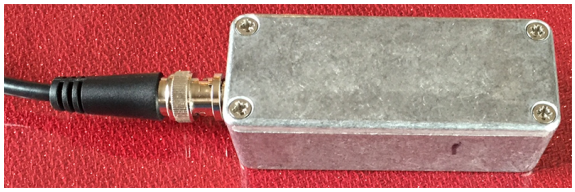

Fig. 2: Enclosed Quantum Detector used in experiment.

I was able to capture nearly identical correlated signals in my laboratory in Longmont, Colorado. However, upon further investigation of these signals I determined that they were of local origin and that the frequency of the waveforms was tied to the resonant frequency of the detector-cable system. I have concluded that the "correlation" Cahill sees is only an apparent correlation because the circuits of the two detectors, when excited by an external disturbance, produce nearly the same transient response due to their being nearly identical circuits with nearly the same natural frequency. An external disturbance, such as a nearby static discharge is required to excite the transient response. The correlated signals start out in phase but slip with time because the two resonant frequencies are not exactly the same. The measured phase difference is simply a function of how much time elapses from the moment of excitation until the scope triggers and captures the waveforms.

This paper documents the experiments I performed and my reasoning for coming to the above conclusions.

2 Cahill's data

Figures 3 and 4 show data from Dec. 13 and 14, 2015, taken by Cahill in his laboratory in Adelaide, Australia, and sent to me via email as an example of what the current fluctuations from the gravity waves look like for collocated detectors. Similar pictures of gravity waves in his detectors can be seen in [1–3]. Notice that the frequencies in these two

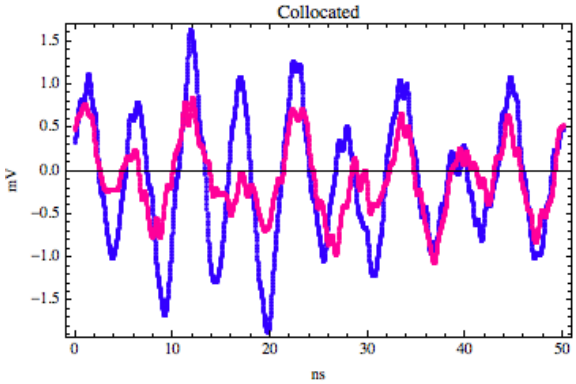

Fig. 3: Cahill Dec 13 Typical Data with detectors collocated.

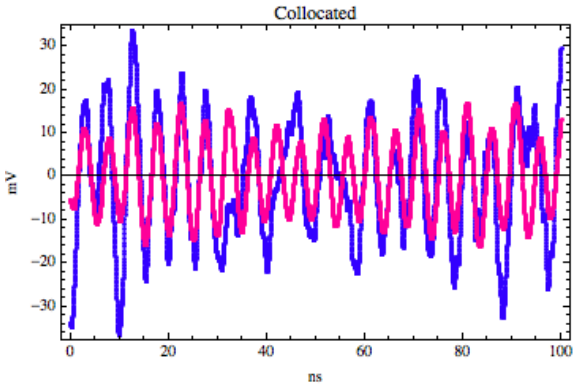

Fig. 4: Cahill Dec 14 Typical Data with detectors collocated.

plots are near 200 MHz and appear almost like a tone superimposed on noise. This seemed odd to me given that Cahill in his papers says that the frequency spectrum of the fluctuations in the detectors has a 1/f amplitude relationship. The reason the tone seen in his data does not show up in the frequency spectrum plots, is because they occur so infrequently. Most of the time the current fluctuations are at very small quiescent levels that look like random, uncorrelated noise. This quiescent current is disturbed at random periods by bursts of energy at mostly a single frequency, which are the waveforms captured in Cahill's pictures. Because these energy bursts are short with long periods of time between them, they have little effect on the Fourier transform over a wide frequency band — hence the 1/f relationship without evidence of these tones.

3 My experimental data

Figure 5 is a photo of my oscilloscope on Dec. 11, 2015, showing the quiescent signal from the detectors. Notice that there is little, if any, evidence of correlation between the two waveforms. The scale is 2 mV per division vertically and 10 ns per division horizontally. Notice also that the peak-to-peak fluctuations are typically less than 1 mV.

On December 11, when I took the picture in Figure 5, I was unable to detect any signals except the quiescent current.

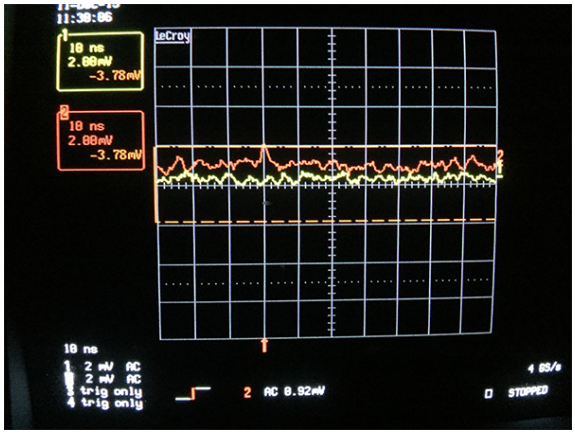

Fig. 5: Quiescent waveforms of collocated detectors.

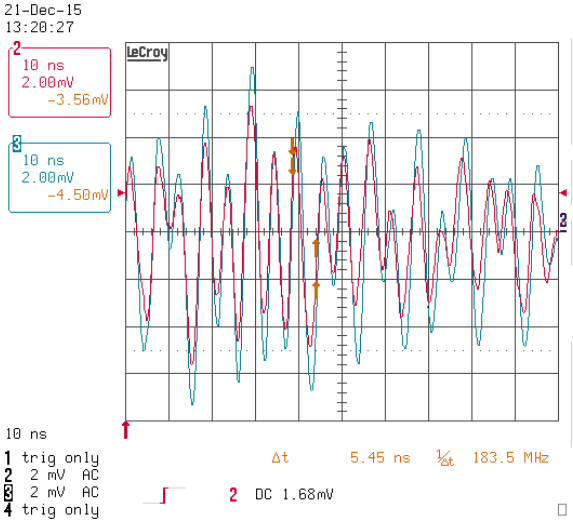

Fig. 6: Burst of energy from collocated detectors in my laboratory on Dec. 21, 2015.

I tried various orientations of the detectors but gave up after a few hours of searching. After communicating with Cahill via email, he sent me the pictures of Figures 3 and 4 showing me what he was seeing in his laboratory. I then went back into my laboratory on Dec 21 and set up my oscilloscope to trigger on any signals above 1.5 mV. After several minutes, I suddenly got a large burst of energy at about 200 MHz just like Cahill. This is shown in Figure 6.

The fundamental frequency of this waveform is highly correlated between the two detectors. However, I noticed a subtle difference between the two waveforms that should not be there if they are truly being modulated by the same source. The phase of the two waveforms is nearly perfectly aligned on the left side of the screen but it is drifting apart as one moves towards the right side of the screen. This is what one would see if two different, but nearly identical frequencies were observed. It is not what one would see from a single modulating

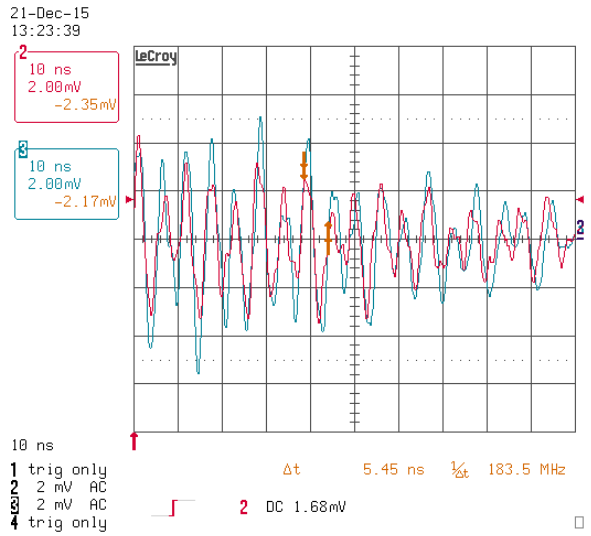

Fig. 7: Another captured waveform from collocated detectors in my laboratory on Dec. 21, 2015.

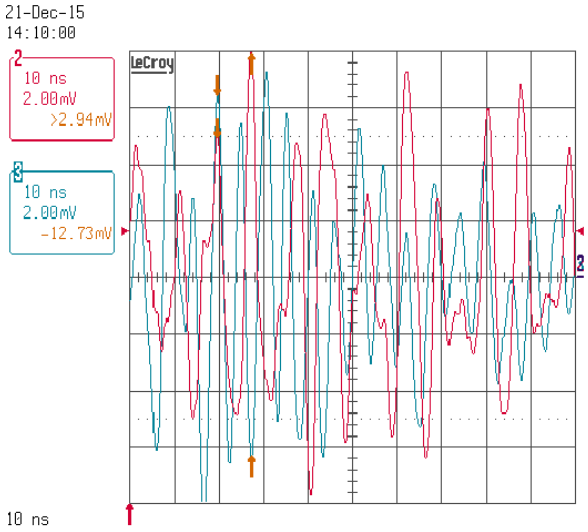

Fig. 8: Waveforms from collocated detectors with different cable lengths.

source observed on two different detectors.

I set the scope up to capture another signal and got the waveform shown in Figure 7. Notice again the same effect. The phase is aligned on the left and is slowly drifting apart as it moves to the right. If collocated detectors were being excited by the exact same gravity waves, the phase between them would not drift. At this point I realized that something was not right. My first suspicion was that my two "identical" detectors were not quite identical, but had natural frequencies in their circuits (including the cables) that were not quite the same. They were being excited by some external signal, but the actual response I was seeing was not a gravity wave, but simply the transient response of each of these circuits as they resonated at their not-quite-equal natural frequencies.

To test this theory, I replaced the cable on one of the detectors with a longer cable. I now had a 3 ft. coax cable on the detector going to channel 3 (blue) of the scope and a 5 ft. cable on channel 2 (red). The result was the waveforms shown in Figure 8. This shows very clearly that the red waveform has a fundamental frequency significantly lower than the blue waveform. I had proof positive that these 200 MHz energy bursts were not from 200 MHz gravity waves.

But there was still the question of what caused the excitation of the circuits to start with. Could it be Cahill's gravity waves that provide the initial excitation? Or was the source of local origin? My next experiment was to separate the detectors by a few millimeters to see if the phases of the two waveforms would start out with an initial phase difference. This is what would happen if they were being exited by passing through Cahill's gravity waves due to the velocity of space past the earth. Cahill asserts that the velocity of the earth is about 500 km/sec which represents about 2 ns/mm in phase shift if the detectors are directly aligned with this velocity. If they are not aligned, an even larger phase shift per mm would be observed. I saw no change in the phase relationship between the two signals as the detectors were moved relative to each other. The waveforms remained in phase at the beginning and drifted with time. This indicates an initial excitation disturbance moving at the velocity of light — not 500 km/sec.

In [4], Vrba noted that the battery, diode and resistor circuit form an electromagnetic wave sensing loop having a substantial cross section. Although the circuit is enclosed inside an aluminum box that shields electric fields, it is not a perfect shield. It will highly attenuate an electromagnetic wave, but with the oscilloscope set to its most sensitive level of 2 mV per division, even an attenuated signal could still be large enough to be detected.*

As I was pondering how to identify the source of the initial excitation, I noticed something very interesting. My oscilloscope would not trigger unless there were people in the laboratory. If everyone left and there was no nearby human activity, the signals would remain at their quiescent (< 1.4 mV) level and the scope would never trigger. But once nearby human activity resumed the scope would begin triggering again every few minutes. It didn't take long to find a correlation between static discharges from human activity and the energy bursts in the scope. By experimenting, I found that I could generate a frequency burst that would trigger the scope from as far away as 20 meters by shuffling my shoes on the car-

*Although not reported in this paper, I designed a second experiment using an architecture similar to Vrba's. It included 200× amplification with a bandwidth of 10 MHz to detect even smaller signals. The resonant disturbances disappeared, which left only the random noise. Visually examining these waveforms, I saw no evidence of correlated signals. The raw data files are available upon request at the email address given above for anyone desiring to perform a more sophisticated search for correlation between the waveforms.

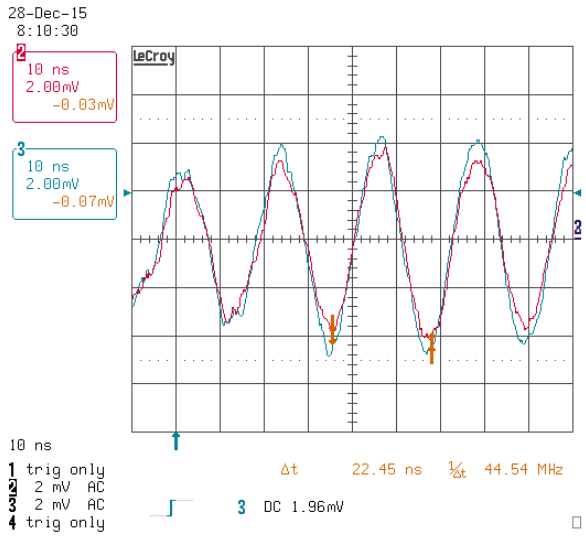

Fig. 9: Waveforms from collocated detectors with battery bypassed with 1 nF capacitor.

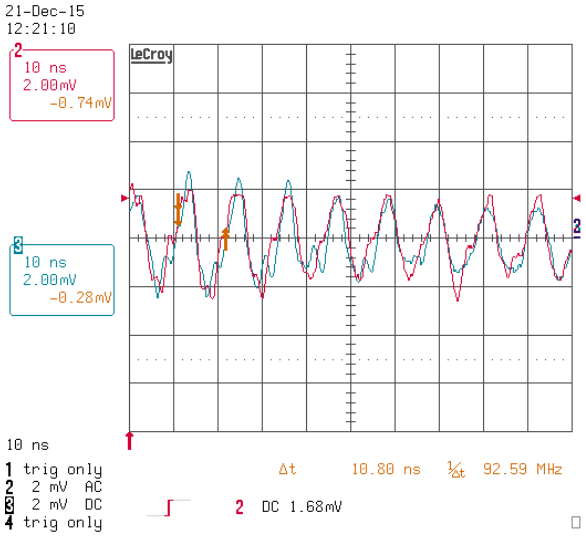

Fig. 10: Waveforms from collocated disconnected coax cables.

pet and touching something metallic. The waveforms looked identical in amplitude and frequency to those above.

As an additional proof that the detected frequency was entirely determined by the circuit, I made 2 modifications to the circuit. First, I put a 1 nF capacitor across the battery to provide a low impedance path for high frequencies. It caused the frequency of the transient response to drop to below 50 MHz as shown in Figure 9. I then removed the quantum detector entirely, and just left the two 3-foot, collocated coax cables disconnected. The waveforms are shown in Figure 10. These results further strengthen the argument that the frequency of the waveforms are determined entirely by the circuit itself.

4 Conclusions

After attempting to repeat the gravity wave detection experiments of Cahill using reverse biased Zener diodes as quantum tunnelling devices, I found no evidence of current fluctuations due to anything but normal random noise or local disturbances followed by a transient oscillation at the natural frequency of the detector circuits. The so-called correlation of the signals between detectors was merely an apparent correlation due to the fact that the circuits have natural frequencies that are nearly identical. This was proven by changing the natural frequencies of the circuits and showing that the frequency of the "gravity waves" changed to the new frequency.

The initial excitation of the circuits was shown to be from local sources — not disturbances in "dynamical space" as proposed by Cahill. The detectors exhibited no evidence of being excited by anything but uncorrelated random noise unless nearby human activity was generating static discharges. No evidence of any correlated signals between detectors was ever seen at any frequency other than the natural frequency of the detector circuits (superimposed on noise and/or reflections in the cables).

Whether Cahill has ever detected disturbances due to dynamical space, I cannot say. But I am satisfied that in Longmont, Colorado in December of 2015, there was no evidence that dynamical space was detectable using the Zener diode circuit Cahill has proposed in his papers.

Acknowledgements

I am indebted to Reg Cahill for his assistance in getting the quantum detectors built properly, providing advice on how to detect the signals and in supplying me with examples of the signals he obtained in his laboratory. It is unfortunate that my experiments ended up contradicting his papers rather than confirming them.

Submitted on September 15, 2016 / Accepted on September 17, 2016

References

1. Cahill R.T. Quantum Gravity Experiments. *Progress in Physics*, 2011, v. 11(4), 317–320.
2. Cahill R.T. Nanotechnology Quantum Detectors for Gravitational Waves: Adelaide to London. *Progress in Physics*, 2013, v. 4(4), 57–62.
3. Cahill R.T. Gravitational Wave Experiments with Zener Diode Quantum Detectors: Fractal Dynamical Space and Universe Expansion with Inflation Epoch. *Progress in Physics*, 2014, v. 10(3), 131–138.
4. Vrba A.L. Reservations on Cahill's Quantum Gravity Experiment. *Progress in Physics*, 2015, v. 11(4), 330.

LETTERS TO PROGRESS IN PHYSICS

Some Insights on the Nature of the Vacuum Background Field in General Relativity

Patrick Marquet

18 avenue du Président Wilson, 62100 Calais, France
E-mail: patrick.marquet6@wanadoo.fr

In our publication "Vacuum Background field in General Relativity" (*Progress in Physics*, 2016, v. 12, issue 4, 313–317) we introduced a kind of "relic" field permanently filling the empty space-time. This proved to be a necessary ingredient to formulate a true vector describing the gravitational field arising from matter, in contrast to the awkward pseudo-tensor usually suggested to ensure the conservation of the energy-momentum in the field equations. In this short paper, we give this field a mathematical description in terms of geodesics.

The background field that persists in vacuum devoid of any matter or energy, finds a physical meaning if we consider the *Landau-Raychaudhuri equation* for a congruence of non-intersecting timelike unit vectorial field $\boldsymbol{X}$, $(X_a X^a = 1)$, i.e.:

$$R^a{}_b\, X_a X^b = -{}^\circ X^a{}_{;a} - \omega_{ab}\,\omega^{ab} + \sigma_{ab}\,\sigma^{ab} + {}^\circ\theta + \frac{1}{3}\,\theta^2, \quad (1)$$

where $^\circ$ means differentiation with respect to proper time τ. In the scalar ζ which is the *Lagrangian density of the vacuum background field*

$$\zeta = \sqrt{-g}\,\nabla_a\,\kappa^a \quad (2)$$

we set up

$$\nabla_a\,\kappa^a = \theta^2, \quad (3)$$

where θ is the *space time volume expansion* characterizing this background field through

$$\theta = X^a{}_{;a} = h^{ab}\theta_{ab} \quad (4)$$

with the expansion tensor $\theta_{ab} = h^c_a h^d_b\, X_{(c;d)}$ ($h_{ac} = g_{ac} - X_{ac}$ is the projection tensor).

The formula of $X_{(c;d)}$ can be regarded as measuring the rate of change of the space-time 4-volume, i.e. either expansion if positive, or contraction if negative.

The form (3) has been chosen so as to preserve the integrity of the gravity tensor equation irrespective of the sign of θ.

In our case (absence of energy/matter), the background field obviously follows a contraction process (negative expansion) of space-time, and the Landau-Raychaudhuri reduces to

$${}^\circ\theta = R^a{}_b\, X_a X^b - \sigma_{ab}\,\sigma^{ab} - \frac{1}{3}\,\theta^2 < 0 \quad (5)$$

(since the vorticity tensor ω^{ab} induces expansion, while the shear tensor σ^{ab} induces contraction and the geodesic equation ${}^\circ X^a{}_{;a}$ is zero).

$R^a{}_b\, X_a X^b$ (sometimes referred to as the Raychaudhuri scalar) is always positive ensuring that the Strong Energy Condition (SEC) is not violated when energy/matter is there. Therefore, we are left with the inequality

$${}^\circ\theta \leqslant \frac{1}{3}\,\theta^2. \quad (6)$$

Integrating it with respect to the proper time τ yields

$$\theta^{-1} \geqslant \theta_1^{-1} + \frac{1}{3}\,\tau\,, \quad (7)$$

where θ_1 is the initial value which can be positive to start with, but very soon after the short expansion, it is followed by re-collapse. The mathematical fate of (timelike) geodesics is a final focusing to a caustic ($\theta \to -\infty$) after a finite proper time of at most

$$\tau \leqslant \frac{3}{\theta_1} \quad (8)$$

after the measurement of the initial value.

Such a state is called *geodesic incompleteness* which is a notion introduced by Hawking-Penrose, to describe (or not !) a geodesics path of observers through space-time that can only be extended for a finite time as measured by an observer travelling along one.

Presumably, at the end of the geodesic, the observer has fallen into a "kink" or encountered some other pathology at which the laws of General Relativity breakdown.

As Landau pointed out, in a *synchronous comoving frame of reference* attached to a homogeneous fluid, such a singularity can be removed by the introduction of a pressure which tends to substantiate our space-time contraction hypothesis.

All these contribute to our impossibility to give a full description of the vacuum background field. In a sense, this marks the lowest horizon level of the space-time.

Submitted on August 31, 2016 / Accepted on September 30, 2016

References

1. Marquet P. Vacuum background field in General Relativity. *Progress in Physics*, 2016, v. 12, issue 4, 313–317.

2. Kramer D., Stephani H., Hertl E., MacCallum M. Exact Solutions of Einstein's Field Equations. Cambridge University Press, Cambridge, 1979.
3. Marquet P. The generalized warp drive concept in the EGR theory. *The Abraham Zelmanov Journal*, 2009, v. 2, 261–287.
4. Raychaudhuri A.K. Relativistic cosmology. I. *Physical Review*, 1955, v. 90, issue 4, 1123–1126.
5. Dadhich N. Derivation of the Raychaudhuri equation. arXiv: gr-qc/0511123v2.
6. Natario J. Relativity and singularities — a short introduction for mathematicians. arXiv: math.DG/0603190.
7. Kar S., SenGupta S. The Raychaudhuri equations: a brief review. arXiv: gr-qc/0611123v1.

Conservation Laws and Energy Budget in a Static Universe

Yuri Heymann

3 rue Chandieu, 1202 Geneva, Switzerland. E-mail: y.heymann@yahoo.com

The universe is characterized by large concentrations of energy contained in small, dense areas such as galaxies, which radiate energy towards the surrounding space. However, no current theory balances the loss of energy of galaxies, a requirement for a conservative universe. This study is an investigation of the physics nature might use to maintain the energy differential between its dense parts and the vacuum. We propose time contraction as a principle to maintain this energy differential. Time contraction has the following effects: photons lose energy, while masses gain potential energy and lose kinetic energy. From the virial theorem, which applies to a system of bodies, we find that the net energy resulting from the gain in potential energy and the loss in kinetic energy remains unchanged, meaning that the orbitals of stars in galaxies remain unaffected by time contraction. However, each object in a galaxy has an internal potential energy leading to a surplus of energy within the object. This internal energy surplus should balance with the energy radiated at the level of a galaxy. We illustrate this principle with a calculation of the energy balance of the Milky Way.

1 Introduction

We are in a universe governed by energy fluxes and exchanges either in the form of waves or particles in motion. Energy flows in space allow life to exist. The universe is characterized by vast concentrations of energy confined in small spaces such as galaxies in the immensity of a surrounding vacuum. Supermassive black holes at the center of galaxies contain a large portion of this energy. However, we do not understand how such energy segregation came into existence. Most of the energy in the universe radiates outward from these dense galaxies. The supermassive black holes at the center of galaxies may be the cosmic embryos that give rise to the birth of the stars and planets. Massive particles and atoms are attracted by gravitation to the dense points of the universe, a process which maintains the segregation between the vacuum and the dense parts. Because galaxies radiate a large amount of energy, they appear to have energy deficits. Here we investigate the physics of how the energy difference between the vacuum and the dense parts of the universe is maintained.

Many profound questions related to this issue have not yet been answered. Most notably, how did the galaxies come into existence? Do the galaxies have a life time? About 90% of galaxies are dwarf galaxies, and most are elliptical or lenticular in shape. Large spiral galaxies such as the Milky Way are the minority. What are the conditions for galaxies to form stars? For a galaxy to form a spiral it must rotate rapidly. We have observed powerful jets of particles ejected from galaxy central supermassive black holes in the direction of the axis of rotation of the galaxy. These jets, together with a vortex in the black hole, supposedly induce the galaxy to rotate, and then form arms and spirals of stars. A galaxy which has few stars radiates less energy than a galaxy forming stars in abundance. Without a doubt, the lives of galaxies should be considered among the greatest mysteries in the universe.

Nowadays, many people consider the static model of the universe outdated. Nevertheless, we believe there is a lesson to learn when considering the energy balance of the universe. After all, energy conservation is a cornerstone of physics. The elusive dark energy encourages us to inspect the energy balance of the universe from a different angle, in a static universe.

2 The entropic principle

The entropic principle in a thermal context is regarded as an indicator of the effectiveness or usefulness of a particular quantity of energy. Mixing a hot supply of energy with a cold one produces a mix of intermediate temperature, which is less effective. If we apply this principle at the level of the universe, it will eventually lead to the so-called “heat death of the universe”, when the outbound and inbound energy fluxes of galaxies reach an equilibrium that should stay at low temperature provided that the universe does not maintain its present energy differential between the vacuum and its denser parts. The inbound energy flow from cosmic radiations is much lower than the outbound flow radiating from a galaxy, giving galaxies the appearance of an energy deficit. Present theories do not permit us to balance this deficit.

3 Photon-particle interactions

We could conceive of a wind of particles that sweeps the remnant undulating energy in the vacuum of the universe in something like the Compton effect and brings it back to the denser parts of the universe to enrich the galactic gas and nebulae where new stars are formed. This scenario appears to be very unlikely as the inbound flux of cosmic rays is very low, and known interactions between low-energy photons and particles do not subtract energy to the photons. In Thomson scattering, the scattered photon energy is left at the same level, and

an increase of the scattered photon energy is obtained in the photon-particle interaction of the Sunyaev-Zeldovich effect. Compton scattering, which subtracts energy from the photons, is known to occur for high-energy light sources such as X-rays and gamma rays. Furthermore, there is no evidence that cosmic rays come from outside the galaxy, although most cosmic rays originate from outside the solar system [1]. Cosmic rays are composed primarily of high-energy protons and atomic nuclei. Some cosmic rays originate from supernovae [2]; however, this is not the only source of cosmic rays. Active galactic nulei also ought to produce cosmic rays [3].

Compton scattering is an interaction between photons and charged particles such as electrons [4,5]. During this interaction, part of the photon energy is transferred to the recoiling electron. The scattering of the photons produces a blurring effect of light.

Thomson scattering intervenes between photons having much lower energies compared to the mass energy of the particle [6–8]. This interaction occurs between free charged particles and photons. Thomson scattering is an elastic scattering, meaning that the energies of the particles and photons remain unchanged in this interaction. However, the wave is scattered, producing a blurring effect. This interaction produces polarization of light in the direction of its motion. The cosmic microwave background ration (CMBR) is linearly polarized and as such must have undergone Thomson scattering.

The Sunyaev-Zel'dovich effect is an interaction occurring between the CMBR and high-energy particles, which produces an inverse Compton effect [9]. It is the result of high-energy electrons transferring some of their energy to the photons. This interaction is observed in the hot gases contained in galaxy clusters, which change the frequency of the CMBR.

The images of galaxies we observe in the sky are not blurred, meaning a priori that no photon-particle interactions occur for these wave frequencies. For all these reasons we dismiss photon-particle interaction as a mechanism to regulate photon energy in the vacuum.

4 Stationary waves

Stationary waves, also called standing waves, are formed by the superposition of two waves of the same amplitude and frequency moving in opposite directions [10]. The result of this interference is a wave with no net propagation of energy. The locations at which the amplitude of the wave intersect with the x-axis are fixed points called the nodes, and the part of the wave contained between two nodes oscillates upside down in a given amplitude range. Because of the vibration of the standing wave, some energy would be stored in the vacuum, but with no energy being transmitted. Because of the isotropy of the universe we can assume that for every wave there exists another wave of same frequency and amplitude moving in the opposite direction. Standing waves may cause an accumulation of energy in the vacuum, but do not explain redshifts. Nevertheless, we would still need additional mechanisms to regulate the energy budget of galaxies and of the universe as a whole.

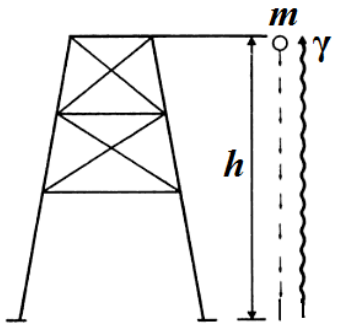

Fig. 1: A photon climbs up to a heigh h. Then, the photon is converted at the top of the tower into a mass m, and falls back to the ground. Perpetual motion is created unless the photon loses energy while climbing in the gravitational field.

5 Time contraction

5.1 Gravitational redshift and potential energy

Another way to look at the problem of energy budget in the universe is by considering gravitational redshift, a phenomenon based on the principle of energy conservation. Einstein imagined the following thought experiment. Let us consider a photon moving away from the ground surface in the direction of the sky up to a given height h. At this height, the photon is converted into mass according to $E = mc^2$, and then falls back to the ground (see Figure 1).

In this system there is an apparent gain of energy from the time the photon left the ground to the time when the mass came back to its initial position due to the potential energy gain when the photon moved upwards. This energy gain, of course is paradoxical. In terms of energy conservation, when considering the energy of a photon, we associate it with the potential energy of its virtual mass counterpart. In order to maintain the system at constant energy, the photon must lose energy when moving away from a mass in a gravitational field, which causes a redshift. The reciprocal is also true: when a photon moves towards a mass in a gravitational field, it is blueshifted. Another solution of the gravitational redshift is obtained with general relativity using the Schwarzschild metric. Both methods give similar solutions that converge asymptotically when the gravitational field is weak.

The gravitational redshift from mass-energy equivalence, which stems from special relativity, is derived as follows. By converting the photon energy into a rest mass we get $E = h\nu = mc^2$. The gravitational potential energy is:

$$U = -\frac{GMm}{r} = -\frac{GMh\nu_0}{rc^2}\,, \qquad (1)$$

where ν is the light-wave frequency, G the gravitational constant, M the mass producing the gravitational field, r the distance between the center of gravity of the mass M and the photon, c the speed of light, and h the Planck constant.

Hence, the frequency change of a photon of frequency ν_0 moving relative to a gravitational mass is $h\nu = h\nu_0\left(1 - \frac{GM}{rc^2}\right)$. Therefore, we get:

$$\frac{\nu}{\nu_0} = 1 - \frac{GM}{rc^2}\,. \tag{2}$$

The equation of the gravitational redshift from general relativity with the Schwarzschild metric is obtained from the equation [21]:

$$\delta\tau = \left(1 - \frac{2GM}{rc^2}\right)^{\frac{1}{2}} \delta t\,, \tag{3}$$

where $\delta\tau$ is the proper time interval, and δt the Schwarzschild time interval.

Because the light wavelength can be expressed as a function of the time interval, $\lambda = c\delta\tau$, we get the gravitational redshift

$$\frac{\nu}{\nu_0} = \left(1 - \frac{2GM}{rc^2}\right)^{\frac{1}{2}}\,, \tag{4}$$

where ν is the light-wave frequency, G the gravitational constant, M the mass producing the gravitational field, r the distance between the center of gravity of the mass M and the photon, and c the speed of light.

For weak gravitational fields, we can use the Taylor approximation $(1 - x)^{\frac{1}{2}} \approx 1 - \frac{x}{2}$ when x is small; hence, we obtain the same equation as the gravitational redshift obtained from mass-energy equivalence.

From general relativity, moving away from the ground surface at increasing altitude causes the clock to tick more rapidly, meaning that time is contracting as in the dichotomous cosmology presented in [11–13]. Based on the principle of time contraction in a static universe, we are able to derive Etherington's distance-duality equation [12]. This principle as an explanation of cosmological redshift is worth considering. One way to look at the problem of photon and matter energy is by linking time with energy, meaning that time contraction is causing both a decrease in the photon energy and an increase in the potential energy of a mass. If this is valid in a gravitational field, does it hold in general? From the mass-energy equivalence, there is an implicit duality between photon and mass, in which energies appear to be indissociable from one another.

Emmy Noether proved a theorem according to which every differentiable symmetry of the action of a physical system has a corresponding conservation law. From the Noether theorem, the law of conservation of energy follows from time homogeneity, meaning the Lagrangian is time-translation invariant. Time is preponderant in energy conservation. In special relativity we learn that time dilation has a direct effect on the energy balance between reference frames. In general relativity, the flow of time and gravitational potential are directly linked. This is a very simple principle that nature could use to regulate energy fluxes in the universe. Accordingly, time contraction would allow maintenance of the energy differential between the vacuum and the massive parts of the universe.

5.2 Effect of time contraction on the photon energy and the energy of a mass

In the dichotomous cosmology [12], we found that the time-contraction factor is expressed as $\gamma_t = \exp(-H_0 t)$. Therefore, the energy of the photon decreases according to an exponential law of the form:

$$E_{\text{photon}}(t) = E_0 \exp(-H_0 t)\,, \tag{5}$$

where H_0 is the Hubble constant, E_0 the initial photon energy, and t the time.

Because the gain in potential energy is in the same proportion as the photon energy loss from mass-energy equivalence, the gravitational potential energy of a mass shall increase according to the law:

$$U_{\text{mass}}(t) = U_0 \exp(-H_0 t)\,, \tag{6}$$

where U_0 is a negative potential energy at time zero, H_0 the Hubble constant, and t the time.

We still need to quantify the effect of time contraction on the kinetic energy of a mass. As time contracts, a clock is ticking more rapidly, and an object in motion appears to slow down. The apparent velocity of an object decreases in direct proportion to the time-contraction factor. Because the kinetic energy is expressed as $K = \frac{1}{2}mv^2$, the kinetic energy of a mass decreases by the square of the time-contraction factor. Hence, the kinetic energy of a mass decreases according to the law:

$$K_{\text{mass}}(t) = K_0 \exp(-2H_0 t)\,, \tag{7}$$

where K_0 is the kinetic energy at time zero, H_0 the Hubble constant, and t the time.

These are the laws that we propose regulate the energy budget of the universe.

Let us show that for a star in orbit in a galaxy, its orbital radius remains unchanged under time contraction. The total energy of the star with respect to other bodies in the galaxy is expressed as follows:

$$E_{\text{tot}}(t) = U + K = U_0 \exp(-H_0 t) + K_0 \exp(-2H_0 t)\,. \tag{8}$$

Let us take the time derivative of E_{tot}; therefore, we get:

$$\frac{dE_{tot}}{dt}(t) = -H_0\, U_0 \exp(-H_0 t) - 2H_0\, K_0 \exp(-2H_0 t)\,. \tag{9}$$

We evaluate this expression at $t = 0$, hence:

$$\frac{dE_{tot}}{dt} = -H_0\, U_0 - 2H_0\, K_0\,. \tag{10}$$

From the virial theorem, which applies to stable systems composed of many bodies, we get:

$$2K_0 + U_0 = 0\,, \tag{11}$$

where K_0 is the kinetic energy and U_0 the potential energy between the bodies.

From (10) and (11), we obtain $\frac{dE_{tot}}{dt} = 0$. Therefore, the total energy of a star in orbit remains unchanged under time contraction, meaning its orbital radius is not affected. This is the condition required to have stable galaxies in the universe.

The virial theorem only considers the potential energy between the bodies of the system. Because each object in a galaxy, either solid or fluid, has an internal potential energy, and that the kinetic energy inside a solid or fluid at rest is negligible, there is a surplus of potential energy from (6). This surplus of potential energy is converted into internal energy within the object. This is the principle we propose to balance the energy radiated by galaxies.

5.3 Energy balance of the Milky Way

From this principle, we would expect that the surplus of internal potential energy due to time contraction, at the level of a galaxy, balances with the outbound radiation flux. Let us do a rough estimation for the Milky Way. The luminosity of the Milky Way is estimated to be about $3.8{\times}10^{10} L_\odot$ [15], with the Sun radiating about 4.6×10^{26} watts, leading to an overall radiation of about $1.74{\times}10^{37}$ watts. We need to estimate the sum of the internal potential energy of each object contained in the Milky Way.

For a spherical solid, the internal potential energy is given by the equation [14]:

$$U_{\text{sphere}} = -\frac{3GM^2}{5R}\,, \tag{12}$$

where G is the gravitational constant, M the mass, and R the radius of the sphere.

Let us consider the estimated mass of the Milky Way including dark matter to be about 1.39×10^{42} kg or $7{\times}10^{11}$ $M_\odot$ [16]. In [17] we show that the dark matter of a spiral galaxy is due to a correction coefficient applied to Newton's force in a disk. Hence, we need an estimate of the total baryonic mass of the Milky Way, which is approximatly one seventh of the apparent mass or about $1.87{\times}10^{41}$ kg. The mass of the cental supermassive black hole Sagittarius A* is about $4.0{\times}10^6$ solar masses [18], and its radius about 31.6 solar radii. Hence, the potential energy of Sagittarius A* from (12) is $-1.15{\times}10^{53}$ joules. We have used a gravitational constant G of $6.67{\times}10^{-11}$ $\mathrm{m^3\,kg^{-1}\,s^{-2}}$.

Because the majority of stars in the Milky Way are red dwarfs, and due to other dense objects such as neutron stars, white dwarfs, and black holes, the average radius of objects in the Milky Way is lower than the radius of the Sun. An estimate of 100 million neutron stars in the Milky Way was obtained by estimating the number of stars that have gone supernova [19]. Let us assume that these 100 million neutron stars in the Milky Way have an average mass of 1.35 solar masses. From the density of neutronium, we can infer that the radius of such a neutron star would be about 15 km. Therefore, from (12), the internal potential energy of those 100 million neutron stars all together is $-1.92{\times}10^{54}$ joules. According to [20] there are about 10 million black holes in the Milky Way. Let us assume that these 10 million black holes have an average mass of ten solar masses and a radius of 45 km. The radius of a black hole is computed from the "photon sphere" which is 1.5 times the Schwarzschild radius. The internal potential energy of those 10 million black holes all together is $-6.42{\times}10^{54}$ joules from (12). Let us assume there are 2 billion white dwarfs having an average mass of half a solar mass and a radius equal to the radius of the earth. The internal potential energy of those 2 billion white dwarfs is $-1.28{\times}10^{52}$ joules. Let us assume there are 200 billion stars lefts (mainly red dwarfs) having an average radius of 0.3 solar radii and average mass of $9.36{\times}10^{29}$ kg. The internal potential energy of those 200 billion stars all together is $-3.34{\times}10^{52}$ joules from (12).

Adding together the potential energies of Sagittarius A*, the 100 million neutron stars, the 10 million black holes, the 2 billion white dwarfs, and the 200 billion stars, the overall internal potential energy of the Milky Way is estimated to be about $-8.49{\times}10^{54}$ joules. The densest objects, although not the most numerous, contribute the greatest share of to the internal potential energy of the Milky Way. For this reason, black holes and neutron stars are responsible for most of the Milky Way's internal potential energy. The calculations for the internal potential energy of objects in the Milky Way are summarized in Table 1.

When multiplying the overall internal potential energy of the Milky Way by the Hubble constant of $H_0 = 2.16\times10^{-18}$ per second (corresponding to 67.3 $\mathrm{km\,s^{-1}\,Mpc^{-1}}$), we obtain a surplus of internal energy of $1.83{\times}10^{37}$ watts. We compare this value with the estimate of the energy radiated of $1.74{\times}10^{37}$ watts. Of course this is a crude estimate, but from our calculations the internal energy surplus of the Milky Way is the same order of magnitude as the energy radiated by the galaxy.

Compact objects such as black holes and neutron stars are known to produce highly energetic jets emitted at relativistic velocities along their axis of rotation. We propose that the surplus of potential energy of compact objects is released to the galaxy through these jets. These jets might be made of neutrons that undergo beta decay to form protons, electrons and antineutrinos.

6 Conclusion

According to the entropic principle in a thermal context, mixing a hot source with a cold source produces a mix of average

Table 1: Internal potential energy of objects in the Milky Way

Object	Number	Mass	Radius	Potential energy
Sagittarius A* (central black hole)	1	$4.0\times10^6\ M_\odot$	2.2×10^7 km	-1.15×10^{53} joules
Black holes	10 million	$10\ M_\odot$	45 km	-6.42×10^{54} joules
Neutron stars	100 million	$1.35\ M_\odot$	15 km	-1.92×10^{54} joules
White dwarfs	2 billion	$0.5\ M_\odot$	6.30×10^3 km	-1.28×10^{52} joules
Remaining stars (mainly red dwarfs)	200 billion	$0.47\ M_\odot$	2.09×10^5 km	-3.34×10^{52} joules
Total	—	—	—	-8.49×10^{54} joules

temperature that is less useful from a mechanical standpoint. The universe is based on energy fluxes and exchanges, and galaxies radiate a large amount of energy. For the universe to be conservative there must be a mechanism to balance the energy deficit of galaxies, otherwise it will lead to the so-called "heat death of the universe". We analyzed photon-particle interactions, and concluded that such interactions cannot regulate the energy budget of the universe. We propose time contraction as a principle to regulate the energy balance in the universe, which would decrease photon energy, increase the potential energy of a mass, and decrease the kinetic energy of a mass. From the virial theorem, which applies to systems of bodies, we find that the net energy resulting from the gain in potential energy and loss in kinetic energy remains unchanged, meaning that the orbitals of stars in galaxies remain unaffected by time contraction. However, each object in a galaxy has an internal potential energy leading to a surplus of energy within the object. At the level of a galaxy, this internal energy surplus should balance with the energy radiated. We illustrated this principle with a calculation of the energy balance of the Milky Way.

Submitted on September 28, 2016 / Accepted on September 29, 2016

References

1. Gaisser T.K. Cosmic Rays and Particle Physics. Cambridge University Press, 1990, p. 1.
2. Ackermann M., Ajello M., Allafort A., Baldini L. et al. Detection of the characteristic Pion-decay signature in supernova remnants. *Science*, 2013, v. 339, no. 6121, 807–811.
3. HESS Collaboration. Acceleration of petaelectronvolt protons in the Galactic Centre. *Nature*, 2016, v. 531, 476–479.
4. Fuchs M., Trigo M., Chen J., Ghimire S., Shwartz S. et al. Anomalous nonlinear X-ray Compton scattering. *Nature Physics*, 2015, v. 11, 964–970.
5. Motz J.W., and Missoni G. Compton scattering by K-Shell Electrons. *Physical Review*, 1961, v. 124, 1458.
6. Gell-Mann M. and Goldberger M.L. Scattering of low-energy photons by particles of spin 1/2. *Physical Review*, 1954, v. 96, no. 5, 1433–1438.
7. Glenzer S.H., Alley W.E., Estabrook K.G., De Groot J.S., Haines M.G., Hammer J.H., Jadaud J.-P., MacGowan B.J., Moody J.D., Rozmus W., Suter L.J., Weiland T.L., and Williams E.A. Thomson scattering from laser plasmas. *Physics of Plasmas*, 1999, v. 6, 2117.
8. Moore C.I., Knauer J.P., and Meyerhofer D.D. Observation of the transition from Thomson to Compton scattering in multiphoton interactions with low-energy electrons. *Physical Review Letter*, 1995, v. 74, 2439.
9. Sunyaev R.A., and Zel'dovich Ya.B. The observation of relic radiation as a test of the nature of X-ray radiation from the clusters of galaxies. *Comments on Astrophysics and Space Physics*, 1972, v. 4, 173–178.
10. Born, M. Principles of Optics: Electromagnetic Theory of Propagation, Interference and Diffraction of Light. Pergamon, 6th Revised ed., 1980.
11. Heymann Y. A Monte Carlo simulation framework for testing cosmological models. *Progress in Physics*, 2014, v. 10, no. 4, 217–221.
12. Heymann Y. A derivation of the Etherington's distance-duality equation. *International Journal of astrophysics and Space Science*, 2015, v. 3, no. 4, 65–69.
13. Heymann Y. The dichotomous cosmology with a static material world and expanding luminous world. *Progress in Physics*, 2014, v. 10, no. 3, 178–181.
14. Kittel C., Knight W.D. and Ruderman M.A. Mechanics. New York, McGraw-Hill, 2nd ed., 1973, 268–269.
15. Flynn C., Holmberg, J., Portinari L., Fuchs B., and JahreißH. On the mass-to-light ratio of the local Galactic disc and the optival luminosity of the Galaxy. *Monthly Notices of the Royal Astronomical Society*, 2006, v. 372, 1149–1160.
16. Eadie, G. M., and Harris, W. E. Bayesian Mass estimates of the Milky Way II: The dark and light sides of parameter assumptions. arXiv: 1608.04757 [astro-ph.GA].
17. Heymann Y. Dark matter, the correction to Newton's law in a disk. *Progress in Physics*, 2016, v. 12, no. 4, 347–352.
18. Boehle, A., Ghez, M., Schödel, R., Meyer, L., Yelda, S. et al. An improved distance and mass estimate for Sgr A* from a multistar orbit analysis. arXiv: 1607.05726 [astro-ph.GA].
19. Camenzind, M. Compact Objects in Astrophysics: White Dwarfs, Neutron Stars and Black Holes. Springer, 2007.
20. Plait P. Death from the Skies!: The Science Behind the End of the World. The Penguin Press, Reprint edition, 2009, p. 302.
21. Moore T.A. A General Relativity Workbook. University Science Books, 2012, Chapter 9.

Progress in Physics is an American scientific journal on advanced studies in physics, registered with the Library of Congress (DC, USA): ISSN 1555-5534 (print version) and ISSN 1555-5615 (online version). The journal is peer reviewed and listed in the abstracting and indexing coverage of: Mathematical Reviews of the AMS (USA), DOAJ of Lund University (Sweden), Scientific Commons of the University of St.Gallen (Switzerland), Open-J-Gate (India), Referential Journal of VINITI (Russia), etc. Progress in Physics is an open-access journal published and distributed in accordance with the Budapest Open Initiative: this means that the electronic copies of both full-size version of the journal and the individual papers published therein will always be acessed for reading, download, and copying for any user free of charge. The journal is issued quarterly (four volumes per year).

Electronic version of this journal: http://www.ptep-online.com

Postal address:
Department of Mathematics and Science, University of New Mexico,
705 Gurley Avenue, Gallup, NM 87301, USA